The palaeoredox condition and morphological variation of microbialites from the Nama Group, South Africa.

Aidan Wilton
WLTAID002

Thesis presented for the degree of Master of Science

Department of Geological Sciences
University of Cape Town
April 2023
Supervised by Rosalie Tostevin
Funded by GENUS (DSI-NRF Centre of Excellence)

Plagiarism Declaration

I, Aidan Alexandré Wilton (WLTAID002),declare the following:
I know that plagiarism is wrong and a punishable offence. Plagiarism is to use another's work without referencing the original sources in the correct format.
I have used the Geological Society of America's Geology journal referencing format for citation and referencing. Each contribution to, and quotation in, this thesis from the works of other authors has been attributed, cited, and referenced.
The thesis presented here is my own work in execution, apart from the guidance from my supervisors, I have received no unacknowledged assistance.
I have not allowed, and will not allow anyone to copy my work with the intention of passing it off as their own work.

Signed by candidate

Date: 14 Apr 2023

Table of Contents

1. Abstract

Microbialites are the fossilised traces of microbial communities and are present in the rock record since the Paleoarchean, 3.5 billion years ago, making microbialites some of the earliest direct evidence for life on Earth. Microbialites exhibit a wide variety of macrostructures and fabrics, including laminated sheets, domes and clotted thrombolites, and formed under a range of conditions. Microbialites also vary on fine scales whereby individual layers in some cases vary within a single microbialite. The ubiquity of microbial reefs across the Precambrian means they were some of the most abundant deposits during major developments in Earth's history, namely the inception of photosynthesis, the oxygenation of the atmosphere and oceans, the development of the earliest metazoans and the origin of skeletonization. While Earth's atmosphere has contained oxygen since the GOE, the oceans only became persistently oxic during the mid-Palaeozoic. Oscillatory redox conditions occurred throughout the Cryogenian and Ediacaran Periods and the early Palaeozoic Era before this stability was reached. While oxic surface waters were present throughout the Proterozoic, there are open questions as to the maximum dissolved oxygen levels, and where oxic waters were located. Microbial reefs, typically composed of photosynthetic cyanobacteria, could have played a vital role in shaping this oxygen landscape. It is possible that cyanobacteria within the reefs created local oxygen oases within a generally low oxygen environment. Here, I test this hypothesis using a suite of microbialites from a section of the Nama Group that crops out in the Northern Cape, South Africa. I have studied the texture and mineralogy using XRD, SEM, petrography, and polished surfaces. I have also analysed high-resolution rare-earth element patterns from microdrilled microbial laminae to study local redox conditions.

Analysis of the mesostructure and microstructure of the microbialites indicates that they were columnar stromatolites that grew into an extensive reef of domal stromatolites within the subtidal zone. Small-scale spatiotemporal feature variations indicate there was widespread turbulence across the reef, potentially indicating rapid fluctuations in water depth or the creation of topographic heterogeneity by the reef. The laminae of the microbial material are composed of micritic calcite peloids, while the intercolumn material is largely microspar calcite. The presence of peloids coupled with the ubiquitous columnar growth patterns suggest an association with microbial activity. In concert with the proposed relatively shallow water depositional environment, it is likely that photosynthetic cyanobacteria are the primary microbes that created these structures. The REE data record primary seawater compositions and are in line with bulk rock analysis from the Nama Group. However, there are no cerium anomalies, suggesting these microbial reefs grew in anoxic waters. This is contrary to the cyanobacterial affinities of the microbialites as well as the presence of in-situ animal fossils in similar microbial reefs in other parts of the Nama Group. We propose three main models to reconcile these observations. First, the microbial communities may not have included oxygenic cyanobacteria, and the micro- and macro-environment surround the reef may have been anoxic. Second, the microbial reefs may have been oxic micro-environments, but this may not be reflected in the REE patterns due to microbial influence on the partitioning behaviour of Ce, or timescales of oxygen production that were much shorter than depositional timescales. Thirdly, the REE may reflect the surrounding water column, rather than the oxic reef environment, if the carbonate was trapped and bound, rather than precipitated in situ.

2. Literature Review

2.1. Oxygen Through Time

Earth's oxygenated atmosphere is inarguably the most unique feature of the planet. Since the Cambrian Explosion, the oxygenated oceans and atmosphere have been paramount to the continued existence and evolution of life as we know it. However, the planet was not always well oxygenated.

2.1.1. Major Events in Earth's Oxygenation

When free oxygen first appeared in the oceans is still a matter of debate, but it was anywhere between ~3.8 Ga (Crowe et al., 2013; Frei et al., 2016; Wang et al., 2018) and ~2.4 Ga (Stüeken et al., 2015), and even then, the atmosphere remained fully anoxic. The three Eras of the Palaeoproterozoic each experienced significant redox changes. The first significant instance of oxygenation was the Palaeoproterozoic Great Oxidation Event (GOE), between 2.45 and 2.2 Ga (Bekker et al., 2004; Holland, 2006, 2020). This period saw the accumulation of atmospheric oxygen at $>10^{-5}$ present oxygen level (PAL), permanently changing Earth's chemical history (Canfield, 2005). The mechanisms of the GOE are still a debated topic (Eguchi et al., 2020; Kopp et al., 2005; Kump and Barley, 2007), but the stratigraphic evidence is well recognised and constrained. The disappearance of prominent redox-sensitive detrital grains from the rock record (Holland, 2020) and the earliest appearance of oxidized deposits such as red beds (Chandler, 1980), gypsum evaporites (El Tabakh et al., 1999) and oxidised palaeosols (Rye and Holland, 1998) are commonly acknowledged markers for the GOE in the rock record.

The next major phase in Earth's oxygenation is the sardonically called the "Boring Billion," which spans the Mesoproterozoic to early Neoproterozoic. Between 1.8 Ga and 800 Ma, the Earth experienced so called biological, geochemical, and tectonic stasis (Brasier and Lindsay, 1998; Buick et al., 1995; Holland, 2006). However, recent studies on the redox landscape have challenged this naming. Estimates of atmospheric oxygen show considerable variation, ranging from 0.1% PAL (Bellefroid et al., 2018) to as high as 4% PAL (Zhang et al., 2016; Zhang et al., 2019b) or 6% PAL (Canfield et al., 2013). Studies from Mesoproterozoic deposits show there were dramatic, potentially regional variations in redox conditions: Mesoproterozoic deposits in North America record instances of oxic to suboxic deep marine waters ~1.85 Ga (Planavsky et al., 2018). Volcanogenic sulphide deposits recorded similar suboxic deep water conditions ~1.8-1.7 Ga (Slack et al., 2007; Slack et al., 2009). ~1.56 Ga Northern Chinese deposits recorded several transient oxygenation events (Diamond and Lyons, 2018; Zhang et al., 2019b). Isolated marine basin deposits from Russia show records of oxygen ~1.42 Ga (Sperling et al., 2014). Additional Northern China deposits even suggests there was deep ocean oxygenation ~1.4 Ga (Liu et al., 2021). Lastly, Guilbaud et al. (2015) recorded a global redox shift from sulphidic to ferruginous conditions in the middle ocean depths ~1 Ga to 0.7 Ga. This ultimately shows the Mesoproterozoic oceans experienced variable levels of oxygenation, far from being boring.

2.1.2. Ediacaran Redox Landscape

The final evolution in Earth's oxygen history was the rise towards stable, modern-like oxygenation levels, during the late Neoproterozoic and early Palaeozoic Eras (Canfield et al., 2007; Canfield and Teske, 1996; Knoll and Nowak, 2017; Marais et al., 1992; Shields-Zhou and Och, 2011; Shields, 2017). This transition was named the Neoproterozoic Oxygenation Event (Och and Shields-Zhou, 2012). Recently, it was suggested to change the name and timing of this geological time period to the Neoproterozoic Oxidation Window or the Palaeozoic Oxidation Event (Poulton et al., 2021; Tostevin and Mills, 2020). These revised names allude to the fact that the Neoproterozoic experienced dramatic spatial and temporal fluctuations in oxygenation (Sahoo et al., 2016): Molybdenum concentrations from South China black shales suggest that there was global deep ocean oxygenation between 630–551 Ma (Scott et al., 2008). Episodic oxygenation events have been recorded between 635–630 Ma, due to post-glacial weathering promoting rapid primary oxygen production following the Marinoan glaciation (Lau et al., 2017; Sahoo et al., 2012). Tostevin et al. (2019) recorded a global expansion of anoxia in the late Ediacaran. Sulphur and carbon isotope records from South China show an oxidation event 635–511 Ma (McFadden et al., 2008), within widespread anoxic oceans (Canfield et al., 2008; Li et al., 2010; Sperling et al., 2015). Fike et al. (2006) instead found three stages of oxygenation between 635-547 Ma, based on sulphur and carbon isotope records from Oman. Persistent, widespread oxygenation was recorded ~580 Ma (Canfield et al., 2007; Scott et al., 2008), while U isotope records show seafloor anoxia fluctuated in the late Ediacaran (Tostevin et al., 2019; Zhang et al., 2019a; Zhang et al., 2018; Zhang et al., 2019b). The marine chemocline potentially varied in depth alongside the global oxygenation events across the Late Ediacaran (Wood, 2018). Other records show the Ediacaran Period was predominantly ferruginous (Sperling et al., 2015).

Iron speciation records show a transition towards oxic conditions ~580 Ma, thought to be a record of a permanent oxygenation in the deep oceans (Canfield et al., 2007). This was originally interpreted to capture a globally significant step change in oxygenation. However, there is no evidence of oxygenation from similar aged rocks from a different basin (Canfield et al., 2008; Johnston et al., 2013) and no significant trends towards increasing oxidation across the Neoproterozoic and early Palaeozoic (Sperling et al., 2015). Iodine to Calcium ratios (I/Ca; an indicator of how much oxygenated iodine is preserved within a sedimentary record.) are variable but low across the Neoproterozoic and Early Palaeozoic, with peaks at 810-800 Ma and 560 Ma (Hardisty et al., 2017). I/Ca ratios peak between 400 and 350 Ma, then decrease and permanently change around 250 Ma (Lu et al., 2018).

Ultimately, the variation and at times contradictory redox conditions recorded from Ediacaran marine deposits shows a complexity in both Earth's oxygen history and variable interactions of different proxy records to these complex redox conditions. These conflicting discoveries could reveal an issue with stratigraphically correlating contemporaneous Neoproterozoic marine rock records, with these different studies potentially recording regional signals. These spatially separate datasets would have thus recorded redox conditions at depositional regimes at different water depths, with each proxy responding differently due to dissimilar variations of their reduction potentials. Alternatively, there could be a preservation bias towards continental shelf carbonate rocks, or some records could be more impacted by diagenesis and metamorphism that previously thought (Sahoo et al., 2016; Tostevin and Mills, 2020).

What can be said about the Neoproterozoic is that it experienced significant climatic and geochemical changes. Consensus is that while the Ediacaran experienced shifts towards oxygenated waters, there was only a prominent permanent shift in oxygenation in the Devonian (Dahl et al., 2010; Lenton et al., 2016; Lu et al., 2018; Sperling et al., 2015; Stolper and Keller, 2018; Wallace et al., 2017). While the deep Ediacaran oceans experienced widespread anoxia (Tostevin et al., 2019; Zhang et al., 2018), the shallow marine waters in contact with a weakly oxygenated atmosphere could have been consistently oxic. The depth of this zone could be tied with proposed cycles of oxygenation, but likely varied considerably on a regional scale.

2.2 Ediacaran Biota

Against a backdrop of regionally variable and dynamic redox, the earliest animal fossils appear in the Ediacaran Period. The Ediacaran Biota, an informal taxonomic classification, are a suite of diverse fossils preserved between 579 and 539 Ma (Fedonkin et al., 2007a; Narbonne, 2005; Xiao and Laflamme, 2009). Controversially, they have been interpreted to be the first macroscopic multicellular metazoans (Laflamme et al., 2013; Wood and Curtis, 2015; Wood, 2011), post-dating the even more enigmatic Palaeoproterozoic *Grypania spiralis* fossils (Han and Runnegar, 1992; Walter et al., 1976). The morphology of the Ediacaran biota is unique, with multiple morphospecies containing growth shapes, body symmetry and branching structures not seen in post-Cambrian lifeforms (Darroch et al., 2015; Laflamme et al., 2013; Wood and Curtis, 2015). There have been many attempts to resolve the taxonomy of the Ediacaran biota and their relationship to each other and to post-Cambrian organisms (Fedonkin et al., 2007b; Laflamme et al., 2013), however our classification ability is limited due to basing relationships entirely on morphological features (Seilacher, 1984; Seilacher, 1985; Seilacher, 1989; Seilacher, 1992), with each morphological group being effectively unique further complicating taxonomic associations. Regardless, the Ediacaran biota can be grouped into distinct fossil assemblages. These are spatially and temporally separated and are commonly used to subdivide the Ediacaran, as a formal stratigraphic subdivision of the period does not exist yet (Laflamme et al., 2013; Narbonne et al., 2012). The assemblage most relevant here is the Nama Assemblage, which encapsulates the final stages of the Ediacaran and potentially extends into the early Cambrian (Grotzinger et al., 2005; Grotzinger et al., 1995; Narbonne et al., 1997).

2.2.1. Skeletal Fossils

While most of the Ediacaran biota are soft-bodied, the Nama Assemblage includes several well documented skeletal fossils. In the Nama Group, this includes *Cloudina* (Cloud and Drake, 1968; Germs, 1972) and *Namacalathus* (Grotzinger et al., 2000). A third skeletal fossil potentially exists, *Namapoikia* (Wood et al., 2002), although this has been disputed as a microbial structure (Mehra et al., 2020). These shelly fossils are thought to be some of the first skeletal metazoans in the fossil record (Grant, 1990; Hua et al., 2005). These fossils are spatially ubiquitous and have well constrained ages between 538.8 and 538.6 Ma (Linnemann et al., 2019), thus making them potential index fossils for Ediacaran aged rock successions (Hua et al., 2005). As with all Ediacaran biota, no modern-day analogues of these organisms exist, but they are thought to be ancestral clades to Cnidaria, Bilateria, Polychaeta and Bryozoa (See sections *2.2.2. Cloudina* and *2.2.3. Namacalathus*).

These skeletal fossil assemblages typically form as dense cemented aggregates, in some cases forming as monospecific colonies, indicating the organisms lived in multigenerational colonies (Penny et al., 2014; Wood and Curtis, 2015). The fossils of both *Cloudina* and *Namacalathus* are composed of high Mg calcite crystals, or potentially dolomite and aragonite (Germs, 1972; Grotzinger et al., 2000; Knoll, 2003; Porter, 2010; Wood, 2011). Due to the global distribution of these skeletal Ediacaran fossils, Wood and Penny (2018) argued that the synchronous and widespread adoption of skeletons must have had a global trigger, such as a change in ocean chemistry (Wood, 2018). The production of any specialized structure requires energy and resources, creating a metabolic cost. Biological systems will tend to the most energetically favourable pathway, minimizing the metabolic costs (Knoll, 2003). In the case of a skeleton, these structures contain both mineral and structural organic components, with the metabolic cost of acquiring the mineral component being lower than the organic component (Lowenstam and Weiner, 1989). Modern exoskeletal organisms will create shells using the physiologically cheapest materials, acquiring the mineral component of a skeleton by scavenging ions abundant in their surroundings (Bengtson, 2004; Warén et al., 2003; Warren et al., 2014). The Ediacaran oceans had high Mg/Ca ratios, had high alkalinity, and were potentially supersaturated with respect to $CaCO_3$ (Grotzinger and James, 2000a; Porter, 2010; Wood, 2011). It would thus make physiological sense to produce shells from the abundant calcium carbonate.

The sessile nature of these first metazoans could have been a selection factor in favour of skeletonization. A skeleton provides rigidity and stability to an organism, potentially allowing the creation of a mechanical anchoring system, whereby the organism can directly attach or embed into the substrate. The skeletal anchoring system would thus facilitate a more stable and resilient lifestyle, especially towards high energy water currents these early animals would have experienced due to living within tidally influenced shallow waters (Bengtson, 2004). A skeleton also allows the formation of specialised feeding structures, such as filtration chambers, while also allocating more space to store metabolites, which are small molecules that are intermediary or end products of metabolic processes (Taber and Thomas, 1940). A skeleton would thus allow an organism to grow larger, providing a framework to both support the increased mass and the increased metabolic activity (Bengtson, 2004; Seilacher, 1999). The skeleton may also be an adaptive response to early active predation. A physical skeleton would have allowed the formation of anti-predation structures (Knoll, 2003), such as rugged rings found at the aperture of *Cloudina* (Wood, 2011) and evident by many bores found within skeletal Ediacaran fossils (Hua et al., 2005; Wood, 2011). In the presence of motile benthic competition from the soft-bodied Ediacaran biota, a skeleton would have also been a novelty adaptation, allowing multiple species to occupy the same environment by utilising separate ecological niches (Darroch et al., 2015; Laflamme et al., 2013). The exact cause of skeletonization is challenging to isolate, but the potential benefits point to numerous ecological foundations. It was likely triggered by the interplay of carbonate ion enriched waters, microbial substrates providing ecological niches, competition from other substrate dwellers and the emergence of predation (Wood, 2011).

2.2.2. *Cloudina*

The skeletal fossils of *Cloudina* occur as stacked, funnel-like tubes that radiate outward from an apex (Germs, 1972). The stacked nature potentially formed from successive calcite tubes growing within the nadir of the funnel. This growth was episodic, whereby each generation of skeletal growth happened within the older, fully formed funnels (Germs, 1972; Glaessner, 1976; Grant, 1990). The actual skeletal remains are thought to be a support structure for the organism. The soft-bodied portion of the organism would sit a top or within the funnel structure (Grant, 1990). The tubes are composed of high-Mg calcite with dolomite microcrystals in the tube walls (Grant, 1990). *Cloudina* is interpreted to be a polychaete or a cnidarian, based on the mode of skeletal production and reproduction. The method of skeletal production is likened to how polychaeta (bristle worms) generate tubes within the benthic substrate (Hua et al., 2005; Vouelle et al., 1991). New skeletal material was most likely precipitated out of a specialised organ (Hanson, 1948; Hedley, 1958; Nott and Parkes, 1975). This material was then shaped by the living organism and oxidised into calcareous walls (Grant, 1990). The mode of reproduction has been theorised to be asexual budding; whereby "daughter" tubes are grown within the apex of the "parent" tube and eventually split off from the "parent" structure (Cortijo et al., 2015; Germs, 1972; Hua et al., 2005).

2.2.3. *Namacalathus*

Structurally, *Namacalathus* fossils consist of two regions. The upper section consists of a thin-walled stalk or goblet shaped cup containing grooves arranged hexaradially symmetrical within the goblet. The lower section consists of a stem that acts as a holdfast into a substrate (Grotzinger et al., 2000). The stem contains regularly dispersed inflections. The exterior wall of these fossils is continuous. However, the upper cup and lower stem are internally separated by a transverse calcareous wall. High resolution analysis of the skeletal walls reveal they are constructed from foliated, platy calcite and contain an inner layer of dolomite microcrystals (Zhuravlev et al., 2015). Initial analysis pointed to a high Mg calcite minerology (Grotzinger et al., 2000), with high resolution analysis by Zhuravlev et al. (2015) confirming the presence of Mg-bearing dolomite. They are not as globally dispersed as *Cloudina* fossils, they are instead exclusive and widespread within the Nama Group stratigraphy (Grotzinger et al., 2000; Wood et al., 2002). *Namacalathus* is thought to reproduce asexually, namely through internal budding. Daughter organisms would have grown from the stem, attached to exterior cup of the parent. This form of reproduction is supported by observations of *Namacalathus* hosting multiple other individuals across the surface of the cup (Zhuravlev et al., 2015). In terms of classification, *Namacalathus* has been related to many sessile invertebrate phyla. A cnidarian affinity has been suggested based on the radial symmetry of the goblet section (Grotzinger et al., 2000). They have been compared to brachiopods (lamp shells) and bryozoans (moss animals) based on both the microstructure, presence of organic rich inner layers and mode of sexual reproduction via internal, bilateral budding (Zhuravlev et al., 2015). They have also been compared to protozoa (Seilacher et al., 2003) and sessile bilaterians (Wood, 2011).

2.2.4. Palaeoecology

The Ediacaran biota of the Nama Assemblage most likely lived within a shallow-marine shelf environment, above the mean storm wave base, and experienced occasional storms and fluvial interactions (Warren et al., 2014). The highest densities of Ediacaran biota fossils are associated with extensive microbial reefs (Penny et al., 2014; Wood and Curtis, 2015).

The soft-bodied Ediacaran biota were motile sediment grazers that fed around and on top of these calcareous reefs created by microbial communities (more on this later) and created shallow horizontal burrows within surrounding non-carbonate substrates (Laflamme et al., 2013; Wood and Curtis, 2015; Wood, 2011). The skeletal metazoans, such as *Cloudina* and *Namacalathus*, were filter feeders or microcarnivores, feeding on nutrient and microorganism rich waters, transported by currents created by wave interactions, fluvial run-off, and topography (Wood, 2011). These sessile suspension feeders had stable holdfasts, using the hard microbial substrates as attachment sites for stability and the microbial structures as defence against strong water currents (Haris, 1990; Seilacher, 1999). The utilization of microbial structures for defence or stability is evident by the discovery of *in-situ Cloudina* fossils within thrombolites (Wood, 2011; Shore et al., 2020) and the discovery of *Namacalathus* attached to microbial substrates or embedded within the benthic substrate between microbialites or encased within microbialites (Grotzinger, 2000; Penny et al., 2014). These skeletal metazoans most likely occurred in large communities. *Cloudina* fossils have been found attached to each other by an external glue-like structure (Shore et al., 2020). These mutually attached fossils form in large horizontal, branching frameworks that are anchored into the microbial substrate. These framework reefs have been suggested to facilitate the growth of successive metazoan generations and to concentrate resources (Penny et al., 2014; Shore et al., 2020; Wood, 1999; Wood and Curtis, 2015). Large *Namacalathus* aggregates have also been discovered, with the goblets of individuals in mutual contact (Wood, 2011), while some *Namacalathus* individuals have been found attached to *Cloudina* individuals, suggesting mixed communities. Stromatolites and thrombolites within the Nama Assemblage contain multiple layers of mixed skeletal metazoan aggregates, suggesting further that microbialites hosted multiple generations of these early metazoan reefs (Penny et al., 2014; Shore et al., 2020; Wood and Curtis, 2015).

Overall, filter feeding reefs appear to be a common feature throughout the late Ediacaran. This contrasts with the older Avalon and White Sea Assemblages, where the dominant feeding mechanism was osmotrophy; whereby nutrients were acquired though the direct absorption from seawater (Laflamme et al., 2013). Osmotrophic forms are noticeably absent within the Nama Assemblage. This, coupled with the fact that the first skeletal organisms appear within the Nama Assemblage, suggests that significant palaeoecological changes were occurring towards the end of the Ediacaran Period. Coupled with the first occurrence of shallow substrate burrowing trace fossils, the Ediacaran palaeoenvironment was evolving into one more like the Cambrian Period (Darroch et al., 2015; Droser et al., 2017; Hummer et al., 2022). It has been suggested that these ecological changes, metazoan reefs, filter feeding, burrowing metazoans, and the disappearance of osmotrophic metazoans, imply an ecological mass extinction occurred (Amthor et al., 2003; Laflamme et al., 2013). Multiple modes of extinction have been suggested (Laflamme et al., 2013); however, it remains contentious whether the Ediacaran-Cambrian transition and subsequent disappearance of Ediacaran biota truly represents a mass extinction (Darroch et al., 2015; Darroch et al., 2016; Droser and Gehling, 2015; Droser et al., 2017; Liu et al., 2015). What is largely agreed is that rapid ecological changes and replacement of Ediacaran forms by Cambrian biota began with the onset of skeletonization and metazoan reefs in the Ediacaran (Darroch et al., 2015; Droser et al., 2017). One cannot talk about the palaeoecology of this Period without mentioning the relationship with Ediacaran oxygenation (See section *2.1.2. Ediacaran Redox Landscape*).

Oscillations between oxic and anoxic conditions observed throughout the Ediacaran could have exerted strong selection pressures on early metazoans (Wood, 2018). Periods of increased oxygenation would see an increase in diversification and radiation, while periods of anoxia would see extinctions and adaptive resilience (Wood and Erwin, 2018). Thus, redox cycles could have caused the novel forms of the Ediacaran biota. Their decline, however, may have been due to the stabilisation of oxic periods, as more complex metazoans with aerobically mediated traits may have outcompeted the Ediacaran biota (Knoll and Nowak, 2017; Shields, 2017; Zhang and Shields, 2022).

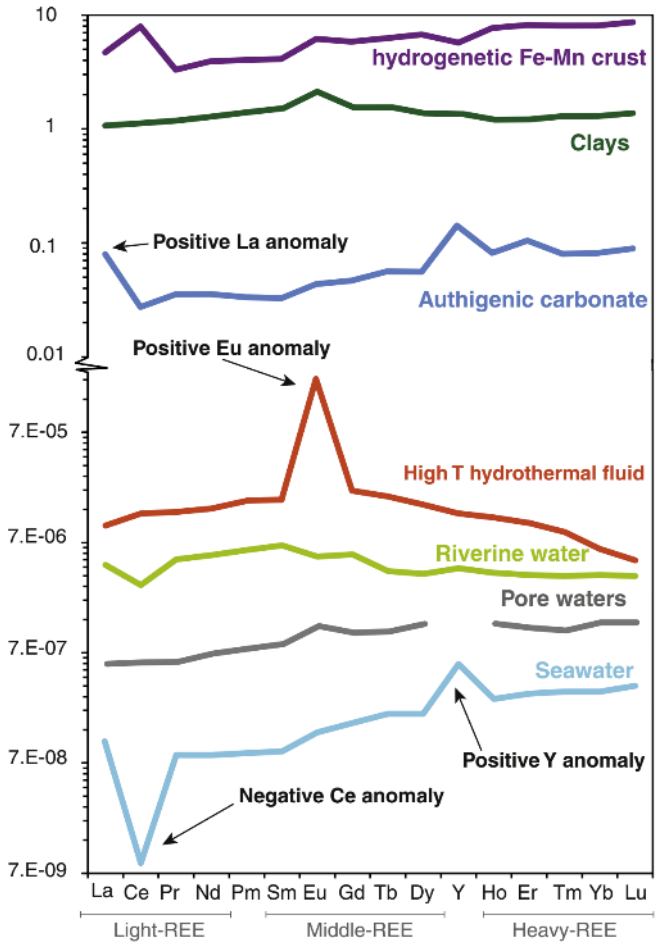

Figure 1*: REE patterns for a range of depositional settings, normalised to PAAS (log_{10}). Based on signal analysis by Tostevin et al., (2016a). Labels at the bottom show the REE subgroupings. Signal attributions: Fe-Mn crust and hydrothermal fluids from Bau and Dulski, (1999); modern seawater from James et al. (1995); pore water from Haley et al. (2005); riverine water from Soyol-Erdene and Huh (2013); authigenic carbonate and clays from Tostevin et al. (2016a).*

2.3. Redox Proxies

To further illuminate the complex interaction between Precambrian oxygenation and the earliest skeletal metazoans, in-depth proxy analysis needs to be performed. Multiple, global scale proxies have been detailed in section *2.1. Oxygen Through Time*, however, a single ecosystem rarely extends over a global scale.

Thus, to get a better understanding of the exact redox conditions associated with these metazoans, an appropriate, high resolution regional to local scale proxy is required. The rare earth elements (REEs), yttrium (Y) and occasionally scandium (Sc) can be used for this purpose. The REEs are a grouping of lanthanide series elements (La-Lu) and Y that share atomic properties. Specifically, these elements experience gradual reductions in ionic radii with increasing atomic number, termed the lanthanide contraction (German and Elderfield, 1990). This results in coherent chemical behaviours across the series, but differing mass dependent complexation behaviours. REEs have been used for decades as geochemical proxies for past ocean chemistry, making them suitable for shallow marine Precambrian redox studies (Corkeron et al., 2012; Hickman-Lewis et al., 2020; Liu et al., 2021; Planavsky et al., 2010). In seawater, REEs are sourced from riverine run-off, terrigenous dust, and hydrothermal fluids (Elderfield, 1988; Elderfield and Greaves, 1981), and removed by elemental scavenging processes related to changes in salinity, water depth and oxygen levels (Frimmel, 2009; Webb and Kamber, 2011).

The controls on seawater REE patterns are thought to be conservative across a range of marine environments and through geological time (Bolhar and Van Kranendonk, 2007; Shields and Webb, 2004). The implication is that REE patterns in marine environments, regardless of geographic distribution and geological age, will share some similar features. If the REE pattern shows a seawater signal, one can expect elevations in La, Gd and Y, uniform light REE (LREE) depletion and the enrichment of heavy REE (HREE) (**Figure 1**; Derry and Jacobsen, 1990; Frimmel, 2009; Nozaki and Zhang, 1995).

Investigating palaeomarine conditions using REE patterns still requires a suitable proxy archive that records marine REE patterns. Decades of study have shown marine chemical sedimentary rocks to be robust archives, capable of retaining the primary geochemical signal of the waters they precipitated from (Bekker et al., 2014; Dumoulin et al., 2011; Kamber et al., 2004; Nothdurft et al., 2004; Webb and Kamber, 2000, Tostevin et al., 2016). More specifically, pure marine calcium carbonate rocks (limestone) have been shown to be ideal, because REEs readily substitute for Ca ions within the calcite crystal structure with little fractionation (Elderfield and Greaves, 1981). This means marine calcite should record the primary chemical conditions from the seawater they formed within (Frimmel, 2009). The ability of REEs to remain within marine carbonates have indeed been demonstratably proven to be robust against diagenesis and dolomitization (Banner et al., 1988; Nothdrurft et al., 2004), weathering processes that lead to dramatic chemical changes in calcite. Thus, the primary seawater REE patterns recorded in marine limestones are excellent geochemical archives (Bolhar et al., 2004; Bolhar and Van Kranendonk, 2007; Byrne and Kim, 1990; German and Elderfield, 1990; Nothdurft et al., 2004). Coupled with the fact these REE signals have been shown to be resilient over million-year timescales (Kamber and Webb, 2001; Komiya et al., 2008; Yamamoto and Isozaki, 2013), one can compare modern and ancient REE signals from the respectively aged marine limestones, allowing the reconstruction of palaeomarine redox conditions.

2.3.1. Cerium Anomaly

There are multiple different geochemical signals recorded by REEs, but the cerium (Ce) anomaly is of particular interest. While the majority of REE reside in the water-soluble 3+ valence state (REE^{3+}), Ce is unique. Under oxic conditions, Ce is oxidised to a tetravalent form (Ce^{4+}), (Elderfield, 1988; Elderfield and Greaves, 1981). Ce^{4+} ions are highly insoluble in seawater and readily adsorb onto Mn-oxides and hydroxides (Tachikawa et al., 1999). The implication is that sufficiently oxygenated seawater will produce Ce^{4+}, which will then sorb onto Mn-oxides or hydroxides and be deposited into marine sediments (Elderfield and Greaves, 1981). This leaves oxygenated seawater depleted in Ce relative to other REE^{3+}, while Mn-oxides and hydroxides would be relatively enriched in Ce (Bau, 1999). If the Ce concentration is normalized against the rest of the REE series, one can gauge the extent of oxidation that has occurred within the water column, termed a Ce anomaly (Ce/Ce*; German and Elderfield, 1990). When a seawater sample Ce anomaly is negative, it indicates oxic conditions under neutral to alkaline pH (Elderfield and Sholkovitz, 1987), while positive Ce anomalies potentially indicate suboxic to anoxic conditions, or inclusion of REE from contaminant Mn oxide and hydroxide particles (Elderfield and Pagett, 1986; Grandjean and Albarède, 1989; Grandjean et al., 1987; Liu et al., 1988; Liu and Schmitt, 1984; Wang et al., 1986; Wright et al., 1987). Ce anomalies have been shown to be highly responsive, recording variations at a metre scale (De Carlo and Green, 2002), and the magnitude of the anomaly has been shown to relate to both the concentration of oxygen and the thickness of an oxic layer (O'Connell et al., 2020).

This potentially makes them ideal recorders of local oxic conditions; however, it should be noted that slow kinetic effects may lead to the overprinting of a local Ce anomaly signal by the signal across a whole basin (Wallace et al., 2017), which is something to consider when interpreting seemingly local redox conditions.

Recall the ability of marine calcite to record the seawater's REE concentrations. If these marine rocks formed in waters that experienced significant oxygenation, they will theoretically record a negative Ce anomaly that represents the integrated redox signal from the water column (German and Elderfield, 1990). This would make the Ce anomaly an indirect indicator of marine oxic conditions. Alternatively, sampling of sediments containing Mn-oxides and hydroxides from the same environment should produce positive Ce anomalies, as these minerals concentrate the Ce ions removed from the ocean system and would indicate oxygen mediated fractionation occurred elsewhere in the environment. This does outline a lithological constraint on sampling marine carbonates for Ce. If the analysed material, be it bulk rock or in-situ sampling, contains Mn nodules, the positive Ce anomaly can be integrated with the primary seawater signal from the calcite, and interfere destructively. Regardless, the Ce anomaly has been successfully used throughout the last decade.

Archean marine carbonates record Ce anomalies close to 1, agreeing with our understanding that Archean oceans were anoxic (Kamber and Webb, 2001; Van Kranendonk et al., 2003). Ling et al. (2013) showed increasing oxidation in shallow marine oceans during the late Ediacaran from southern Chinese carbonates, again in agreement with increases to modern day oxygen level towards the Cambrian. Tostevin et al. (2016) showed mostly positive Ce anomalies for similar aged rocks from southern Africa, indicating oxygen mediated fractionation occurred somewhere within the depositional environment. Wallace et al. (2017) showed there was widespread oxygenation across the Late Palaeozoic-Mesozoic, corroborated by Fe speciation, $Fe^{3+}/\sum Fe$ ratio and I/Ca ratio values (Kunzmann et al., 2017; Sperling et al., 2017; Stolper and Keller, 2018; Lu et al., 2018). More recently, Zhang and Shields (2022) compiled a database showing Ce anomaly variations throughout the Precambrian, with Archean marine carbonates typically recording Ce anomalies between 0.8-1.2. Variations in Ce anomalies at localised scales have been attributed to regional environmental changes, such as sea-level fluctuations altering the depth at which carbonates form across the shelf, basin restrictions, which will alter water circulation and oxygen aeration and more importantly changes in the oxygen content of the shallow oceans and atmosphere (Ling et al., 2013). Utilising Ce anomalies could thus further detail or explain the heterogeneity of the Late Neoproterozoic oceans with respect to oxygenation, as outlined in section *2.1.2. Ediacaran Redox Landscape*.

2.4. Microbialites

Microbially induced carbonates, or microbialites, are considered reliable archives for recording primary marine REE signals throughout geological history (Kamber and Webb, 2001), from the Archean through to the recent Holocene (Hickman-Lewis et al., 2020; Kamber et al., 2004; Kamber and Webb, 2001; Nothdurft et al., 2004; Olivier and Boyet, 2006; Wilmeth et al., 2019).
Coupled with the fact that extensive microbialite reefs have been associated with and hosted the earliest known metazoan ecosystems in the Ediacaran (Penny et al., 2014; Wood, 2017; Wood and Curtis, 2015), the analysis of these Ediacaran microbialites could be beneficial for multiple reasons. But what are they?

2.4.1. Microbialite Formation

Microbialites are thought to form through the *in-situ* precipitation of minerals within and around microbial mats as well as detrital agglutination (Riding, 2011a). However, of all the potential minerals a microbialite could be made of, carbonate minerals are the most commonly observed, and specifically calcite. The precipitation of *in-situ* calcite is based on a series of microbial metabolic processes. However, the specific chemical reactions are not fully understood for even modern microbialites (Kamennaya et al., 2012). A potential scenario for the *in-situ* precipitation of calcite takes into consideration the products and effects of oxygenic photosynthesis and anaerobic decomposition within the microbial mat. The breakdown of H_2O during photosynthesis releases hydroxide anions (OH^-) into the surrounding extracellular polymeric substance (EPS). These ions react with carbon dioxide dissolved in the water to form bicarbonate ions (HCO^{3-}), which will further react with more liberated hydroxide to form carbonate ions (CO_3^{2-}). Simultaneously, dead microbes and EPS are decomposed constantly, leading to the liberation of Ca^{2+} and Mg^{2+} (Weiner and Dove, 2003). The newly formed carbonate ions readily react with these free cations of Ca^{2+} and Mg^{2+}, and potentially with cations released during unrelated seawater chemical reactions, leading to the spontaneous precipitation of calcite within the EPS of the active microbial surface (Kawaguchi and Decho, 2002).

The sediment accumulation mechanism is a process of entrapment and subsequent lithification of terrigenous particles as they pass over the living microbialites, entrained in the surrounding water. The EPS readily binds small particles through weak electrostatic forces. Overtime, the capture of suspended sediment will mask the living microbes, leading to them shifting above and over these detrital layers, forever incorporating them into the structure (Burne and Moore, 1987; Kennard and James, 1986). Regardless of formative mechanism, the calcification, and lithification of successive microbial growths and detrital accumulation will preserve buried microbial mats, leading to the creation of various structures at different scales.

2.4.2. Classification

There are four accepted structural classifications of microbialites: stromatolites, thrombolites, leiolites and dendrolites. These are not mutually exclusive classifications, and we could add a fifth group, composite microbialites. Microbially induced sedimentary structures (MISS) are like microbialites but are primarily formed from siliciclastic material with unique structures and thus are not true microbialites (Grey and Awramik, 2020). Stromatolites are microbialites with clearly defined microbial laminations (Awramik and Margulis, 1974), They are created by filamentous microbe colonies. A stromatolite is typically composed of multiple successions of laminations with interbeds of detrital material that contain little or no microbial matter (Kennard and James, 1986). Thrombolites differ from stromatolites in that they are composed of clotted or clustered coccoid-shaped microbial structures, termed mesoclots, that form as bushy aggregations with complex internal fabrics (Shapiro, 2000). These mesoclots are thought to be the remains of coccoidal bacterial cells that have been calcified due to the *in-situ* precipitation of calcium carbonate (Gabelein, 1974; Kennard and James, 1986; Monty, 1976). The original microbial community are thought either to have formed as separate colonies that grew into each other or as coccoid forming bacteria that radiated outward (Kennard and James, 1986). Dendrolites are microbialites composed of branching, dendritic microbial structures called shrubs. These shrubs lack laminations or mesoclots (Grey and Awramik, 2020).

Microbialites that lack mesoclots, laminations or shrubs are classified as leiolites (Grey and Awramik, 2020). Leiolites typically contain mottled, irregular, patchy, or massive microbialite textures with no distinct structure (Aitken, 1967; Kennard and James, 1986). Due to their regularity and adherence with lateral succession, stromatolites have been ideally used for palaeoredox and environmental analysis. The layering makes determining or approximating growth direction easier. An aspect of microbialite studies that should be noted is the taxonomic classification of microbialites. Studies attempt to make these classifications based on morphological constraints, by seeing if a distinct microfossil morphology is unique to a time-restricted stromatolite structure (Awramik, 1991). These classifications are diverse, with branched columnar stromatolites being associated with *Conicodomenia*, *Conophyton*, *Anabaria* and *Baicalia* microbial genera (Cao, 2003; Semikhatov and Raaben, 2000). The assignment of genera and species for microbialites seems to thus be indirect morpho-species classifications. Consequently, controversy has arisen as microbialites are diverse communities of innumerable microbes, with microbialite morphology being influenced by the internal biology and interactions of these complex communities as well as the external environment (Shapiro and Wilmeth, 2020)

2.4.3. Research History

The study of microbialites has an ambiguous and contentious history. Many classification schemes have been developed to define microbialites and describe their various morphologies (Aitken, 1967; Kennard and James, 1986; Riding, 2011b). However, their classification is marred by inconsistency, with the community struggling to even agree on the definition of a microbialite. Finding the original sources for key information is challenging (Grey and Awramik, 2020). This is compounded by the fact that the bio-metabolism and environmental physio-chemical conditions that control microbialite growth are inherently complex (Arenas et al., 2017; Grotzinger and Knoll, 1999; Hoffman, 1973; Riding, 2011a; Semikhatov et al., 1979; Serebryakov, 1976) and there seems to be a skew in research towards stromatolites and thrombolites (Grey and Awramik, 2020). Controversy also exists with regards to the chemical processes that result in microbialite formation. The extent of agglutination vs microbial precipitation, or even discriminating between these constituents, is still challenging, especially for fine-grained ancient microbialites that would have experienced grain recrystallisation (Corkeron et al., 2012). With regards to mineral precipitation, there is even a continuum between microbial and inorganic formative processes (Burne and Moore, 1987; Grotzinger, 1990; Hoffman, 1973; Riding, 2011a). Additional controlling factors include the pH and alkalinity of the water, the speed of water currents and the space available for microbial growth (Grotzinger and Knoll, 1999; Sumner and Grotzinger, 1996; Webb and Kamber, 2011).

The morphological diversity of microbialites has changed over Earth's geological history. Archean microbialites tend to form as simple planar or shallow domical stromatolites (Awramik, 1971; Awramik, 1991; Awramik, 1992). Microbialite forms, and in particular stromatolites, begin to show an increase in diversity in the Early Proterozoic. Awramik (1991) speculated this was a consequence of cyanobacterial adaptive radiation with the onset of the GOE: It could thus be extrapolated that the oxygenation of the atmosphere associated with the GOE could have been pivotal in the evolution and spread of cyanobacteria and affected microbial morphologies thereafter.
The ability to cope under low oxygen levels, and indeed produce their own oxygen, could have allowed for the rapid dispersal and extensive colonisation of low oxygen shallow marine environments.

These adaptations could have allowed for the formation of novel microbial mat configurations, mechanisms resulting in more efficient sediment accretion, or the more effective formation of EPS fabrics (Awramik, 1991). Stromatolites dominated the Proterozoic (Awramik, 1971; Awramik, 1991; Awramik and Semikhatov, 1979).

While thrombolites and oncoids are common, the shear diversity of conical, columnar, branched and stratiform composite reefs are most apparent and possibly exclusive to the Proterozoic (Awramik, 1971; Cloud and Semikhatov, 1969; Grotzinger and James, 2000a; Grotzinger and James, 2000b; Pierson et al., 1992; Raaben, 1969; Raaben et al., 2001; Semikhatov and Raaben, 2000). Modern stromatolites are rarely found as columns or even branched forms, and are usually found in fringe locations, regions with high solute concentrations that are unconducive for habitation by other lifeforms (Arenas et al., 2017; Logan, 1961; Louyakis et al., 2017; Reid and Browne, 1991; Webb and Kamber, 2000). It was only leading up to the Ediacaran-Cambrian transition that the distribution and morphological diversity of microbialites begin to decrease (Awramik, 1971; Awramik, 1991; Monty, 1976; Walter and Heys, 1985).

It has been suggested that the inception of motile metazoans, and with them the rise of substrate burrows and bioturbation, destroyed microbial structures and disrupted the benthic substrate. Essentially, newly evolved animal forms outcompeted and likely fed upon the reef building microbes during the Ediacaran-Cambrian transition, leading to the relegation of microbialites to fringe environments uninhabited by substrate burrowers in the Phanerozoic (Grotzinger and James, 2000b; Riding, 2008; Penny et al., 2014; Wood and Curtis, 2015; Grey and Awramik, 2020; Shore et al., 2020; Shapiro and Wilmeth, 2020). Accompanying these biological turnovers are changes in the hydrodynamics, changes in the calcite saturation conditions of the oceans and competition of resources by more efficient planktonic algae (Grotzinger, 2000; Grotzinger and Knoll, 1999; Riding, 2006; Sanchez-Baracaldo, 2015). For example, stratiform stromatolites began to disappear leading into the Cambrian across Ediacaran-Cambrian deposits in China (Li et al., 2022). Additionally, Ediacaran thrombolites were composed of thin to moderately bedded mesoclots with thin stromatolitic sheet interbeds. Cambrian thrombolites, however, were made of larger mound shaped thrombolite aggregates that contained fanlike and dendrolitic columns (Li et al., 2022). These unlaminated columns also contained prominent calcified microbial and fossiliferous assemblages, features rare or completely absent from Ediacaran microbialites (Furuyama et al., 2013; Gandin and Debrenne, 2010; James and Gravestock, 1990; Rowland and Shapiro, 2002; Zhuravlev et al., 2015). Overall, there was a notable predominance of diverse stromatolitic forms across the Precambrian, with thrombolites becoming more prevalent post-Cambrian, until microbialites were relegated to specific, isolated environments largely uninhabited by ecosystem engineers and substrate burrowers (Grey and Awramik, 2020; Grotzinger and James, 2000b; Riding, 2008; Shapiro and Wilmeth, 2020).

2.4.4. REE Proxy Potential

With regards to using ancient microbialites as REE proxies, they have already been proven to be some of the most informative records of early Earth (Hofmann et al., 1999; Lowe, 1980; Walter et al., 1980). They are records of the first lifeforms, and the first ecosystems, and are found in some of the oldest sedimentary rocks on Earth. More exceptionally, they could be the target organism in the search for extra-planetary life (Barbieri and Cavalazzi, 2004; Cady et al., 2003; Gibson Jr et al., 2001).

They have proven to be critical paleoenvironmental indicators and can provide information about palaeoclimates (Abell et al., 1982; Serebryakov et al., 1972; Solari et al., 2010; Whalen et al., 2002). One issue with carbonate rocks, in general, is that primary signals can be overprinted by diagenesis. However, microbialites have been found to retain primary signals, regardless of diagenetic alteration (Webb and Kamber, 2011). Perceived diagenetic alterations may instead have been due to the input of non-marine REE enriched fluids (Nothdurft et al., 2004). Microbialites also incorporate higher levels of marine REE into the mineral compared to skeletal carbonate rocks. Precambrian microbialites record similar seawater REE signals to modern microbialites (Johannesson et al., 2014; Nothdurft et al., 2004; Scherer and Seitz, 1980; Shaw and Wasserburg, 1985). Due to the laminated, successive structure of stromatolites, their chemistry has been extensively studied to determine how these early photosynthetic bacteria interacted with the Precambrian oceans. They have long been theorized to be so called "oxygen oases" for the early suboxic to anoxic oceans (Fischer, 1965; Herman and Kump, 2005; Lalonde and Konhauser, 2015; Sumner et al., 2015; Wilmeth et al., 2019). Therefore, REE analysis of microbialites deposited around the Ediacaran-Cambrian boundary could record the geochemical history of this pivotal time in Earth history.

3. Project Goal

3.1. Aims

The overall goal of this project is to shed light on microscale differences between microbialites and constrain their influence on local redox conditions. The study will form a launch pad for detailed, microbialite focussed palaeoredox throughout the geological record.

3.2. Research Questions

1. *Can we extract reliable REE signals from ancient microbialites?*

2. *Were these microbialites centres of oxygenation in an otherwise low oxygen ocean?*

3. *Do these signals correlate with conditions found within contemporaneous Nama Group deposits based on bulk rock analysis?*

4. *Are there notable spatiotemporal variations in the macroscale morphologies, microscale fabrics and REE patterns across previously unstudied South African Nama Group microbialites?*

5. *Can an ecological relationship be established between the formative microbes of the microbialites and their environment?*

6. *What was the provenance of the carbonate within the stromatolites? Did the formative microbial mats scavenge carbonate sediments from the water column or was carbonate precipitated in situ? Is there a correlation between the carbonate provenance and different microbial fabrics?*

4. Regional Geology

4.1. Geological History

The Nama Group largely consists of marine siliciclastic and limestone rocks deposited during the latest Ediacaran to early Cambrian periods. The group is located across southern Namibia, with outcrops in northern South Africa (**Figure 2A**). The rocks of the Nama Group were deposited in the Nama Basin, a late Ediacaran foreland basin on the western edge of the Kalahari craton. The basin formed due to continental flexure across the Kalahari craton, resulting from the collision of the Damara mobile belt to the north and the Gariep mobile belt to the west (Germs and Gresse, 1991; Germs, 1974, 1995; Germs et al., 1986). This is one of many foreland basins that formed due to the larger Pan-African Orogenesis that occurred between 680–580 Ma (Germs, 1974). A peripheral bulge formed across the Nama basin during orogenesis, trending east-west. This ancient geographical high is known as the Osis arch, and it divided the Nama basin into the Zaris Basin in the north and the Witputs Basin in the south (**Figure 2A**). Both basins experienced closely related but independent geological histories, evident by the differing lithologies and structures across the basins (Germs and Gresse, 1991; Germs, 1995; Germs et al., 1986). The Nama Group was deposited in shallow marine, deltaic and fluvial depositional environments bordering shallow westerly deepening ancient waterbodies; the Adamastor Ocean and later the Khomas Sea (Hartnady et al., 1985; Stanistreet et al., 1991). This stable shallow marine region formed a stable continental shelf, which lead to the formation of an extensive carbonate ramp. This ramp was dominated by microbial communities, which eventually formed large microbial pinnacle reefs along the edge of the continental shelf (Wood and Curtis, 2015). Flexure of the continental crust under the Nama basin eventually led to subsidence across the carbonate ramp, causing marine transgression and drowning of the shallow marine environment. This transgression was the final result of orogenesis across the region (Geyer, 2005).

4.2. Regional Stratigraphy

The stratigraphy of the Nama group has gone through many iterations (Blanco et al., 2011; Bowyer et al., 2020; Germs, 1974, 1995; Nelson et al., 2022; Saylor et al., 1995), making a unified stratigraphy challenging. This is ultimately due to the Nama Group being exposed in multiple spatially isolated subdivisions across Namibia and South Africa (Germs and Gresse, 1991). The Nama Group can be subdivided into three main subgroups, consistent across all subbasins. The oldest divisions are the Ediacaran aged Kuibis Subgroup. The Schwarzrand Subgroup was deposited during the latest Ediacaran Period, potentially extending into to the earliest Cambrian Period. The Nama Group is capped by the early Cambrian Fish River Subgroup, which unconformably overlies the Schwarzrand Subgroup (**Figure 2;** Germs, 1974). The Kuibis Subgroup contains coarse quarzitic and feldspathetic sandstones, micritic limestones and thick siltstone beds. The depositional environment was a shallow marine sea on the stable continental shelf. The Schwarzrand Subgroup consists of clastic sandstones, micritic limestones, siltstones as well as conglomerate beds. The Subgroup was deposited in a transition zone between the distal section of a fluvial delta and the deeper offshore marine plane. The deposition is marked by periods of uplift, glaciation, and high volcanic activity. The Fish River Subgroup consists of conglomerates, sandstones, and shales that were deposited within a fluvial river system (Germs and Gresse, 1991; Germs, 1974, 1995; Saylor et al., 1995).

5. Study Site

5.1. Local Stratigraphy

The study site is located on the Neint Nababeep Plateau along the Orange River, Northern Cape, South Africa (**Figure 2A** & **Figure 2C**; Almond, 2009; Nelson et al., 2022). The plateau is contained within the Vioolsdrif subbasin. The Vioolsdrif subbasin is either a subdivision of the Witputs basin (Germs and Gresse, 1991) or merely a distal southern extension of the Witputs subbasin (Germs et al., 2009). Regardless, The Neint Nababeep Plateau contains rocks of the Kuibis and Schwarzrand Subgroups (Germs, 1974; Germs and Gresse, 1991; Almond, 2009; Nelson et al., 2022). The Kuibis Subgroup is subdivided into the Dabis and Zaris Formations (**Figure 2B**). However, the Dabis Formation is not present across the Neint Nababeep Plateau. Refer to **Figure 2** for a stratigraphic map of the region.

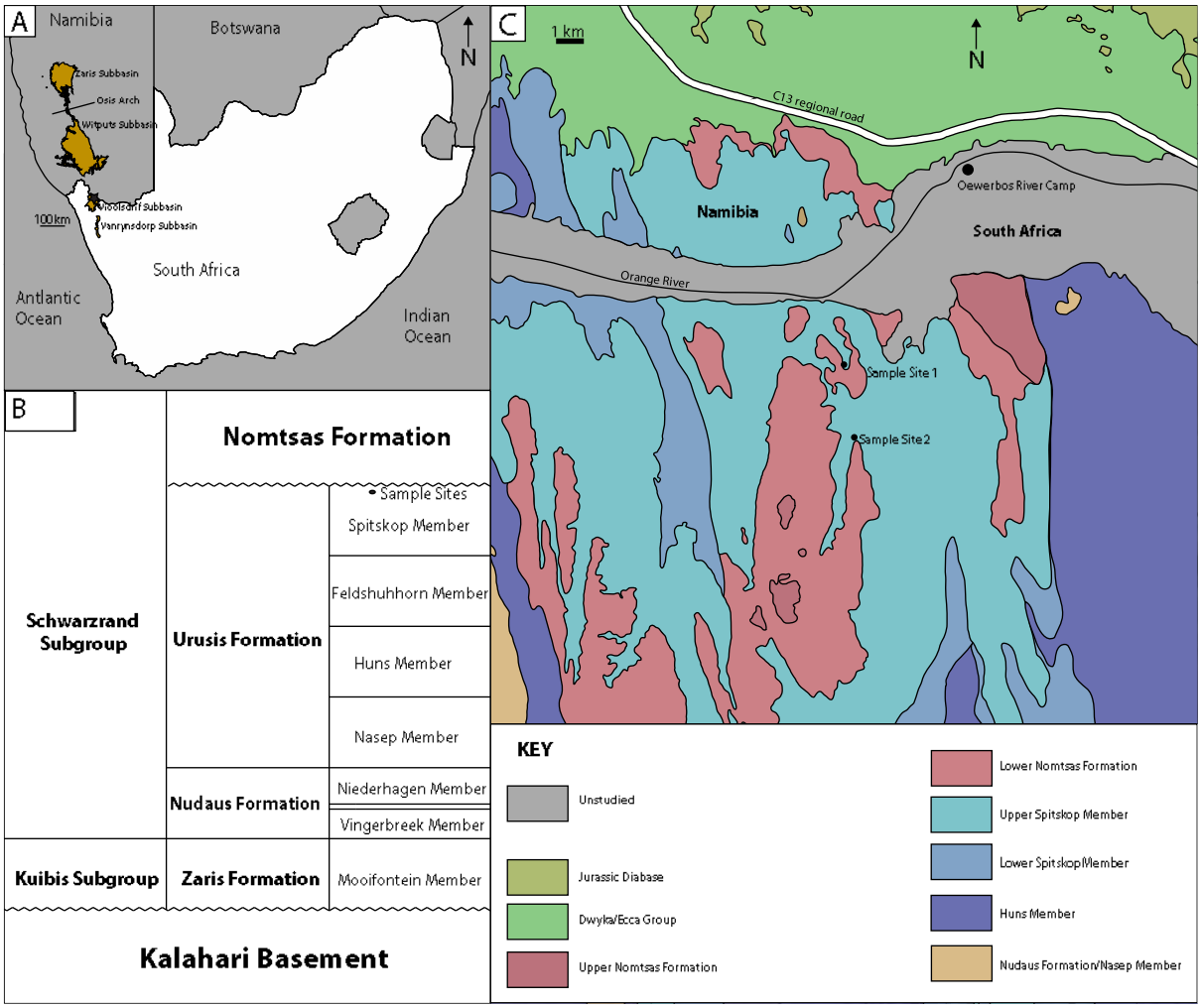

Figure 2: *A) Geographic location of the study site, indicated as a black star, with respect to the Nama Subbasins. B) Simplified stratigraphy of the Neint-Nababeep Plateau, with the study site marked with a black dot. C) Regional geology of the Neint-Nababeep Plateau and the rocks that outcrop across it, with the study sites marked as black dots. Based on geological maps by Almond (2009) and Nelson et al. (2022)*

The oldest identified stratigraphy within the Neint Nababeep plateau is the Mooifontein Member of the Zaris Formation. The Mooifontein is a fossiliferous limestone unit with thin *Cloudina* and *Namacalathus* bearing beds. The Member is composed of thin, micritic limestone beds and calcarenites.

Clast-supported conglomerates occur, with silts, sands, ooids and skeletal fragments making up the clast composition (Saylor et al., 1995). Overlying the Mooifontein Formation is the Nudaus Formation of the Schwarzrand Subgroup, which contains the Niederhagen and Vingerbreek members. The Niederhagen Member consists of thinly bedded, medium-grained sandstones (Saylor et al., 1995). The Vingerbreek Member contains grey, rippled mudstones with thick tabular sandstone units. Hummocky cross-bedded sandstones and siltstones also occur within the member. Grooved and striated bed bottom structures across the Member indicate a major disconformity, potentially created by glaciers scouring channels into the original beds (Saylor et al., 1993; Germs, 1995). Overlying the Nudaus is the Urusis Formation, which includes the Nasep, Huns, Feldshuhhorn and Spitskop members. The Nasep contains thick, massive to cross-bedded medium sandstone beds overlain by hummocky cross-bedded sandstones, siltstones, calcarenites. The member is capped by thick cross-bedded sandstone beds (Saylor et al., 1995). The Huns Member consists of thick, cross-bedded limestones that weather into characteristically dark blue or grey cliffs (Almond, 2009; Nelson et al., 2022). These limestones contain coarse clast bearing conglomerates along with ooids and *Cloudina* fragments (Saylor et al., 1995, Nelson et al., 2022). Thin siltstones containing laminated fine sandstones and cross-stratified limestones occur, which have been interpreted as flooding surfaces (Nelson et al., 2022).

Microbial limestones have been identified in the older beds of the Huns Member (Saylor et al., 1995; Nelson et al., 2022). The Feldshuhhorn Member consists of siltstones with tabular sandstone beds that grade into micaceous tangentially cross-bedded sandstone with channelized beds (Saylor et al., 1995; Nelson et al., 2022). The Spitskop Member contains thin-bedded calcite bearing siltstones and dark oolitic limestone beds (Saylor et al., 1995) that grade into coarser micaceous sandstones (Nelson et al., 2022). The most characteristic feature of the Spitskop Member are the extensive microbialite pinnacle reefs that form at the top of the Member. These microbialites range from columnar stromatolite mounds, large domes, and conical stromatolites containing thrombolitic cores (Nelson et al., 2022). Overlying the microbialite reefs of the Urusis Formation are sandstones containing manganese rich horizons, and silty limestones of the Nomtsas Formation. This Formation additionally contains brecciated channels that incise into the lower Urusis Formation. These channels consist of clast and matrix supported breccias, marine siltstones and diamictites (Saylor et al., 1993; Nelson et al., 2022).

5.2. Sample Acquisition

The microbialite samples in this thesis came from two regions in the Neint Nababeep Plateau. Both these locations contained laterally extensive microbialite beds, coinciding with the boundary between the Spitskop Member and the lower Nomtsas Formation. The microbialite samples were collected during a five-day fieldtrip to the Neint Nababeep Plateau, from the 11th to the 15th of May 2021. Sample locations were marked with a handheld GPS. Samples with representative features were selected that appeared to be in situ, well preserved and the right way up. The rock samples varied in size, from ~4 cm wide and ~3 cm thick sections to large ~10 cm wide and ~30c m long cones. Preference was given to rock samples that were near or clearly contained columnar microbialite features.

6. Microbialite Analysis

6.1. Sample Processing

Microbialite samples were cut in half with a circular saw to reveal a cross-section through the centre of the microbial dome with fresh surfaces. A few samples were too large for cutting with UCT's Department of Geological Science's in-house saws. Cutting of these larger microbialites was performed externally, at the University of the Western Cape's (UWC) Department of Earth Science. The UWC sample preparation lab uses 40 cm radius saw blades to accommodate larger rock samples. The blade is connected to a custom two-stroke engine to provide sufficient power to the blade, and the blade is lowered onto the rock, allowing more control and stability. Cut segments of each rock were then selected for polishing. Polishing was performed with a handheld variable speed orbital sander fitted with diamond polishing pads, whereby a novel polishing technique was developed for future in-house research (See section *10.3. Appendix 3: Rock Polishing Technique*). High-resolution photographs were then taken in a dark room for a digital record and for descriptive analysis. Samples were then selected for thin section creation at UCT's Department of Geological Sciences and analysed using a Zeiss Scope.A1 imaging microscope under polarising light. Images were taken with an Axiocam attached to the objective lens and exported to a computer to be processed using Zen 2 Lite. Ore mounts were then created to perform higher resolution microstructural analysis, using a backscatter scanning electron microscope (B-SEM) configuration (See B-SEM images in section *10.1. Appendix 1: B-SEM Images*) on a Tescan MIRA SEM from UCT's Department of Chemical Engineering. Boundaries between the microbial material and the intercolumn sediment as well as novel features were targeted for both thin section and mount creation. Overall, 9 polished slabs, 14 thin sections and 8 mounts were created to perform petrographic analysis.

6.2. Petrographic Analysis

The description of the characteristics of the samples was performed using the terminologies and standardised systematic analysis outlined by Grey and Awramik (2020). Microbialite analysis can be divided into different scales of analysis. The most important divisions for this study are between features visible with the naked eye, which informs us about environmental conditions, and features resolved with the aid of microscopes, which informs as about the origin and biogenicity of the microbialites (**Table 1**; Grey and Awramik, 2020). The macroscale analysis involves field observations across the outcrop (meters to tens of meters). The mesoscale refers to features seen across each polished rock sample (mm to dm scale). Finally, the microscale refers to features below 0.01 mm, resolved under microscopic view.

There are some constraints on the petrographic analysis of these rock samples. The first constraint is on quantitative metrics, as i) we lack plan view sections of the columns to gain a full three-dimensional understanding of the samples and ii) the material preserved in these sections may not initiate or terminate within the sample, so we only have snap shots of the full structure. The other constraint is in both defining a lamina and distinguishing between individual laminae. The classic definition of a lamina is a "~10 mm rock layer of similar texture, distinct from under and overlain rock layers by sharp boundaries or gradual changes in colour or texture" (Walter, 1972).

An alternative description for composite laminae is, a “grouping of multiple single laminae with distinct colour, textures and thickness that differ from other simple or composite laminae” (Arenas et al., 2017; Mercedes-Martín et al., 2014). However, many of the successions in these microbialites are very fine, bordering on microscopic, making these demarcations unclear. This ultimately makes determining the thickness of laminae, the boundaries between individual lamina, and even detecting individual lamina, highly subjective. With these limitations in mind, only the clearly discernible features of a microbialite have been listed and described (**Table 2**).

6.3. Morphology

6.3.1. Macroscale

Site 1 was a locality nicknamed the “onions” (**Figure 2C**). The microbialites from this region formed at the top of the Spitskop Formation as a laterally extensive biostrome or reef that crops out over a 100-meter-wide area (**Figure 3A**). The reef outcrop is located five metres below thick beds of reddish limestone containing manganese nodules and no other microbial features (**Figure 3B**). The outcrop size varied, and the tallest section of microbial build up was 5 metres. The reef is composed of tightly packed, nested domical stromatolites of varying dimensions. Stereotypical karstic weathering exposed the interior plan view. Dome dimensions varied between two size ranges, from 10–30 cm and from 1–4 m in diameter, with the layers of adjacent domes merging in places. Segmental domes grew asymmetrically over larger hemispherical domes, and some of the largest domes contained multiple smaller domes within (**Figure 3C**). Each dome was composed of predominantly stratiform microbial layers that gently bulged towards an apex. However, weathered surfaces perpendicular to the lamination plane showed columnar and simply branched stromatolite structures.

Each of the rock samples presented in this study came from these columnar sections. It is likely that these columns formed as laterally extensive parallel ridges instead of isolated cylindrical columns (Tosti and Riding, 2017a). Weathering exposed the cores of these domes, revealing significantly branched and linked columnar stromatolites. Field analysis on columnar and branched stromatolites revealed distinctly harmonized laminated internal structures (i.e., laminae of similar composition and at the same depositional height from separate but parallel columns; see **Table 1**). The microbial material seen across this site were all layered, and thus stromatolitic (**Figure 3D**).

Site 2, nicknamed the “poofies”, had a different macroscale layout (**Figure 2C**). Microbialites formed as funnels, ~30 cm deep and ~10 cm wide at the top, constrained by the surrounding sediment or neighbouring microbialite funnels. These microbial structures were unlaminated thrombolites and branched dendrolites. These sites were less than 2 Km apart and occurred at the same boundary, yet both the macroscale and mesoscale morphologies varied considerably. As this study set out to analyse the nature of the columnar microbialites found at the cores of the stromatolitic domes, these unlaminated microbialites were not studied further. This does however outline a clear lateral microbialite growth heterogeneity for the Neint-Nababeep Plateau.

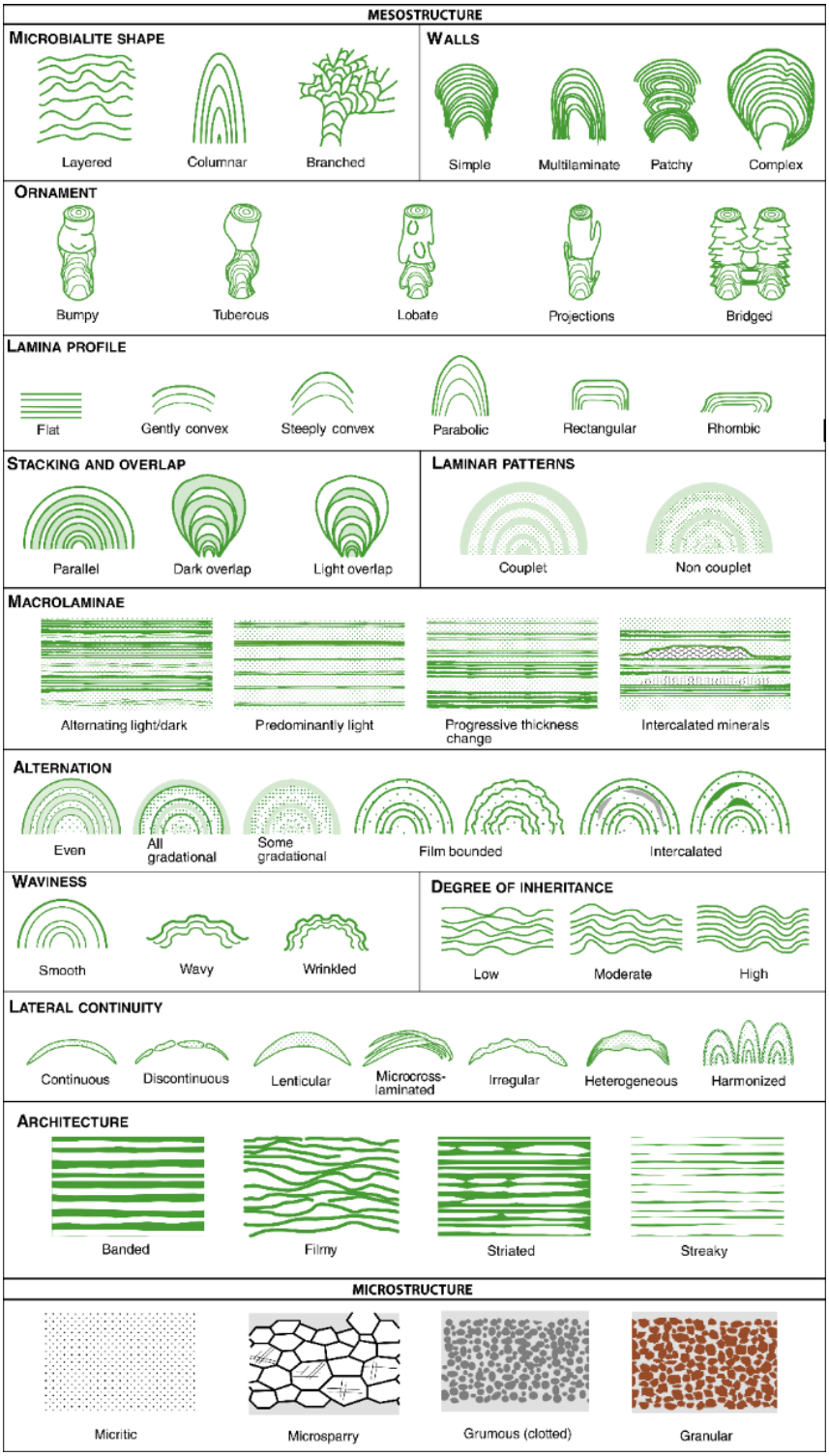

Table 1: *The features have been grouped into mesostructural (across the rock sample) and microstructural (under thin section). The illustrations, names and classification style are from Grey and Awramik (2020).*

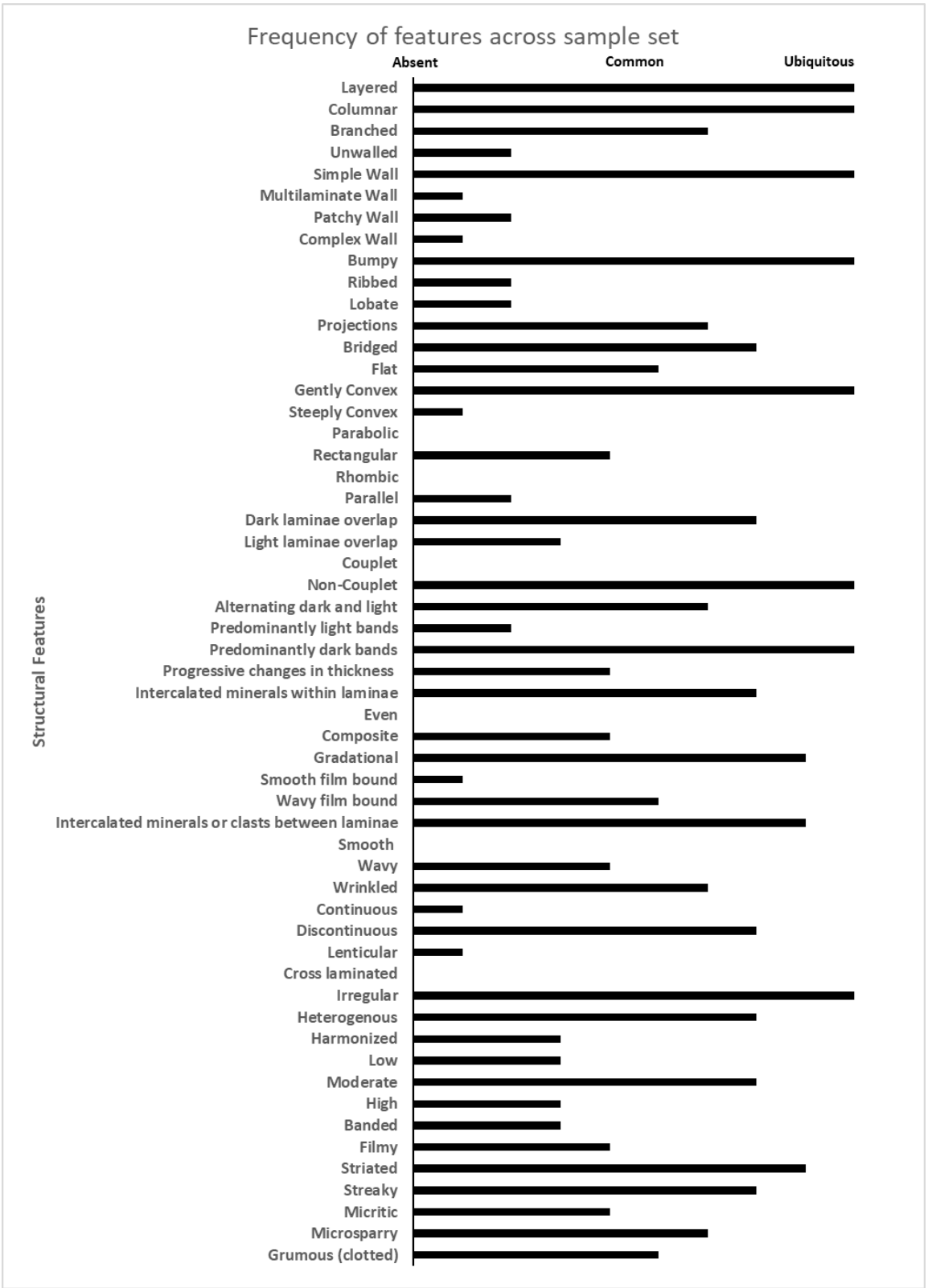

Table 2: *Frequency of the structural features listed in Table 1 across the microbialite rock sample set. This is based on the occurrence of each specific feature in both hand sample specimens and thin section specimens.*

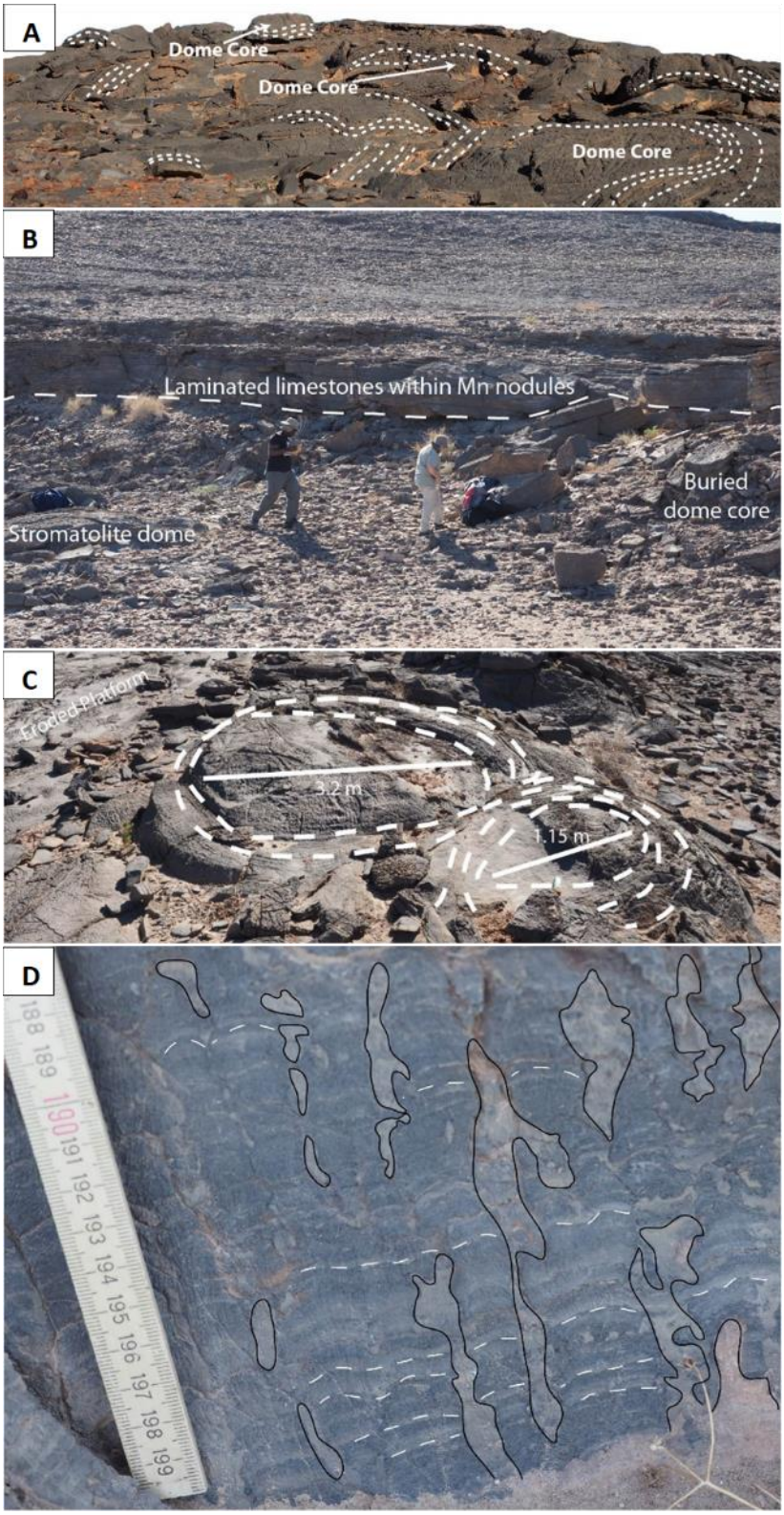

Figure 3: *Field photographs of Site 1. A) Maximal height of the outcrop showing exposed dome cores and complex layering of successive domes. B) Contact between microbialite reef and laminated limestone unit. C) Dimensions and laminar layout of adjacent domes, showing how the domes fuse over time. D) In-situ exposed interior of a dome core, showing distinct laminations (white dotted lines) of successive columnar structures (Outlined in black).*

6.3.2. Mesoscale

Sample RT1

Sample RT1 contains five microbialite columns, labelled A to E (**Figure 4**). Column A and E are not fully represented but appear to have vertically consistent walls. Column D is cylindrical with a constant width of ~3 cm. Column B and C could initiate and terminate part way through the sample, however, the irregularity in termination and initiation hints at the preservation of longer columnar microbialites that were cut tangentially to the growth axis. RT1 is dominated by dark microbial laminae, with a low degree of detrital sediment intercalations. The walls and internal fabrics of Columns B, C and D have been disrupted or overprinted by bright orange sediment. In addition, there are nebulous white structures in the intercolumn sediment that show apparent branching. The origin of these structures is unknown, however Monty (1976) identified similar structures in modern microbialites and associated them with filamentous algae and Li et al. (2021) associated similar irregular structures to micritic burrows. Additionally, there are fragments of dark material in the sediment that commonly have a sub-spheroidal shape. These could potentially be skeletal fossil fragments or broken, semi-lithified pieces of microbialite mat akin to roll-up structures seen in Archean microbial limestones (Simonson and Carney, 1999; Sumner and Grotzinger, 2004).

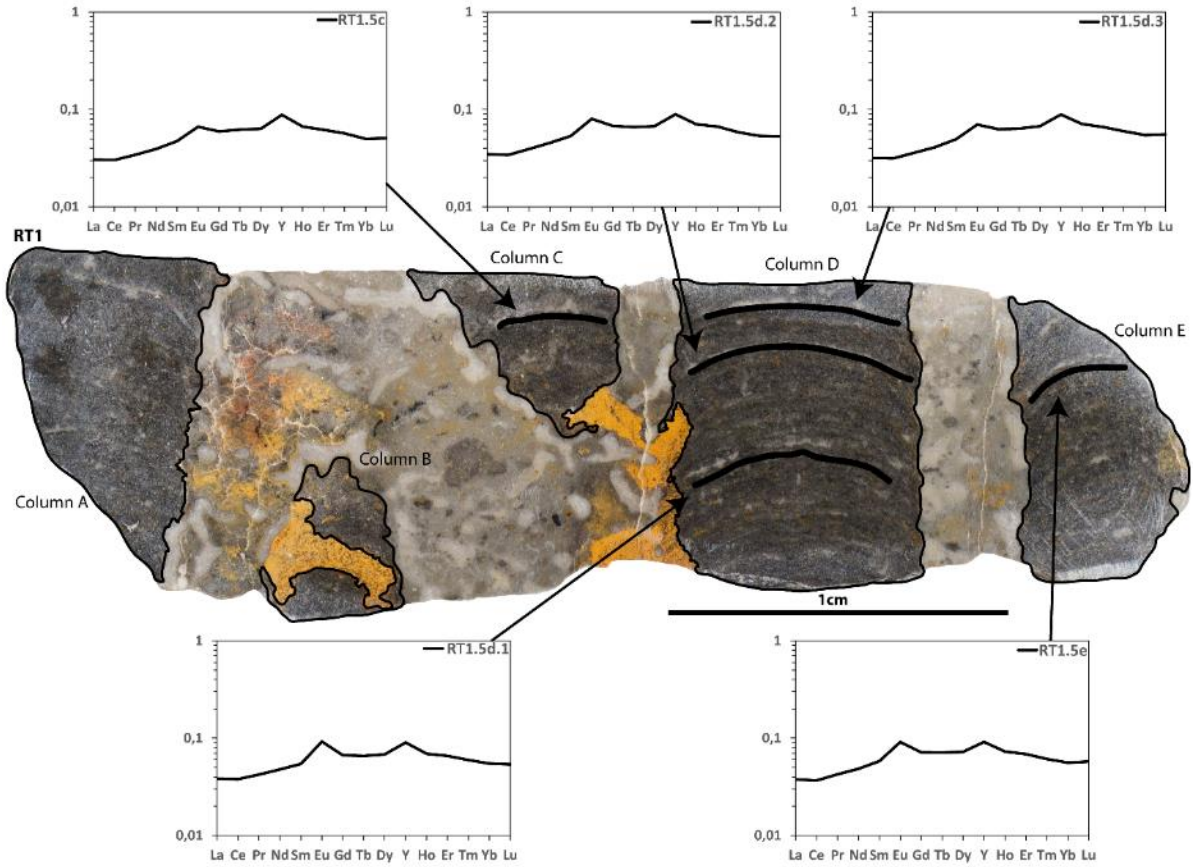

Figure 4: *Labelled photograph of microbialite sample RT1. Microbial material outlined in black with ascribed column names nearby and subsample drill transects as black lines. The REE plots show the patterns of select subsamples, with black arrows pointing to the associated subsamples.*

Sample RT3

Sample RT3 contains six microbialite columns, labelled A to F (**Figure 5**). There are prominent intercalations of a dull orange sediment throughout most of the columns, ~0.1 mm thick. These intercalations are predominantly continuous, indicating complete laminae of this material were deposited across the entire width of the columns. Column D appears to be two fused columns. The walls of the microbial columns in RT3 are rough, with short crenulations projecting into the intercolumn sediment. Similarly, to RT1 there are subrounded clasts and nebulous branched structures in the intercolumn sediment. Key features within the intercolumn sediment are the occurrence of a seemingly double walled structure between Columns C and D, similar nebulous white structures seem in Sample RT3 as well as the orange-red material in the intercolumn sediment.

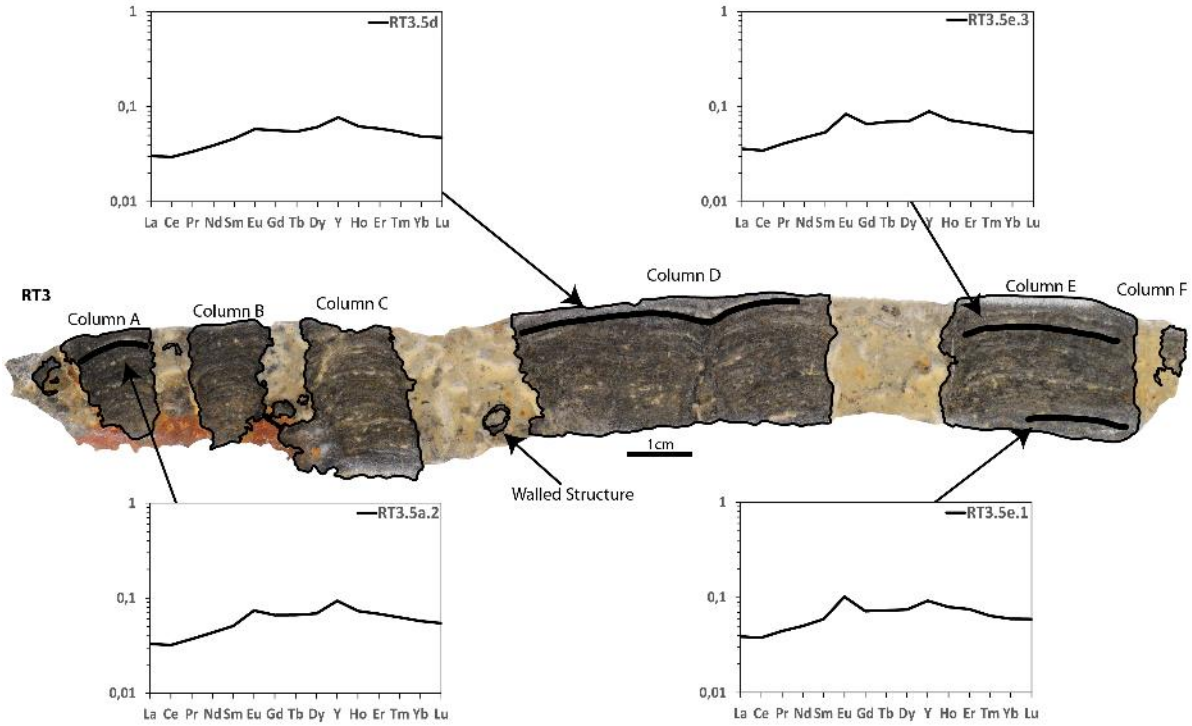

Figure 5: *Labelled photograph of microbialite sample RT3. Microbial material outlined in black with ascribed column names nearby and subsample drill transects as black lines. The REE plots show the patterns of select subsamples, with black arrows pointing to the associated subsamples.*

Sample RT4

Sample RT4 is a complex mixture of columnar and layered microbialite fabrics spread over three growth periods (**Figure 6**). These growth periods are defined by the cessation of microbial formation, where sequences of detrital sediment completely buried the microbial structures present at the time. There are multiple thin detrital intercalations spread throughout the sample. There is a predominance of light microbial laminae in this sample. These groups of non-periodic light laminae occur as sections of variable thickness. Almost all the microbial walls are ragged, distorted, or non-existent, except in the case of Section C and J, where the surrounding sediment is interwoven with the dark microbial matter. Growth linkages between adjacent columns are erratic, such as between Section H and Column E and between sections B and D. The microbial structure linking sections B and D seems to drape over a section of detrital material.

Substantial portions of the microbial matter in Section J are irregular, with ~1 mm sediment clasts scattered within this section and poorly defined walls. There are thick, amorphous sections of detrital sediment between microbialite growths, such as within the middle section of Column A and the lower middle section of D. The growth across Column A follows the previous generations growth style and column width. The growth form switches from lateral sheets to columnar growth between Section B and D. Similar occurrences appear in subsections G and I, where these growth structures were temporarily halted before growth resumed in sections B and H and Column E.

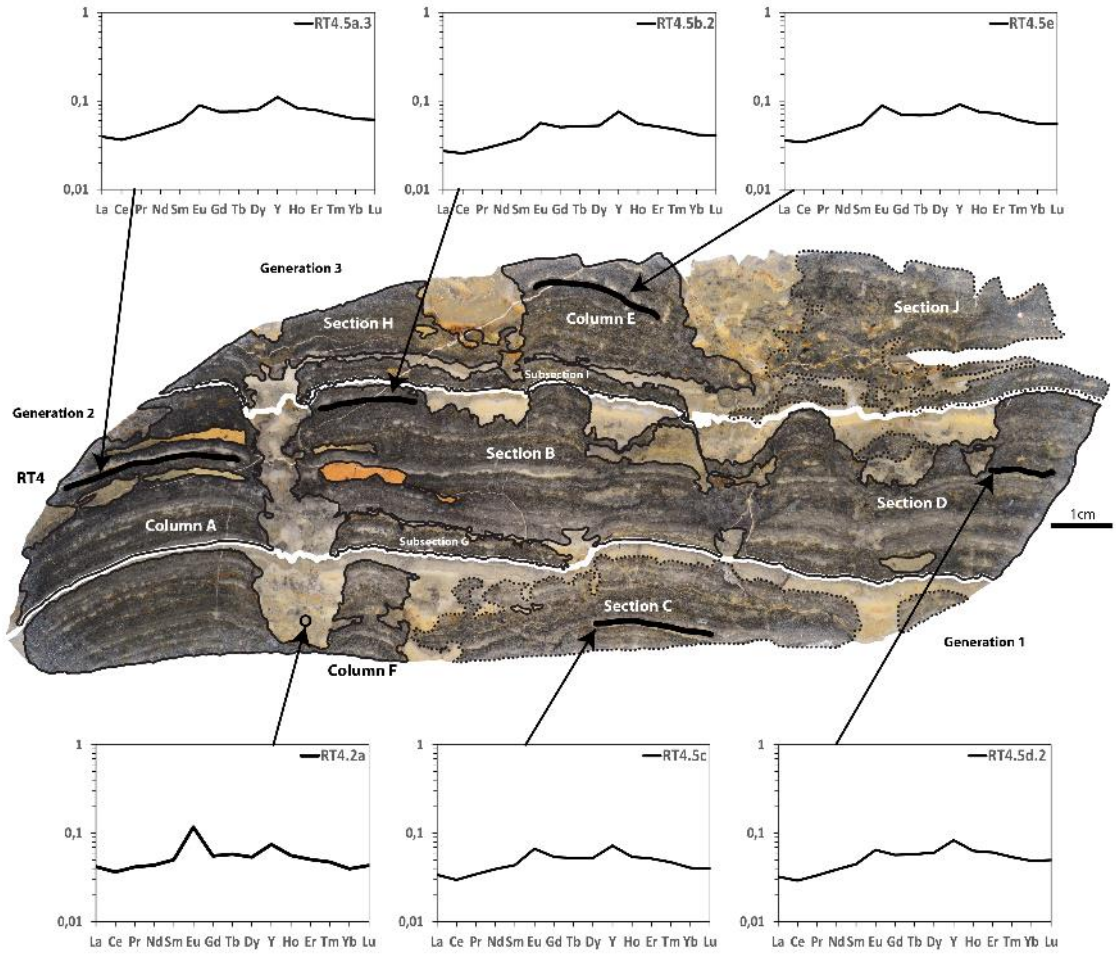

Figure 6: *Labelled photograph of microbialite sample RT4. Microbial material outlined in black with ascribed column and section names nearby and subsample drill transects as black lines. White lines separate different generations of microbial growth, with the names of each generation listed. Generation differences are defined by breaks in lateral microbial continuity. Section C and J have dotted boundaries to indicate poorly defined microbialite walls, with the dark material mixing with the surrounding sediment. The REE plots show the patterns of select subsamples, with black arrows pointing to the associated subsamples.*

Sample RT5a

RT5a contains numerous columnar microbialites, with Columns A, B, C, H, D and G showing parallel branching (**Figure 7**). Columnar linkages are present between Columns E and F and Columns C and H. There is an uneven variation between light and dark microbial laminae. While the dark laminae tend to be laterally extensive and continuous across the growth axis (they extend across the microbial columns), the light laminae appear as discrete, domed lenticular bands spread between the dark laminae. Detrital intercalations are widespread and vary in thickness, lateral extent, and continuity. Section I has a mottled texture and a vaguely disenable columnar shape.

The intercolumn sediment contains fragmented and subrounded clasts or potentially skeletal fossil fragments, such as the ring structures between Column G and E and the double walled clasts between Columns B and C. Such structures are akin to the conical shapes associated with *Cloudina* fossils found throughout the Ediacaran (See section *2.2 Ediacaran Biota*).

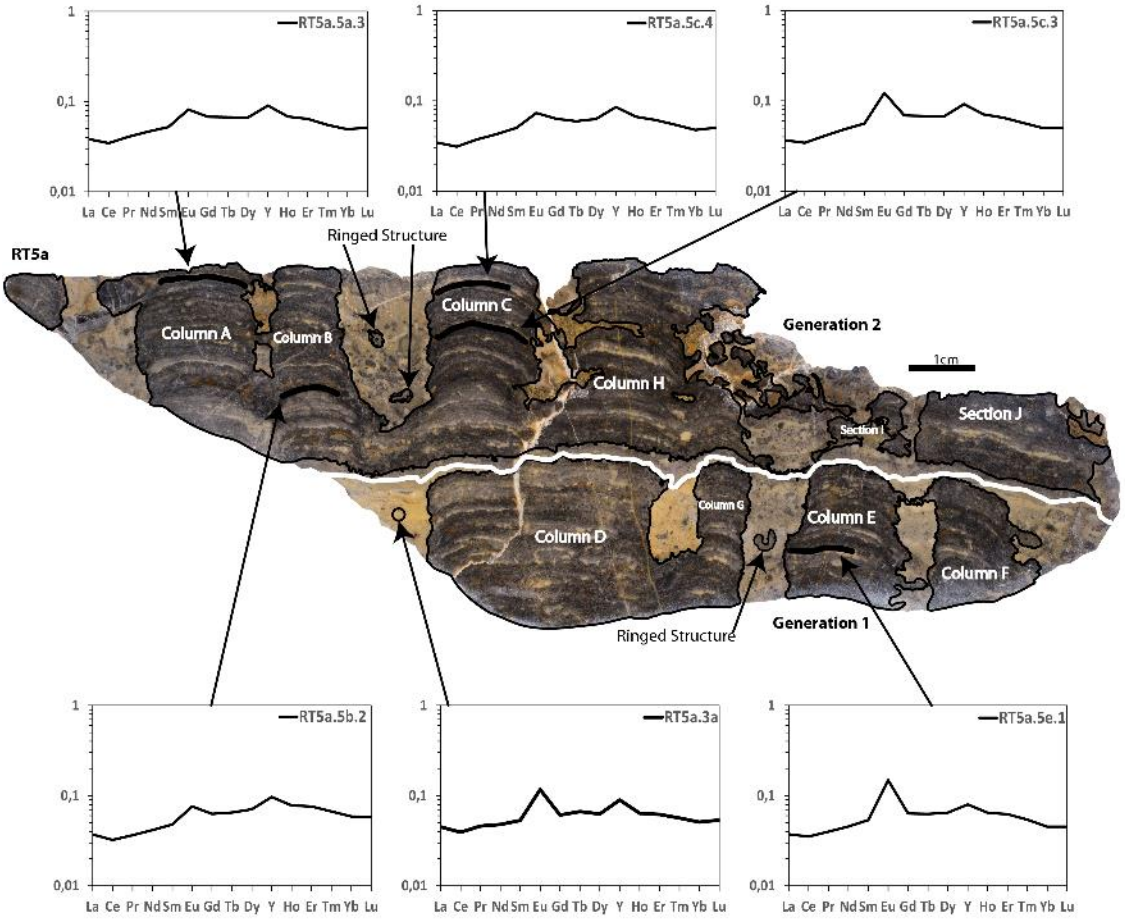

Figure 7*: Labelled photograph of microbialite sample RT5a. Microbial material outlined in black with ascribed column and section names nearby and subsample drill transects as black lines. White lines separate different generations of microbial growth, with the names of each generation listed. Generation differences are defined by breaks in lateral microbial continuity. The REE plots show the patterns of select subsamples, with black arrows pointing to the associated subsamples.*

Sample RT6a

The most notable feature of rock sample RT6a is the complex intercolumn material (**Figure 8**). There are fragmented microbial structures within Detrital Material A, this same material surrounds the skewed and irregular walled Columns B and C. Another notable feature is the presence of subrounded red sediment at the top of the branches of Column F and within a microbial structure in Section D. The microbial material seems to have grown around or entrapped these fine-grained cements (Red Material in **Figure 8**). The microbialite growth structure is also quite varied across the sample. Branched and linked microbial columns occur within Columns B, C, F and Section D. The rest of the microbial material occurs as microbial sheets, which grade into columnar microbialites in the case of Section H.

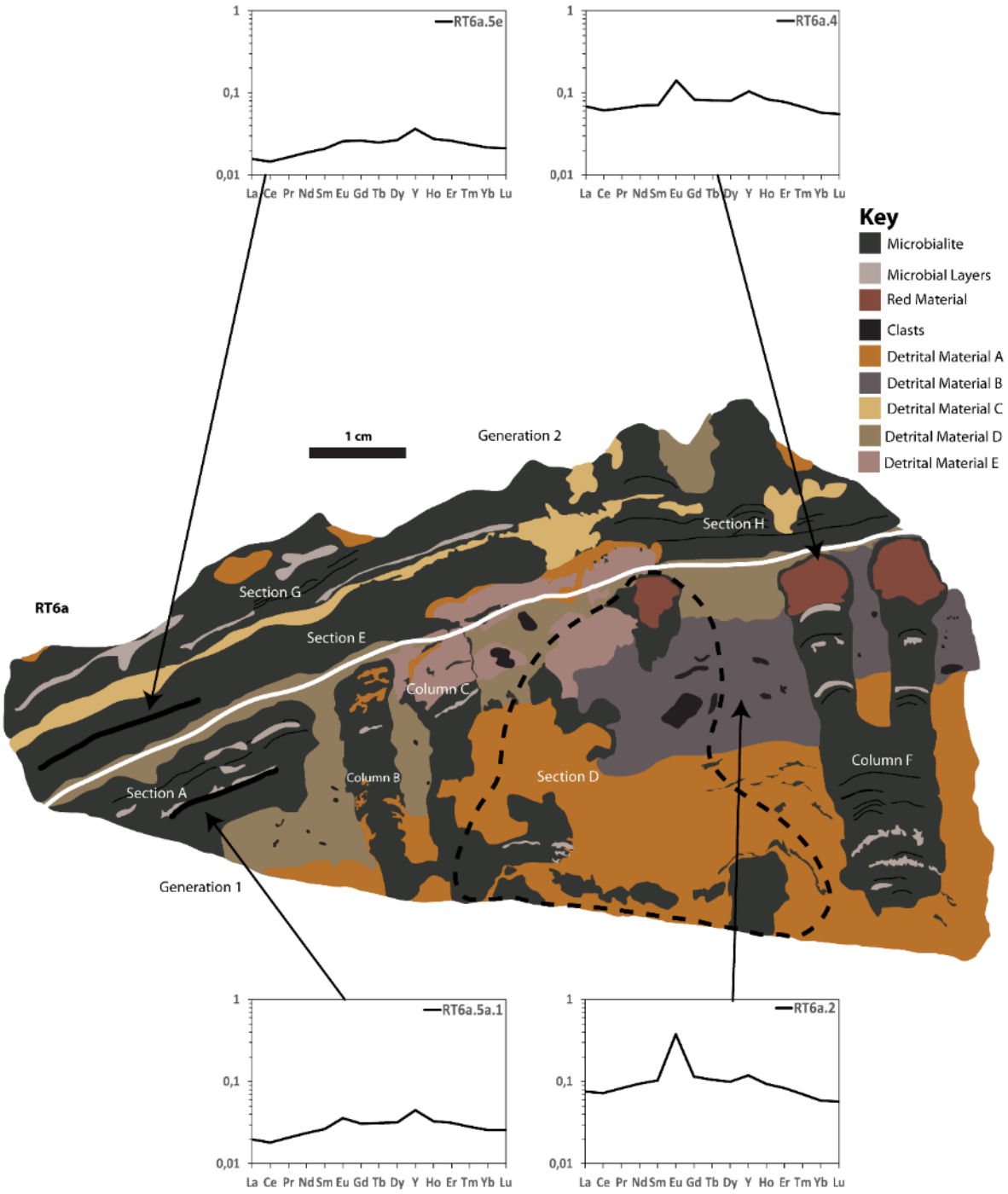

Figure 8: *Reconstruction of the microbial and detrital fabrics in sample RT6a. The purpose of this illustration is to convey the diverse range of intercolumn material and how it interacts with the microbialite columns. Five distinct detrital materials have been identified and coloured based on the most likely colour hex code of the original sediment. The key indicates the nature and morphology of the material present in the rock sample. As with prior figures, assigned microbial column and section names are listed, white lines separate microbial growth generations and the REE plots show the patterns of select subsamples, with black arrows pointing to the associated subsamples.*

Dark microbial laminae dominate the sample, with minor amorphous or lenticular sheets of light microbial material scattered throughout (microbial layers in **Figure 8**). Detrital Sediment C in Generation Two draped across the microbial growth, after which microbial build-up continued to form Section H. When growth resumed over Section I, these microbial mats potentially fused, but columnar growth was favoured in Section H while lateral growth continued in Section I.

Sample BO1a

Rock sample BO1a is an almost idealised example of harmonised, synchronous columnar growth (**Figure 9**). Both the light and dark microbial laminae in one column are perfectly repeated in the other columns preserved in this rock. There are many column links, wide wall projections and some simple branching, with Columns A to D seemingly originating from the same lateral microbial unit. There is a predominance of light microbial laminae, regular alternations of light and dark laminae and potentially a degree of laminae cyclicity. Intercalations are minor, found as <1 mm red grains across the columns. The light laminae seem to have more structured profiles than the dark laminae, crenulations and ridges occurring along the top and bottom of these light laminae. The intercolumn sediment is composed of orange and grey-orange sediment with ~0.5 cm rounded sediment clasts and minor amounts of subrounded dark lithic fragments.

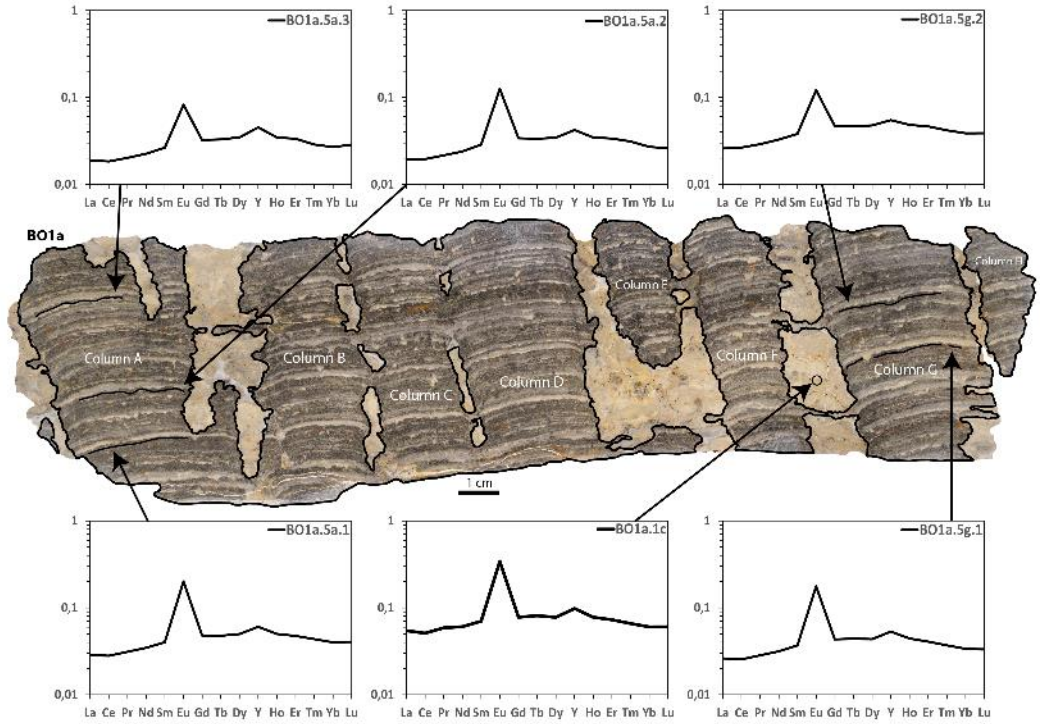

Figure 9: *Labelled photograph of microbialite sample BO1a. Microbial material outlined in black with ascribed column names nearby and subsample drill transects as black lines. White lines separate different generations of microbial growth, with the names of each generation listed. Generation differences are defined by breaks in lateral microbial continuity. The REE plots show the patterns of select subsamples, with black arrows pointing to the associated subsamples.*

Sample BO2

While sample BO2 shows two growth generations, the microbial material preserved in Generation One is sparse (**Figure 10**). The majority of the microbialite material across this sample is a mixture of simple columnar and complex branched and linked columnar microbialites made of predominantly dark microbial laminae. Also notable is the change in growth style and complex columnar linkages. Columns A, B, C and E grew into columnar structures from a thin lateral microbial sheet. Column C also fused with Column D and Section H, forming a white lateral microbial sheet in Section G. Six separate columns grew from Section G at different growth heights. There are distinct lateral variations in both the detrital intercalations and intercolumn sediments across the sample.

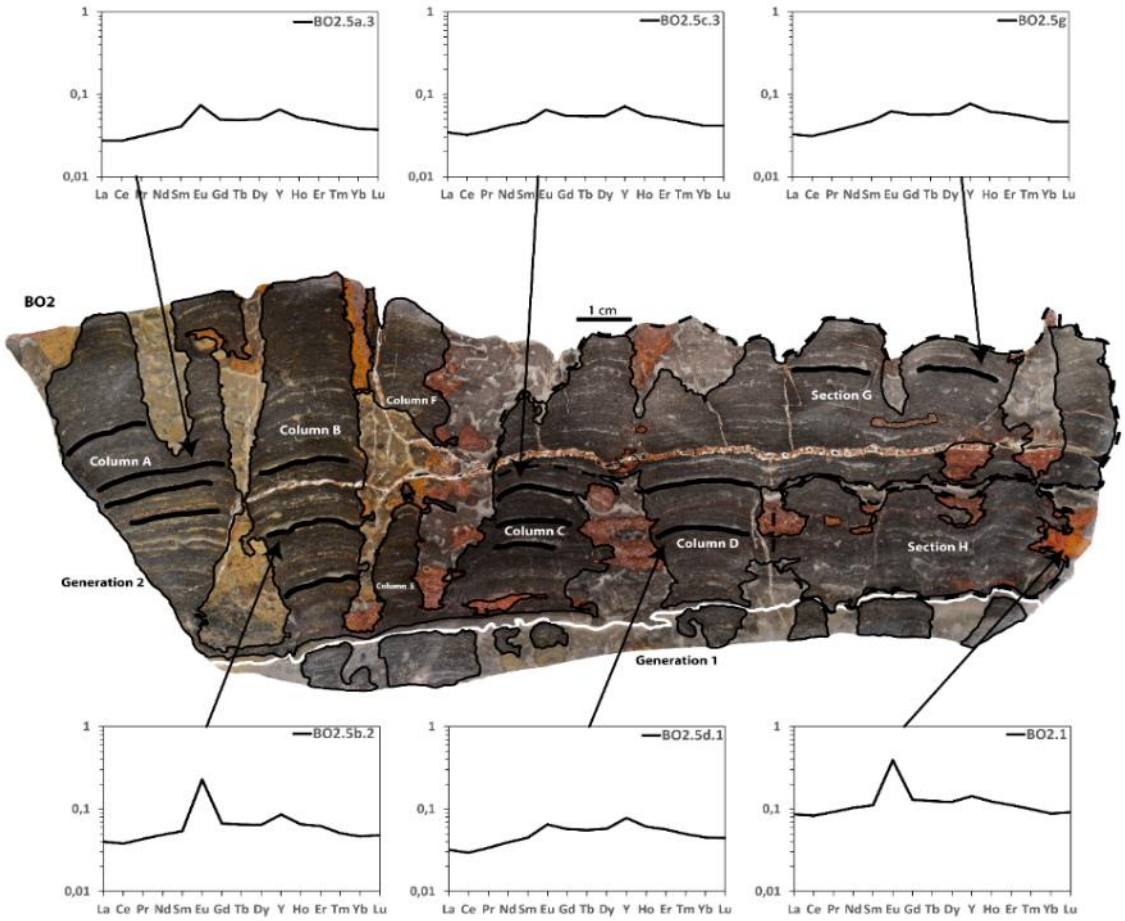

Figure 10: *Labelled photograph of microbialite sample BO2. Microbial material outlined in black with ascribed column and section names nearby and subsample drill transects as black lines. White lines separate different generations of microbial growth, with the names of each generation listed. Generation differences are defined by breaks in lateral microbial continuity. The REE plots show the patterns of select subsamples, with black arrows pointing to the associated subsamples and horizontal black lines showing the paths of the microdrill.*

Columns A, B and F contain laterally continuous laminae of pastel orange detrital material, while Section G, Columns C, D and Section H contain dark grey lateral intercalations, as well as subrounded intercalated clasts of this grey material across Section G. The intercolumn sediment mirrors this intercalation zonation, with different shades of orange sediment surrounding the columns to the left, and grey intercolumn sediments with patches of dark orange to red sediment across the middle and right side of the rock sample. This sample also contains the same nebulous branched structures seen in RT1, as well as potentially fossiliferous ring fragments and subrounded spheres between Columns A and B.

Sample SNO

Sample SNO contains successive columns, like sample BO1a (**Figure 9**). Unlike BO1a, SNO does not have consistently harmonized laminae, along with less developed laminae (**Figure 11**). There is a marginal dominance of dark microbial laminae over light microbial laminae. The light laminae occur as discrete lobes and sheets, while the dark laminae are thinner, more laterally consistent and lack clear laminar boundaries. Multiple detrital sediment layers occur across the columnar microbialites, each indicating periods of increased sediment burial before the living microbes grew through these units.

Sections H and J contain poorly discernible laminar architecture, seemingly containing subrounded ~2 mm detrital clasts embedded within the microbial fabrics. Columnar linkages are common, with highly erratic linkages occurring between Sections H and J. The intercolumn contains subrounded, potential fossil fragments as well as a vein of post-depositional calcite between Columns F and G.

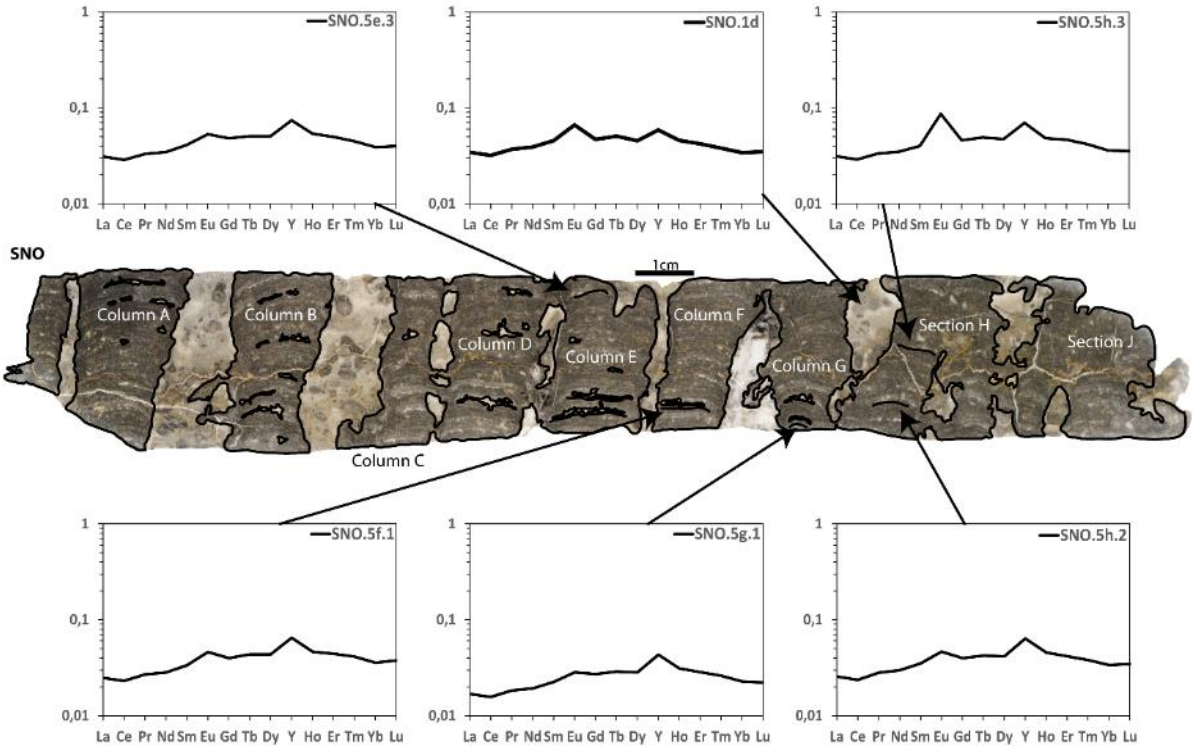

Figure 11*: Labelled photograph of microbialite sample SNO. Microbial material outlined in black with ascribed column and section names nearby and subsample drill transects as black lines. The REE plots show the patterns of select subsamples, with black arrows pointing to the associated subsamples.*

Sample SPO

Rock sample SPO is an example of complicated columnar microbialite branching (**Figure 12**). There are two cessation periods, however the microbes were able to persevere or grow through the sediment cover, visible as tendril like growths from Columns C and D into Section H. There is a dominance of dark laminae, with sections of thicker light laminae dispersed throughout. The initial microbial growth was erratic and poorly defined, as seen in Generation One. After this, Generations Two and Three contain columnar microbialites with a large degree of parallel branching and even anastomosed branching, whereby separate columns branch, fuse and then branch again, as seen between Columns D and E. There are multiple instances of microbialite initiation within the intercolumn sediment, however it is unclear if these are broken off fragments of adjacent columns, such as structures between Columns D and E, Column F and Section G and sections H and I. The microbial laminae in Generation Three are very thin, becoming indistinguishable in most parts, and the columns contain large sections of detrital sediment. There is an extensive degree of branching, erratic columnar wall projections, and more of the nebulous white structures within the intercolumn sediment across all three growth. There is also a relatively high degree of branch coalescence across SPO.

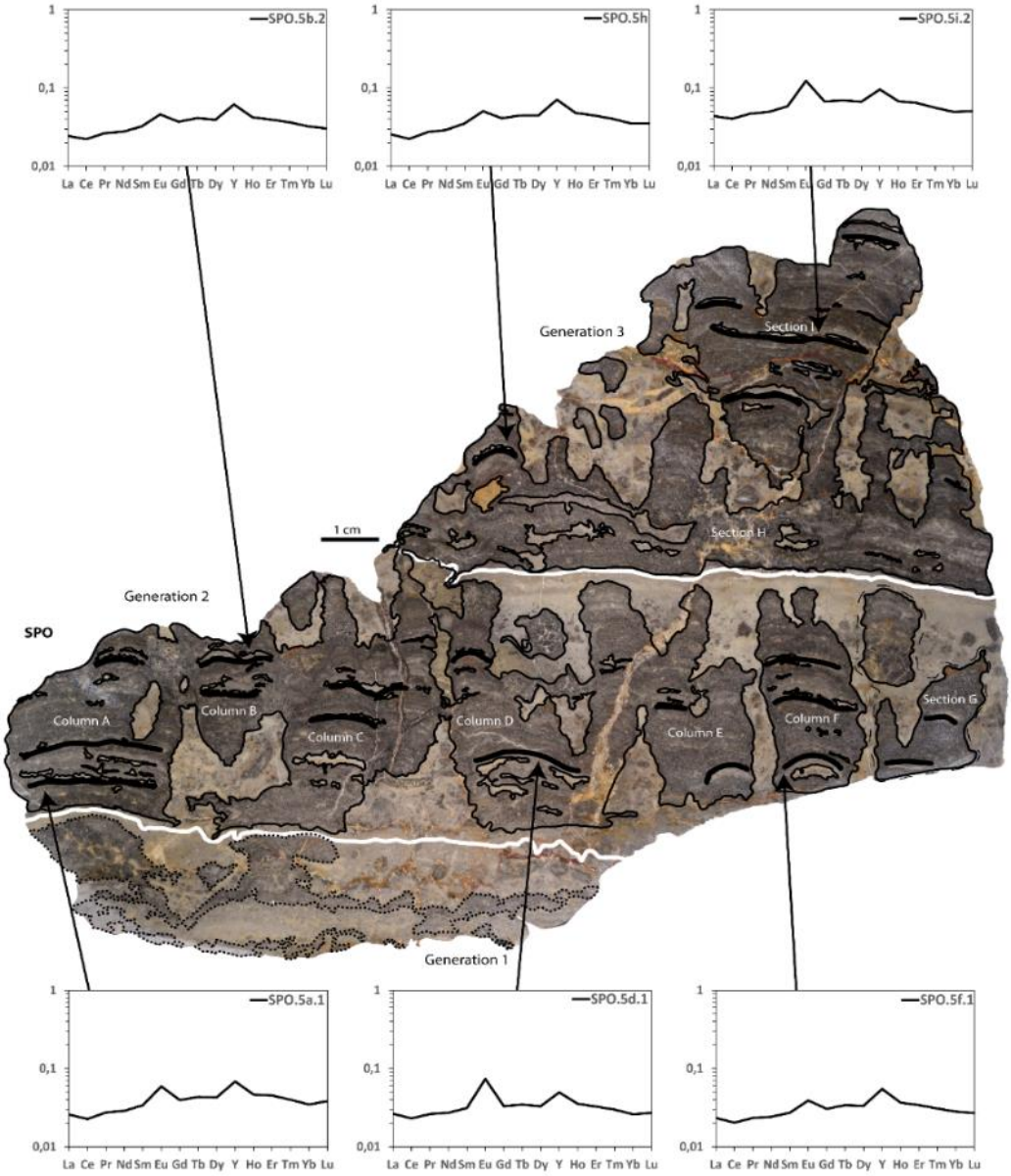

Figure 12*: Labelled photograph of microbialite sample SPO. Microbial material outlined in black with ascribed column and section names nearby and subsample drill transects as black lines. White lines separate different generations of microbial growth, with the names of each generation listed. Generation differences are defined by breaks in lateral microbial continuity. The REE plots show the patterns of select subsamples, with black arrows pointing to the associated subsamples.*

6.3.2.1. General Mesoscale Features

The stromatolites are predominantly columnar with infrequent simple branching and columnar linkages, composed of predominantly microspar and micritic calcium carbonate grains with variable grain sizes and subrounded to subangular shapes. The columns are composed of dark and light laminae, with the dark laminae being the most predominant, that grade into each other. Boundaries between laminae are unclear or diffuse, with rare occurrences of distinct, wavy, or crenulated film boundaries separating sections of dark laminae. Laminae continuity tends to be irregularly continuous to discontinuous, with some outliers of thicker light microbial layers with consistent or even harmonised continuity. The overall profile of the laminae in the columnar material are gently convex and rarely steeply convex. Alternating detrital laminae are common within the columnar structures, with the abundance varying between each rock sample.

While columns are the most common growth form, layered microbialites are found either after a break in microbial growth or where columns fuse to create a stratiform microbialite with internal columns. These thin layers contain flat, undulatory laminae boundaries. The intercolumn sediments have a range of colours, which could be compositional or diagenetic (See section *6.4. Discussion*), and contain a variety of intraclasts, fragments and structures, which are detailed in *6.4.5. Feature Summary.*

6.3.3. Microscale (Thin Section)

The intended purpose of the microscale analysis was to test for the biogenicity of these carbonate rocks, thus only the most common mesoscale features were selected from a fraction of the sample set. Regardless, these microstructural descriptions focus on sedimentary grain morphology, fabric, texture, and other features visible under magnification (Grey and Awramik, 2020; Schopf and Walter, 1982). This provides information about the fabrics and texture that lead to the creation of the larger microbialite morphologies, as well as evidence of microfossils. It is necessary here to clarify the difference between fabric and texture with regards to microstructure analysis, as the two are commonly conflated. Microstructure fabric refers to the orientation, lamination or pattern of discrete grains, crystals, and cement while microstructure texture refers to the morphology of the grains in a sedimentary rock. It should also be noted that a prominent constraint on microstructure analysis and preservation is that diagenesis and post depositional compression can and does destroy the original microbialite microstructure. The microbialite samples are almost entirely composed of calcium carbonate, primarily calcite with minor dolomite. The average grain size of the calcium carbonate across the rock is cryptocrystalline, making distinguishing grain boundaries challenging even at 25x magnification.

Sample RT1

The columnar microbialites in RT1 (**Figure 13A**) are made up of grumous textures (subrounded clots of micrite) which grade into unstructured cryptocrystalline micrite (in situ calcium carbonate grains) and microspar. No clear fabric or evidence of lamination is apparent in this material. The intercolumn sediment is a homogenous micritic texture, containing globular sections of low relief microspar and sparry calcite clasts, which are the nebulous white structures seen in rock samples RT1 (**Figure 4**) and RT3 (**Figure 5**). The microbial column walls are well defined by the contrast between dark grumous texture and the dominant micrite in the intercolumn, terminating abruptly at the margin with the intercolumn sediment (**Figure 13B**). Post-depositional cracks filled with microspar run through both the microbial and detrital regions.

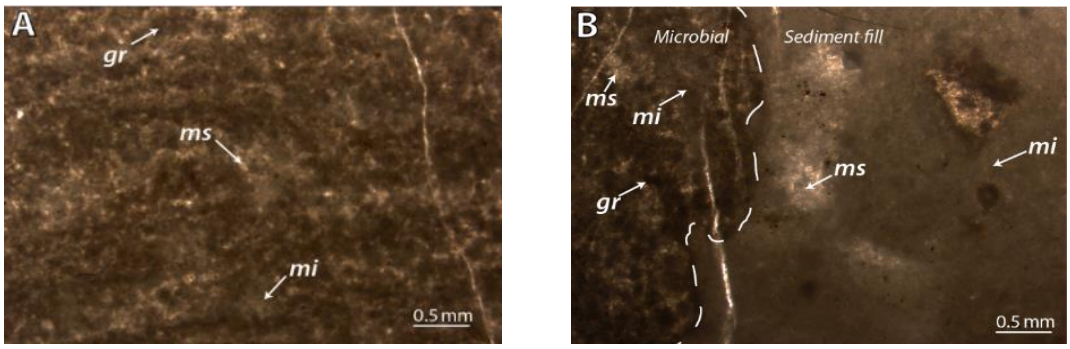

Figure 13: *Plane polarised photograph of sample RT1 at 25x magnification. A: the microbial region; B: the interface between the microbial column and intercolumn sediment, with the wall outlined in a dotted line. Grumous (gr), microspar (ms) and micritic (mi) textures are indicated on the photographs.*

Sample RT3

RT3 shows grumous clots defining laminated fabrics (**Figure 14A**). **Figure 14B** shows that the dark, subangular intercolumn fragments are composed of the same micritic texture as the sediment, albeit darker. Veins crosscut the intercolumn sediment, with some larger veins sedimented with microspar.

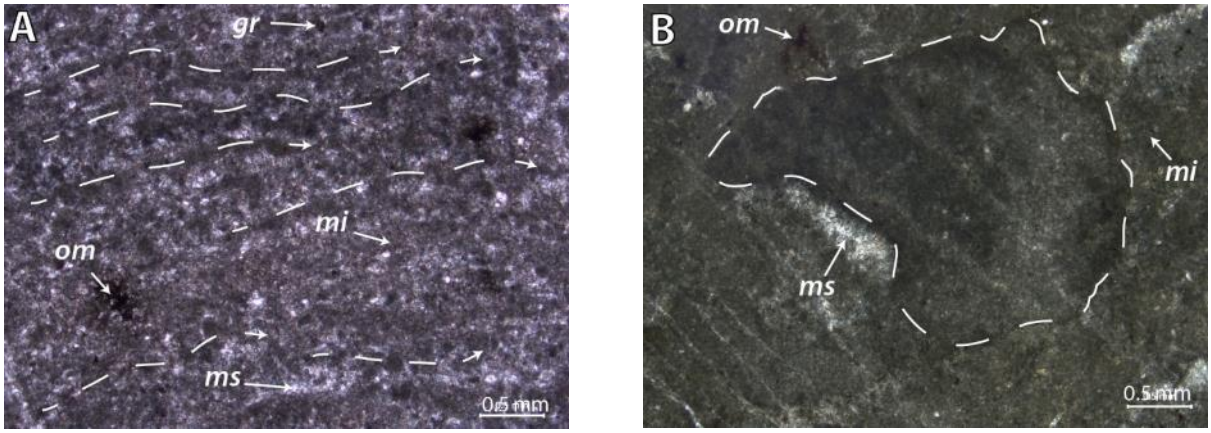

Figure 14*: Plane polarised photographs of sample RT3 at 25x magnification. A: the microbial material with weakly orientated textures indicated with directional dotted lines; B: the intercolumn sediment with a large sedimentary clast. Grumous (gr), microspar (ms) and micritic (mi) textures are indicated on the photographs, along with potentially organic matter (om) fragments.*

Sample RT4

RT4 contains microstylolites, filled with opaque oxides or organic matter, which cut across both the microbial and detrital regions (**Figure 15A**), most likely artifacts of sediment compaction. Unique to RT4 are dome-shaped structures within a layered band of micrite. These domes run parallel to the laminae in the column and are composed of fine-grained microspar and micrite (**Figure 15B**). These could potentially be voids or fenestrae (Sumner, 2000), that have been filled with recrystallised calcium carbonate.

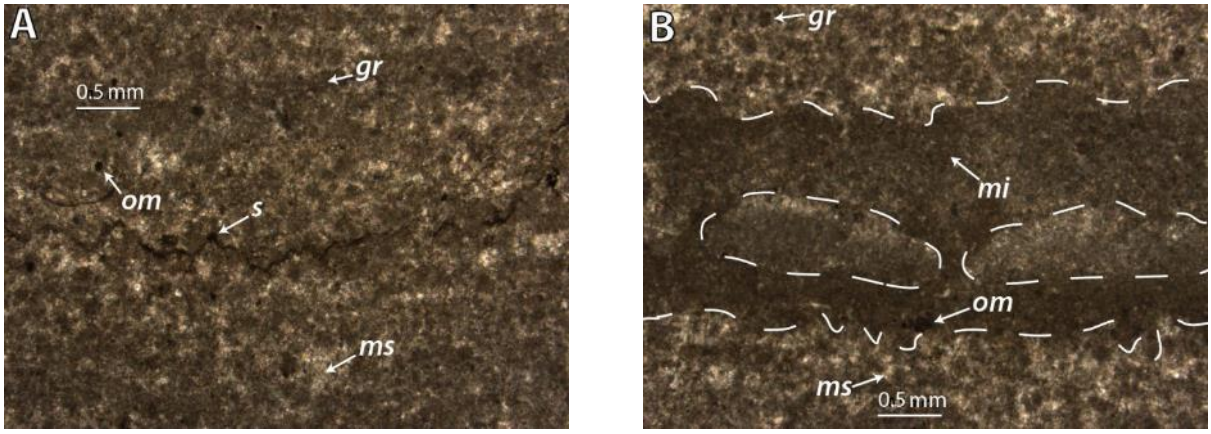

Figure 15: *Plane polarised photograph of sample RT4 at 25x magnification. A: Stylolite within the microbial material; B: domed structures inside a micritic laminae within the microbial material, dotted white lines demarcating these features. Grumous (gr), microspar (ms) and micritic (mi) textures are indicated on the photographs, along with organic matter (om) fragments and the stylolite (s).*

Sample RT5a

RT5a exhibits typical columnar and detrital textures seen thus far, but uniquely, contains large (0.5-3 cm) detrital intraclasts made of recrystallised microspar (~0.02 mm) in both the microbial and intercolumn material (**Figure 16A**). Some thick and dark micrite walled cavities occur throughout the intercolumn material, filled with coarsening inward calcite (**Figure 16B**). This sparry calcite shows clear lamellar twinning. These walled fragments are similar in shape to the proposed fossil fragments seen on the macroscale (**Figure 7**).

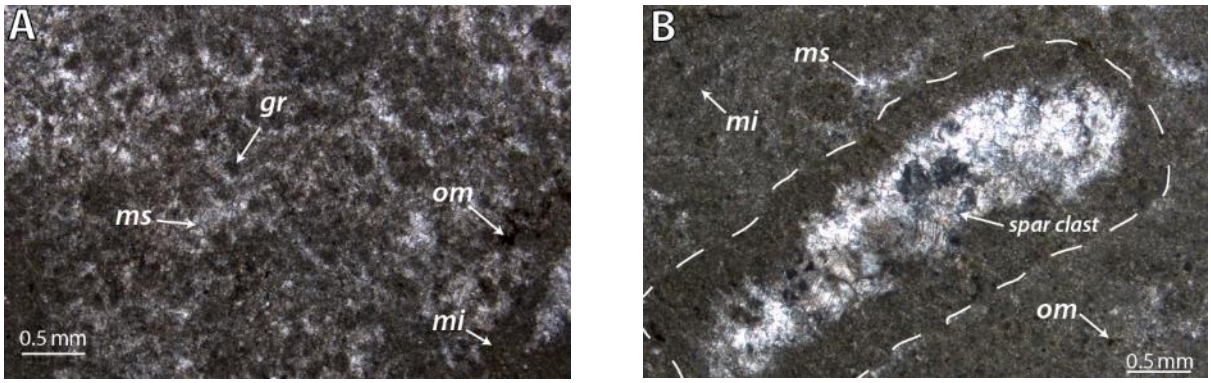

Figure 16: *Plane polarised photograph of sample RT5a at 25x magnification. A: Columnar microbialite textures; B: Intercolumn sediment with a sparry calcite crystal surrounded by an isopachous micrite wall, indicated with a dotted line. Grumous (gr), microspar (ms) and micritic (mi) textures are indicated on the photographs, along with organic matter (om) fragments. Note, the micritic textures across this sample are coarser than previous samples.*

Sample SNO

SNO contains more microspar than micrite within the microbial columns (**Figure 17A**). An interesting feature captured in thin section is a detrital intercalation made of sparry calcium carbonate defining the lamination at the microscale (**Figure 17B**).

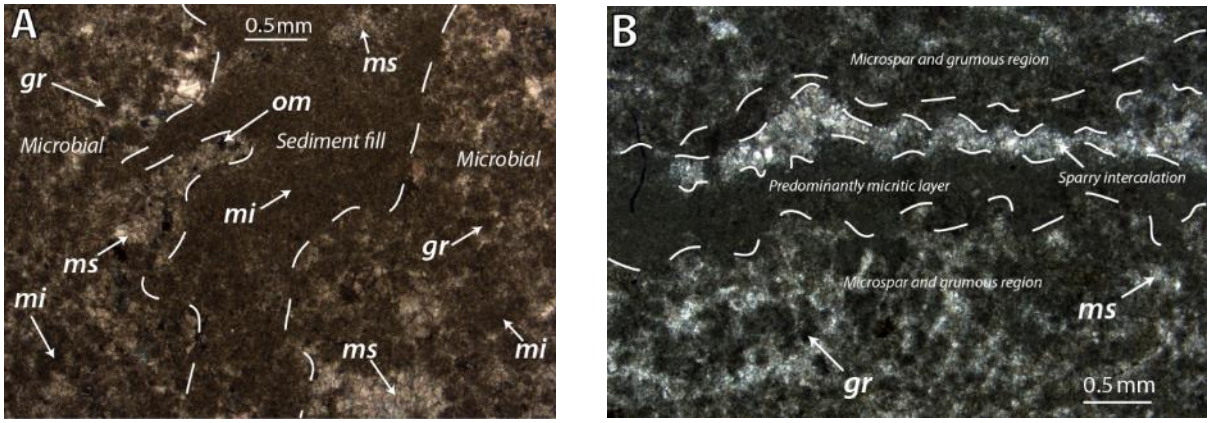

Figure 17*: Photographs of sample SNO at 25x magnification. A: Intercolumn sediment between two columnar microbialite projections, boundaries marked with a dotted line; B: Microbial material with a micritic laminae containing a layered detrital intercalation, with dotted lines separating these boundaries. Grumous (gr), microspar (ms) and micritic (mi) textures are indicated on the photographs, along with organic matter (om) fragments.*

Sample SPO

In SPO, the columnar regions are dominated by microsparry calcite with minor micritic textures and grumous clots (**Figure 18A**). The grain shapes vary dramatically, ranging from subhedral rhombs to lath crystals to exceptionally fine anhedral grains. The intercolumn sediment is dominated by a much darker fine-grained micritic texture. Coarse grained calcite intraclasts are scattered throughout the intercolumn sediment. Dark clasts are also more prominent in the intercolumn sediment than the microbial regions. The interface between the sediment and the microbial material clearly shows the difference in grain size and texture variation (**Figure 18B**). The grumous texture in this section shows clear lineation, potentially showing the formative units of the laminae visible at the macroscale.

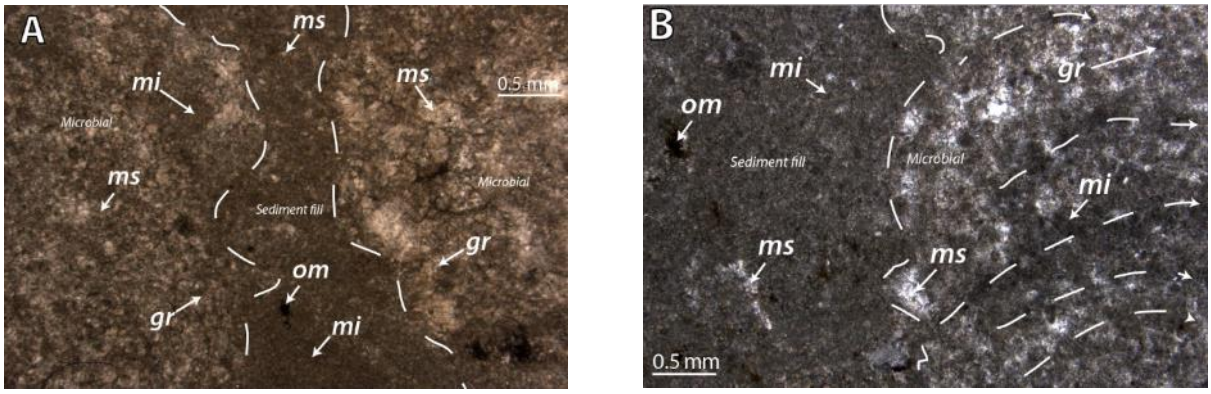

Figure 18: *Plane polarized light photograph of sample SPO at 25x magnification. A: Intercolumn sediment between two columnar microbialite projections, boundaries marked with a dotted line; B: Interface between the intercolumn sediment and a microbial column, which contains preferential lamination defined by grumous textures and dotted lines yet again highlighting the wall and laminar orientation. Grumous (gr), microspar (ms) and micritic (mi) textures are indicated on the photographs, along with organic matter (om) fragments.*

6.3.3.1. General Microscale Features

Thin section images show the microbialite are made up of a mosaic of cryptocrystalline calcium carbonate, either as grumous clots, microspar or micrite. The columnar microbial material contains a mixture of calcite microspar crystals and dark grumous clots. The calcite in the microspar typically ranges from 0.05 mm to 0.1 mm and are anhedral to subhedral rhombic shaped. The intercolumn sediments are dominated by micritic textures with coarse microspar to sparry grains and cm scale spar filled, dark micrite walled cavities (**Figure 16B**). The horizontal laminations that are clearly visible in the macroscale are not apparent in thin section. In general, evidence of consistent laminae is poorly defined to non-existent in the columnar material, except for patches of recrystallized calcite intercalations or lineated grumous clots. Of particular note is that both the intercolumn and microbial material are composed entirely of calcium carbonate. Select samples were additionally imaged under back scatter scanning electron microscopy (B-SEM) to determine if there were any differences between the crystal structure of the columnar microbial material compared to the intercolumn sediment. However, the sample preparation and scanning method were not successful in generating meaningful information, showing widespread, etched clasts of calcium carbonate across a cemented surface. The SEM images are included in the appendix in section *10. Supplementary Data.*

6.4. Discussion

6.4.1. Depositional environment

The morphologies of the microbialite samples from the Nama Group differ from contemporaneous microbialites. Li et al. (2021) among others note that columnar stromatolites are rare on the Ediacaran side of the Precambrian-Cambrian transition, but they are present in the Nama Group (Site 1, **Figure 2C** and **Figure 3D**). At the macroscale, the domal stromatolite reef at Site 1 is interpreted to have been deposited in an intertidal region on the western shore of the continental shelf. This is because stromatolitic domes are thought to form within shallow, wave influenced subtidal zones that are consistently submerged (Grotzinger, 2000; Saylor et al., 1998; Smith and Mason, 1998).

At the mesoscale, the variation of unlinked columnar, linked, and simple branched columnar and rarely thin planar laminae and thicker stratiform stromatolites suggest that there was some small-scale environmental complexity. Most of the laminae across the sample set are gently convex, which is the most common laminae shape in Precambrian microbialites (Zhang and Hoffmann, 1982). Columns are growth forms associated with deeper marine waters, where these laterally restricted features form due to high energy currents preventing lateral microbial mat expansion. The exact mechanism for column formation has been related to biological responses to sunlight, known as heliotropism. Microbes will prefer configurations that can net the highest sun coverage, lowest turbulence, and optimal interaction with suspended sediments (Golubić, 1973). In the case of a columnar stromatolite, the microbial community need to minimise the distance from the photic zone, and thus accrete upwards, becoming laterally constrained and vertically exaggerated (Hand and Bartberger, 1988). It should be noted that multiple studies suggest that short, columnar stromatolites could have developed in shallower tidal settings akin to modern marine stromatolites found in Australia (Jahnert et al., 2013; Li et al., 2021). However, the presence of scours in the column walls, periods of detrital sediment accumulation burying stromatolites and fragments of microbial material within the intercolumn sediment indicate that abrupt, syndepositional, high-energy events (likely storm events or mass movement events) occasionally impacted the microbialite reef (Martin-Bello et al., 2019). The presence of thin microbial sheets after cessations that are overlain by laterally restricted columnar stromatolites potentially indicates a biological response to increasing water depths accompanied by increasing environmental energy levels (Martin-Bello et al., 2019).

At the microscale, the variation in microbial laminae continuity, thickness, laminae boundary shape and waviness are due to several previously determined factors, namely variations in microbial growth, fluctuations in sediment supply, changes in microbial mat chemistry and current turbulence (Hofmann, 1973; Martin-Bello et al., 2019; Monty, 1976; Petryshyn and Corsetti, 2011). Zhang and Hoffman (1982) attributed microbial laminar shape to strong biological controls, regardless of the environmental conditions. The fact that the laminae vary both laterally and vertically indicates these variations occurred in space and over time, respectively. A possible scenario could be the formation of erratic current eddies as waves break on the nearby shore, with these eddies not hitting the whole reef with equal energy or in the same direction.

Together, the features across these three scales point to formation at a transition between a tidally influenced intertidal zone and a subtidal, near offshore zone that occasionally experienced storm related wave action. Fluctuations in sea level would push the microbial reef into these different environmental regimes, changing the localised environmental energy strength and prompt biological responses, leading to the vertical and lateral changes in morphology seen throughout the columns at Site 1. Thicker sections of stratiform microbialites adjacent to columnar stromatolites are more difficult to explain (**Figure 10**), as this implies formation in shallow, occasionally exposed surface waters and low energy conditions, which means they were unlikely to have formed in the subtidal zone. The likelihood of near surface conditions is further decreased by the lack of any planar microbialites at the macroscale (**Figure 3A** and **Figure 3C**). Martin-Bello et al. (2019) also noted thick, stratiform build ups between or adjacent to columnar stromatolites and suggested that this could occur at the transition to the open ocean. The low energy, passive sediment accumulation in the open ocean would allow for lateral expansion, with the presence of columnar peaks indicating periods when the microbes attempted to increase their sunlight acquisition. It could thus be that this laterally extensive domal reef formed at the distal edge of the carbonate ramp, at a location more associated with open ocean sedimentation rates.

6.4.2. Sample specific energy levels

RT1 and RT3 are the only samples with even columnar widths, indicating stable current energy levels (Gebelein, 1974; Monty, 1976). The rest of the samples contain structures that vary along their length, indicating spatial heterogeneity in current energy levels and stability. What was the current direction across the domal stromatolite reef build up? Turbulence due to tightly grouped columns could lead to eddies of variable direction forming, which would have impacted the lateral expansion of microbial mats, and thus impacted the lateral shape of the microbialites. The samples also show diversity in the intercolumn sediment composition and content, something not always observed for ancient stromatolites (Tosti and Riding, 2017a, b). BO2, RT1 and RT3 contain potential biologically influenced structures, and all samples show colour variations in the sediment, potentially pointing to compositional variations within the sediment, but more likely a result of interactions with diagenetic fluids. BO1a, BO2, RT1, RT3, RT5a and SNO have layers of light microbial or detrital laminae that preserve the equivalent of bed bottom scours, where the lighter material gouges into the darker laminae below. These could indicate turbulence creating pockmarks as currents flowed over the unlithified microbial mat. BO1a is an almost pristine example of harmonized, continuous laminations across unlinked microbial build ups. This sample does however have uneven branching, showing that while the overall environmental energy allowed for stable build up, there was some degree of lateral sedimentation variation or turbulence.

A common feature across rock samples RT5a, RT6a, BO1a, BO2 and SPO, are irregular microbial walls, erratic wall projections, sections of branching and linked columnar growth as well as complex anastomosing and coalescing columns in the case of SPO. These features point to microbial growth in a relatively high energy environment. Microbial column branching and coalescing could be due to rapid water currents or intermittent periods of increased sedimentation rates, potentially from marine regressions or storm surge events (Awramik, 1971; Gebelien, 1974; Tosti and Riding, 2017a; Zhang et al., 2019b). These events would result in abrasive waters or interruptive currents that would have reduced microbial mat growth rates and potentially influenced the shape of the column walls.

Tosti and Riding (2017b) expanded on this by relating periods of growth cessations and subsequent sediment burial to consistent high energy currents preventing microbial growth from keeping pace with the background sedimentation rate. The space around the columns would gradually fill, eventually leading to burial. When the sea returns to baseline levels, or following a storm event, a new generation of microbial mats will nucleate on the detrital substrate. Closer examination reveals many more sample specific features, all essentially pointing to one thing: small-scale, lateral variation in energy levels, current stability, and sedimentation rates.

Also of note is that both the mesoscale and microscale show no orientation or layering of the intercolumn material. This means that the intercolumn sediment experienced reworking by high energy currents, creating a normalised unstructured material relative to the microbial calcite, which could have lithified more quickly, preventing severe reworking. It is also possible that the intercolumn sediment was postdepositional (Tosti and Riding, 2017a, b). However, the occurrence of microbial fragments within the intercolumn sediment, gouged or uneven walls and slanting columns (**Figure 8**) indicates syndepositional processes did occur. Thus, sedimentary deposition could have been a largely gradual process, punctuated by short periods of syndepositional sediment disruptions and column breakages during microbialite build up.

6.4.3. Microfabric-macroscale disparity

Microbial laminae are clearly visible at the mesoscale, forming columnar, branched and rarely layered stromatolites. However, at the microscale, these laminae are made from poorly sorted, clotted micrite grains that lack a preferred orientation, akin to the mesoclots that define thrombolitic microbialites. Using previous categorizations of microscale textures, the microbialites in this study should indicate coccoid cyanobacteria preservation (Gabelein, 1974; Kennard and James, 1986; Monty, 1976; Semikhatov et al., 1979). This poses an interesting dilemma about the nature of the microbial laminae preserved in these samples. Ancient, micritic stromatolites would have experienced some degree of alteration, creating widespread neomorphic micritic grains and destroying primary fabrics, making analysis of the microstructure challenging (Bosak et al., 2013; Corkeron et al., 2012; Fairchild, 1991; Martin-Bello et al., 2019). Exceptional conditions may be required to consistently preserve primary microstructure, with some papers noting the rarity of cyanobacterial fossil preservation in the rock record, regardless of age (Arp et al., 2001; Planavsky et al., 2010). The bacterial cells themselves may need to be calcified during the living microbial build up to be properly preserved (Riding, 1991; Riding, 2011b). Widespread calcified cyanobacteria preservation was notably common between the Cambrian and the Late Triassic (Arp et al., 2001), potentially indicating that preservation potential is linked to global changes that favoured calcite precipitation, which is more resistant to fluid alteration, silicification or chemical replacement (Ries et al., 2008; Wood, 2018; Wood, 2011; Wood et al., 2015; Zhang et al., 2018). The lack of clear microfossil evidence may not necessarily be dead-end. Many studies have noted that dark, spherical micritic aggregations that have been classified as grumous are evidence of organic matter, potentially representing moulds of cyanobacteria or the fragmented remains of them (Awramik and Grey, 2005; Lan and Chen, 2012; Monty, 1976; Riding, 1993; Riding, 2000; Semikhatov, 1976; Vandenbroucke and Largeau, 2007; Zhang et al., 2019b). Awramik and Semikhatov, (1979) observed that dark laminae can contain a combination of coccoidal and filamentous forms when microfossils are preserved. So, the grumous textures within the microbial columns could be the remains of destroyed filamentous microbial fossils or simply, compacted microbes.

Ultimately, this lack of any unambiguous evidence of filamentous or coccoidal cyanobacteria means determining the biodiversity or microbial complexity of the formative mats is impossible. The absence of clear fabrics could be an artefact of destructive thin section sample processing. For example, variation in the thickness of the thin sections has resulted in perceived colour variations. Some regions of the thin sections are so worn down that one can only see microspar textures, while the original rock contained both columnar and sediment material. The poor features seen in the B-SEM mounts could also be a result of inappropriate sample preparation (See section *10. Supplementary Data*). Regardless of the above discrepancies and in the absence of further information, the microstructural texture in these thin sections suggests that the dark columnar material is biologically mediated (grumous textures) and the intercolumn sediment is detrital material (microspar and coarse grained micrite), likely terrigenous in origin.

6.4.4. Laminae Creation

Understanding the chemical, physical and biological processes that generate modern microbialites can help us interpret the genesis of ancient microbialite structures and fabrics (Awramik and Grey, 2005; Hofmann, 2000; Monty, 1976; Riding, 1991). It was from observations on modern day cyanobacterial mats that the association of layering in ancient stromatolites with microbial mediation was made (Gabelein, 1974; Monty, 1976). The overall shape of a microbial build up is associated with predominantly environmental controls such as water depth, hydrodynamics, salinity, and sedimentation rates (Andres and Pamela Reid, 2006; Jahnert and Collins, 2011; Jahnert et al., 2013; Martin-Bello et al., 2019; Mercedes-Martín et al., 2014; Reid and Browne, 1991; Tosti and Riding, 2017b). Secondary alteration, sediment compaction and diagenesis alter the chemistry and crystalline structure of the material that makes up an ancient microbialite, but the mesoscale morphologies usually remain unchanged. Microscale features such as the morphology of individual or groups of laminae are influenced by water depth, energy levels and sediment supply (Dupraz et al., 2006; Hofmann, 1973; Logan et al., 1964; Riding, 2000). However, the most significant factor controlling microscale features are the ecological interactions and behaviours of the formative microbes (Awramik and Semikhatov, 1979; Gabelein, 1974; Omelon et al., 2013; Tosti and Riding, 2017b). Microbialites form by either accretion of transported sediment or *in-situ* carbonate mineral precipitation (See section *2.4.1. Microbialite Formation*), both leading to the preservation of calcified microbial cells, EPS sheaths and entrained sediment (Black, 1933; Logan et al., 1964). Where they differ is the extent to which the environment or microbial behaviour influences the microbialite shape.

However, as both mechanisms produce similar grain textures that are difficult to distinguish even at the microscale, made worse by varying extents of alteration and low-grade fluid metamorphism, determining which mechanism likely led to the creation of the preserved microbial features is contentious and may have a large degree of subjectivity (Fairchild, 1991; Corkeron et al., 2012; Bosak et al., 2013). Nevertheless, decades of research on microbialites from different ages and depositional environments have shown that a continuum likely exists between sediment accretion and *in-situ* microbially mediated microbialites (Black, 1933; Criado-Reyes et al., 2023; Dupraz et al., 2009; Dupraz et al., 2004; Kamber and Webb, 2001; Monty, 1977; Visscher et al., 2000; Webb et al., 1998). However, there are some features that point to the formative mechanism.

Lack of microbial fossils, low to moderate relief columns, complex laminar alternation, and microscale texture variation all point towards a sediment accretion mechanism (Hofmann, 2000; Riding, 1993; Riding, 2008; Tosti and Riding, 2017b). Tosti and Riding (2017b) suggested further that frequent branching is also an indicator of grain trapping formation, as well as the presence of laterally continuous laminations within both the microbial and intercolumn sediment. Under this mechanism, the main control on microbialite growth are abiotic forces, as the microbes are buried by detritus, and the mat community growing during interrupted burial periods.

In contrast, vertically oriented crystals, clear terminations along column walls, clotted or peloidal grains, sparry crusts or intercalations, fenestrae, calcified microbes, and clear textural difference between microbialite and intercolumn sediment all point towards *in-situ* precipitation (Riding, 1993; Tosti and Riding, 2017b). There is a disparity in the exact formative conditions created through microbial mediation. One of the first microbialite formation theories postulated by Gabelein (1974) and Monty (1976) involved a motile, photosensitive cyanobacterial response. The motile filamentous cyanobacteria associated with stromatolites would align themselves vertically during the day, creating a layer of erect filaments within the surface. This tightly packed layer leaves no space for detritus to settle, and is preserved as light, glassy laminae, with little detrital material. During the night, the filamentous bacteria migrate into a horizontal position, creating a surface of thinly stacked bacteria that becomes covered and further compressed by detrital deposition. This compacts the microbes, leading to the preservation of darker, densely packed layers with a higher detrital content. Semikhatov et al. (1979) proposed an alternative theory, where dark laminae indicate periods of increased microbial growth and elevated productivity, with the dark colouration due to a high concentration of organic matter. Light laminae would thus indicate periods of decreased or supressed laminae growth, potentially due to interruptive currents or increased sedimentation rates. This would lead to detrital sediment accumulation within the microbial mat, causing the mat to be lithified as lighter, organic matter poor lamina. The dark laminae would thus be composed of organic rich automicrite, while the light laminae would be composed of recrystallized clastic grains with minor organic constituents. While an interplay of microbial growth and sediment supply is essential to either mechanism, this sequence is antithetical to the model postulated by Gabelein (1974) and Monty (1976).

Based on the features identified in the samples from Site 1, it is likely that the columnar stromatolites formed predominantly through biologically mediated precipitation, with the dominance of grumous dark laminae indicating growth was largely rapid or favourable and beds of light laminae indicating more biologically stressed conditions, such as sunlight fluctuations, current turbulence, or increased sedimentation deposition.

6.4.5. Feature Summary

Altogether, the evidence suggests that the reef was located at the transition between the subtidal offshore zone above storm-wave base, and the deep intertidal zone that experienced tidal and wave action. The widespread occurrence of wide stromatolite domes indicates that the reef was within the intertidal zone more frequently. Smaller scale columns potentially formed as ridges between the domes, potentially indicating regular water depth fluctuations, as columns tend to form in deeper waters that experience higher energy levels. However, they can also form in shallower waters if there is high synoptic relief. Current turbulence was common, as there are both lateral and vertical shifts in microbialite morphology and laminae architecture. This turbulence was caused or enhanced by the reef itself, potentially creating pockets of increased turbulence or regions protected from it, explaining how both anastomosed columns and thick planar stromatolites formed within 20 m of each other. This also could explain how certain columns experienced consistent harmonized laminar growth within pockets that experienced consistent sediment supply and low turbulence. These harmonized laminae are usually lighter, so even though environmental energy levels were stable, sunlight may have been inadequate. The lateral variation in laminae architecture combined with a lack of vertical cyclicity further supports that turbulence was common, probably due to being at the transition of two regimes with different energy levels.

The dominance of dark laminae indicates high microbial activity, but these dark laminae could also be influenced by organic matter preservation and diagenetic overprinting. Light laminae are usually thin veneers but are more prominent in certain columns and may form thick tented beds. These lighter layers indicate periods of time or sections of the reef that experienced strained microbial mat growth, due to a range of factors such as decreased sunlight penetration, localised current turbulence, or increased sedimentation rate. Diffuse or graded boundaries between adjacent laminae could indicate calcite recrystallization or rapid precipitation (Awramik and Semikhatov, 1979). Infrequent column linkages show that there were periods of stability after the intercolumn space was filled. The microbial mats were able to expand laterally and colonise more substrate during these short-lived periods before turbulence or sedimentation rates prompted columnar growth. Branching in some columns indicate periods of current or sediment disruption, causing the mat communities to aggregate vertically to minimise the amount of turbulence experienced, and potentially to further improve sunlight acquisition. Rarely, laminae become more parabolic towards the tops of a column, indicating the microbes were intensely trying to minimise the distance from the photic zone.

The predominance of crystalline spar within the non-microbial and intercolumn sediments suggest these materials likely experienced reworking and post-depositional deformation. The non-microbial material and intercolumn sediments were thus transported to the microbial reef, contrasting with the micrite and grumous clots of the columnar material, which were precipitated in-situ by the microbial communities. The dark grains common throughout the thin sections are likely oxides or organic matter that were entrained within the non-microbial sediments. The nebulous white structures better seen at the mesoscale (**Figure 4**, **Figure 5** and **Figure 10**) were revealed at the microscale to consist of low relief, recrystallised microspar (**Figure 13B**). It is possible that these were cavities subsequently filled with cement, potentially even burrows. The origin and petrography of the darkened angular fragments, subrounded clasts and ringed structures within the intercolumn best seen in the mesoscale (**Figure 4**, **Figure 5**, **Figure 7**, **Figure 11** and **Figure 12**) are still a mystery.

Microscale analysis shows that some of the ringed and subrounded structures (See the ringed structures in **Figure 5** and **Figure 7**) are micrite walled cavities filled with sparry cement (**Figure 16B**). These well-defined walls could point to shells or skeletal structures that have been filled with secondary cements. These structures contrast with the darker, angular fragments ranging from ~0.1 mm to 3 mm seen scattered throughout every rock sample. Microscale analysis shows that these intraclasts are composed of high relief dark micrite relative to the surrounding lighter micrite and microspar intercolumn sediments. These could be partially agglutinated carbonate muds that were entrained and redeposited between the intercolumn space of the columnar stromatolites (Tosti and Riding, 2017a). More rigorous palaeontological and petrographic analysis of the microbial columns and the reef as a whole would be required to determine whether these ringed structures are fossils, or we simply have a wide morphological range of rock fragments.

The thin section petrography, XRD analysis (See *7.2.1. XRD Analysis*) and SEM imaging (See *10.1. Appendix 1: B-SEM Images)* all show that, regardless of location within the intercolumn or microbial structures, there is a homogeneity of calcium carbonate across the rock sample set. Tosti and Riding (2017a, 2017b) noted an abundance of carbonate mud in and around stromatolite columns and suggest that this abundance was due to periods of dramatic water column calcite precipitation, referred to as "whitings" (Grotzinger, 1994; Knoll and Swett, 1990). Decreasing CO2 partial pressure, due to oxygenic photosynthetic microbes, could have rapidly altered the calcite saturation of the local waters, leading to the spontaneous precipitation of calcite, the whiting of the water column and the widespread preservation of calcium carbonate muds in both microbial and intercolumnar spaces (Grotzinger and Knoll, 1999). It is possible a similar situation occurred during the formation of the microbial reef.

7. Chemical Analysis

7.1. Sample Processing

In situ sampling and digestion was performed at the Department of Geological Sciences at the University of Cape Town. Specific microbial horizons across the sample set were microdrilled using an 8 mm drill bit fitted to a variable speed rotary tool, allowing for precise extraction of the target material from a single, laterally continuous horizon or areas within the intercolumn sediment. Three chemical analyses were performed on the powdered subsamples: *7.2.1. XRD Analysis* to confirm the calcite mineralogy, *7.3.1. SLI Analysis* to compare against bulk analysis of contemporaneous Nama Group deposits and *8. Rare Earth Element Analysis* to determine the redox conditions the microbialites formed in.

7.2. Mineralogy

7.2.1. XRD Analysis

15 Powdered subsamples were selected for XRD analysis at UCT's Department of Chemical Engineering. A Bruker AXS D8 Advanced X-ray diffractometer with Co-anode and K radiation was used for analysis. The data from the analysed subsamples were analysed using the Profex program, generating 15 diffractograms.

7.2.2. Results

The goal of this analysis was to confirm that the samples were predominantly made of calcium carbonate, in the form of calcite. The samples selected included representative material from the intercolumn sediments, the microbial laminae within the columns and detrital intercalations within the columns. This sampling ultimately showed the material, regardless of location in column or intercolumn, is composed out of calcite and quartz, with two samples containing dolomite (**Figure 19**). The peaks for calcite, dolomite and quartz were based on experimental analysis by Reinhard Kleeberg at the Freiberg University of Mining and Technology and from the RRUFF™ Project mineral database created at the University of Arizona's Department of Geosciences.

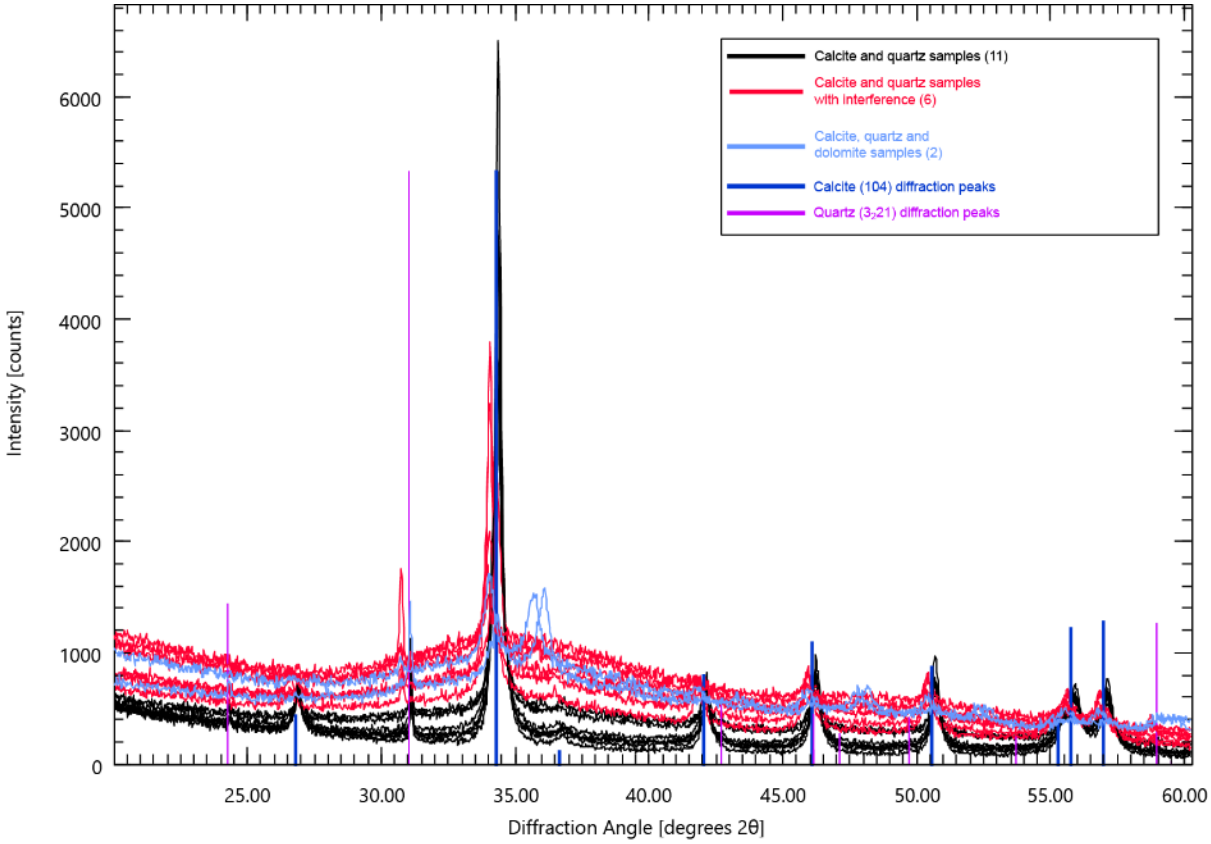

Figure 19: *Diffractograms of the randomly selected powdered samples, showing the rough alignment of the rocks with calcite,* quartz, *and dolomite. Dolomite peaks have not been listed, but the two peaks in blue between 35.5 ºΘ and 36.5 ºΘ align with dolomite.*

7.3. Carbon and Oxygen Isotopes

7.3.1. SLI Analysis

46 of the powdered subsamples were selected for $\delta^{13}C$ and $\delta^{18}O$ isotope analysis. The goal of this was to compare the general trends of the targeted samples to the bulk analysis performed by Tostevin et al. (2016b). Analysis was performed in the Stable Light Isotope Lab in the Department of Archaeology. Vials were pre-treated before analysis. An in-house cleaning method was performed, whereby the analysis vials were washed with alternating phases of dilute H_3PO_4, distilled water and Milli-Q water before being heated in a furnace at 500°C for three hours. The cleaned vials were filled with 0.2 to 0.3 mg of powder from each powdered subsample. Three inorganic carbonate standards were also weighed out (between 0.18 and 0.22 mg): IAEA-CO-8 and IAEA-603 (referred to as Carrara-Marmor New internally) , corrected to Vienna Pee Dee Belemnite (V-PDB), as international marine CO_2 and O_2 standards and Cavendish Marble ($\delta^{13}C$ = 0.34 ‰; $\delta^{18}O$ = -8.95 ‰) as an internal.

The method outlined in Luyt et al. (2019) was then followed, running the pre-treated samples through a Thermo Scientific GasBench II, and finally analysing the evolved gas with a Delta Plus XP isotope ratio mass spectrometer. The corrected isotope data is presented and discussed along with the rare earth data in section *8. Rare Earth Element Analysis* below.

8. Rare Earth Element Analysis

8.1. Sample Analysis

15 ± 0.1 mg of material was weighed out and then each powdered subsample was placed into 15 ml analysis tubes. A modified sequential digestion procedure for targeted digestion of the carbonate phases, while excluding any non-carbonate phases was performed, as outlined in Tostevin et al. (2016a). The following adaptations where made:

(1) the first (0–20%) and second (20–60%) digestion steps were combined due to the small, powdered subsample size.

(2) 1% HNO_3 was used in the dissolution to increase liquid volumes.

887 µl of dilute acid was pipetted into each analysis tube and mechanically mixed for 30 seconds. The tubes were then placed in a centrifuge and spun at 4000 rpm for 10 minutes. 840 µl of the leachate was then pipetted out from each tube, with care taken not to disturb the remaining powder, and transferred into clean analysis tubes. The samples were then placed in a drying oven for 15 hours at 80°C. The dried down tubes were sent to UCL, where they were resuspended in 2% nitric acid and analysed via ICP-MS. The acid digested subsamples were further diluted to 10 ml with 2% HNO_3 at UCL. The major elements (Al, Ba, Ca, Fe, Mg and Mn) were analysed through solution ICP-OES on a Varian 720. REE + Y were analysed via solution ICP-MS on an Agilent 7900. UCL's Cross-Faculty Elemental Analysis Facility uses In and Re as internal standards, however they were not corrected to the analysed data due to uncertainty about their appropriateness for REE + Y analysis. The raw data was then pre-screened at UCL to test for oxide interference on CeO, PrO and BaO. No significant oxide contributions were found, thus matrix effects can be discounted as a potential source of contamination, even though some samples contained high Ba concentrations. Ca concentrations were high in some cases, due to the correction to UCT's marble standard that contained 39.6%. The raw concentrations were mass corrected based on the digestion process and then the REE + Y concentrations were normalised to the Post-Archaean Australian Shale (PAAS) composite (Taylor and McLennan, 1985). The results were further screened to remove any signals outside of the detection range of the spectrometer, resulting in the acquisition of 84 clear REE signals.

8.2. Results

Anomalies and elemental ratios are reported for each subsample in **Table 3** and **Table 4** below. Elemental ratios show the relative enrichment of an element or a suite or elements relative to adjacent REEs. The Bell-Shaped Index (BSI; equation [1]) approximates any post-depositional phosphate or Fe oxide enrichment by comparing the abundance of the middle REE (MREE) to the light REE (LREE) and heavy REE (HREE) (Haley et al., 2004; Martin et al., 2010; McArthur and Walsh, 1984), the Pr_{SN}/Yb_{SN} ratio indicates the abundance of the LREEs compared to the HREEs, while the Yb_{SN}/Nd_{SN} ratio is an indicator of HREE enrichment (Johannesson et al., 2014). We also report the Y anomaly as the Y/Ho ratio (*not* shale normalised), a key indicator of seawater conditions (Bau, 1999; Bau and Dulski, 1999; Diakonov et al., 1998).

Anomalies quantify the measured abundance of an element compared to the expected concentration based on an interpolation between neighbouring REEs (Neuweiler et al., 2003). Ce, Eu and La can all exhibit anomalous behaviour relative to their neighbours (equations [2, 3 and 4]).

$$BSI = \frac{2*\left(\frac{([Sm]_{SN}+[Gd]_{SN}+[Dy]_{SN})}{3}\right)}{\left(\frac{[La]_{SN}+[Pr]_{SN}+[Nd]_{SN}}{3}\right)+\left(\frac{[Ho]_{SN}+[Er]_{SN}+[Tm]_{SN}+[Yb]_{SN}+[Lu]_{SN}}{5}\right)} \quad [1]$$

$$Ce_{SN}/Ce^{*}_{SN} = \frac{[Ce]_{SN}}{([Pr]_{SN})^{2}/[Nd]_{SN}} \quad [2]$$

$$Eu_{SN}/Eu^{*}_{SN} = \frac{2*[Eu]_{SN}}{[Sm]_{SN}+[Gd]_{SN}} \quad [3]$$

$$La_{SN}/La^{*}_{SN} = [Pr]_{SN}^{3}/[Nd]_{SN}^{2} \quad [4]$$

The sum of the REE content (∑REE) of the samples are generally low, with an average of 0.77 ± 0.31 ppm (**Table 3**). The samples have positive La anomalies (mean La_{SN}/La^{*}_{SN} = 1.36 ± 0.06) and are HREE enriched relative to LREE (mean Pr_{SN}/Yb_{SN} = 0.82 ± 0.13; mean Yb_{SN}/Nd_{SN} = 1.12 ± 0.13). There is a small enrichment of the MREE (mean BSI= 1.21 ± 0.05), large Y anomalies (mean 34.46 ± 2.32, ranging from 29.46 to 40.63), positive Eu anomalies (mean Eu_{SN}/Eu^{*}_{SN} = 1.74 ± 0.82, ranging from 1.10 – 4.62) and no significant Ce anomalies (mean Ce_{SN}/Ce^{*}_{SN} = 0.96 ± 0.05, ranging from 0.86 – 1.04). To summarise, the main geochemical properties of the samples are weak HREE and MREE enrichment, no Ce anomalies, and pronounced positive Eu and Y anomalies. The HREEs experience increased complexation with carbonate ions, while lighter REEs form complexes with other particles that remove them from the water source, explaining the increasing trend towards the HREEs (Byrne and Kim, 1990; Shaojun and Mucci, 1993).

Subsample Name	Sample Nature	Rock Location	Horizon	BSI	Ce_{SN}/Ce^{*}_{SN}	Eu_{SN}/Eu^{*}_{SN}	La_{SN}/La^{*}_{SN}	Yb_{SN}/Nd_{SN}	Y/Ho	∑REE (ppb)	$\delta^{13}C$	$\delta^{18}O$
Overall				1.21 ± 0.05	0.96 ± 0.05	1.74 ± 0.82	1.15 ± 0.09	1.12 ± 0.13	34.46 ± 2.32	0.77 ± 0.31	1 ± 0.37	-14.05 ± 2.41
BO1a.1c	IS	Middle intercolumn between Columns F and G		1.2	0.89	4.62	0.98	0.99	32.76	1.31	N/A	
BO1a.5a.1		Column A	1st	1.21	1	4.55	1.14	1.16	31.37	0.79	-0.14	-13.98
BO1a.5a.2		Column A	2nd	1.24	1	4.01	1.11	1.13	31.61	0.53	-0.75	-13.54
BO1a.5a.3	ML	Column A	3rd	1.22	1.01	2.8	1.17	1.19	33.95	0.49	0.36	-12.41
BO1a.5g.1		Column G	1st	1.24	1	4.42	1.14	1.07	31.21	0.7	0.56	-12.56
BO1a.5g.2		Column G	2nd	1.23	1.03	2.86	1.14	1.18	29.46	0.68	0.64	-14.97
$_{mean}$**BO1a**$_{microbial}$				1.23	1.01	3.73	1.14	1.15	31.52	0.64	0.13	-13.49
BO1b.3	IS	Grey sediment between section 4 and 5, above the orange sediment and below the green sediment		1.24	0.92	1.94	1.12	0.8	33.74	0.95	N/A	
BO2.1	DS	Red sediment to the right of section H		1.23	1.01	3.25	1.17	0.85	30.2	1.9	0.81	-10.20
BO2.5a.1			1st	1.28	0.97	2.13	1.16	0.96	36.85	0.55	0.82	-9.53
BO2.5a.2		Column A	2nd	1.28	1.01	1.57	1.21	1.11	32.99	0.47	0.69	-11.67
BO2.5a.3			3rd	1.25	1	1.65	1.16	1.08	32.83	0.66	0.92	-15.01
BO2.5a.4			4th	1.21	1.04	1.26	1.22	1.25	32.97	0.87	0.95	-15.77
BO2.5b.1			1st	1.24	1.02	1.38	1.29	1.11	33.42	0.79	1.06	-14.50
BO2.5b.2		Column C	2nd	1.25	0.99	3.79	1.18	0.95	34.2	1.01	1.09	-15.53
BO2.5b.3			3rd	1.24	1.01	1.47	1.22	1.19	32.88	0.93	0.98	-13.96
BO2.5c.1	ML		1st	1.23	1	1.17	1.25	1.2	34.12	0.75	1.10	-18.85
BO2.5c.2		Column F	2nd	1.25	0.99	1.98	1.18	1.07	32.58	0.85	1.20	-16.65
BO2.5c.3			3rd	1.22	1.03	1.28	1.29	1	33.51	0.72	1.12	-17.26
BO2.5d.1		Column G	1st	1.23	1.02	1.28	1.29	1.15	33.09	0.75	1.11	-18.35
BO2.5d.2			2nd	1.24	1	1.18	1.22	1.11	32.51	0.77	1.12	-18.78
BO2.5f		Section I, second column from the right		1.23	1.02	1.19	1.24	1.12	32.09	0.74	1.49	-13.76
BO2.5g		Section I, 1st column from the right		1.21	1.01	1.19	1.21	1.15	32.34	0.76	1.08	-18.13
$_{mean}$**BO2**$_{microbial}$				1.24	1.01	1.61	1.22	1.1	33.31	0.76	1.04	-15.2
PSP.1	DS	Orange sediment between columns		1.29	0.96	3.46	1.15	0.8	30.5	2.62	1.32	-7.71
RT1.5d.1			1st	1.22	1.01	1.52	1.16	1.15	33.88	0.91		
RT1.5d.2		Column D	2nd	1.26	1.01	1.32	1.19	1.18	32.95	0.88		
RT1.5d.3	ML		3rd	1.27	0.99	1.41	1.15	1.16	32.67	0.94	N/A	
RT1.5c		Column C		1.24	1.01	1.25	1.18	1.27	34.38	0.81		
RT1.5e		Column E		1.23	1	1.24	1.15	1.33	32.53	0.85		
$_{mean}$**RT1**$_{microbial}$				1.24	1	1.35	1.17	1.22	33.28	0.88		

Table 3: *REE characteristics and SLI ratios of each microdrilled subsample from rocks BO1a to RT1. Sample nature states whether the subsample is from the intercolumn sediment (IS), detrital sediment (DS) or microbial laminae (ML). Horizon indicates at which layer the related subsample came from, numbered bottom to top.*

Although the HREE and MREE enrichment is slightly different to seawater (Nozaki and Zhang, 1995), they are consistent with modern carbonate sediments. All together the REE patterns indicate the preservation of a seawater signal (Bau et al., 1997; Nozaki and Zhang, 1995). The key differences from modern seawater are a lack of any significant Ce anomaly and large Eu anomalies.

Subsample Name	Sample Nature	Rock Location	Horizon	BSI	Ce_{SN}/Ce^*_{SN}	Eu_{SN}/Eu^*_{SN}	La_{SN}/La^*_{SN}	Yb_{SN}/Nd_{SN}	Y/Ho	∑REE (ppb)	$\delta^{13}C$	$\delta^{18}O$
RT3.5a.2	ML	Column A		1.23	1.01	1.26	1.21	1.32	33.17	0.88	0.95	-14.50
RT3.5d		Column D		1.23	1.02	1.13	1.21	1.24	32.41	0.76	1.01	-14.28
RT3.5e.1		Column E	1st	1.22	0.96	1.55	1.12	1.19	30.25	0.98	1.12	-12.97
RT3.5e.3 (rep)			2nd	1.22	0.97	1.4	1.17	1.18	32.18	0.9	1.07	-14.21
		$_{mean}$**RT3**$_{microbial}$		1.23	0.99	1.34	1.18	1.23	32	0.88	1.04	-13.99
RT4.2a	IS	Lower intercolumn between Columns A and B		1.18	0.92	2.22	1.11	0.91	34.63	0.81	N/A	
RT4.5a.1	ML	Column A	1st	1.24	1.02	1.14	1.25	1.2	33.87	0.8	1.13	-16.62
RT4.5a.2 (rep)			2nd	1.18	1	1.13	1.22	1.16	33.85	0.82	1.20	-16.17
RT4.5a.3			3rd	1.25	1.03	1.34	1.31	1.28	34.3	1.01	1.07	-12.01
RT4.5b.2		Section F	1st on left	1.22	1.03	1.28	1.25	1.28	35.74	0.67	1.13	-14.43
RT4.5b.3			2nd on left	1.27	0.97	1.24	1.16	1.28	33.15	0.82	1.23	-15.46
RT4.5c (rep)		Section C		1.21	0.99	1.37	1.29	1.03	34.72	0.71	1.01	-9.47
RT4.5d.2		Section F	1st on right	1.2	1.02	1.28	1.31	1.25	34.31	0.78	1.07	-13.23
RT4.5d.3			2nd on right	1.23	0.98	1.22	1.23	1.23	32.82	0.67	1.08	-12.82
RT4.5e		Column I		1.25	1.02	1.43	1.24	1.2	31.5	0.92	0.88	-15.44
		$_{mean}$**RT4**$_{microbial}$		1.23	1.01	1.27	1.25	1.21	33.81	0.8	1.09	-13.96
RT5a.3a	DS	Left of Column A		1.14	0.89	2.05	1.06	1.06	36.49	0.91	N/A	
RT5a.5a.1	ML	Column E	1st	1.25	0.99	1.23	1.31	1.24	33.85	0.7	0.97	-12.68
RT5a.5a.3 (rep)			2nd	1.25	0.97	1.36	1.23	1.06	34.34	0.87	0.86	-14.18
RT5a.5b.2		Column F		1.14	1.01	1.37	1.33	1.42	32.27	0.9	1.08	-12.30
RT5a.5c.1		Column G	1st	1.27	0.99	2.04	1.2	1.03	32.65	0.84	1.19	-14.41
RT5a.5c.2			2nd	1.24	0.99	1.86	1.19	1.24	33.86	0.82	1.04	-14.56
RT5a.5c.3 (rep)			3rd	1.28	0.99	1.95	1.25	1.03	33.67	0.93	1.11	-13.60
RT5a.5c.4			4th	1.25	0.95	1.29	1.21	1.11	33.24	0.82	1.00	-14.28
RT5a.5e.1		Column C		1.27	1	2.54	1.21	0.99	31.98	0.9	1.17	-12.53
		$_{mean}$**RT5a**$_{microbial}$		1.24	0.99	1.71	1.24	1.14	33.23	0.85	1.05	-13.57
RT6a.2	IS	Very dark grayish pink sediment left of Column E		1.35	1	3.46	1.18	0.62	33.05	1.61	1.27	-15.75
RT6a.4	DS	Dark moderate red clasts at the top of Column E branches		1.15	1.01	1.84	1.22	0.82	32.42	1.17	1.38	-10.39
RT6a.5a.1	ML	Section A		1.18	1	1.26	1.23	1.09	35.29	0.43	1.22	-12.83
RT6a.5e	ML	Section F		1.2	1.01	1.1	1.24	1.15	34.4	0.35	1.16	-13.84
		$_{mean}$**RT6a**$_{microbial}$		1.19	1.01	1.18	1.24	1.12	34.85	0.39	1.26	-13.2
SNO.1d	IS	Intercolumn between Column H and Section I		1.21	0.91	1.44	1.04	0.87	33.45	0.65		
SNO.5e.1	ML	Column F	1st	1.17	0.9	1.16	1.04	1.11	36.53	0.55		
SNO.5e.2			2nd	1.17	0.9	1.31	1	1.2	35.69	0.62		
SNO.5e.3			3rd	1.19	0.91	1.19	1.03	1.13	35.89	0.67		
SNO.5f.1		Column G		1.15	0.9	1.26	1.01	1.26	36.34	0.58		
SNO.5g.1		Column H		1.17	0.9	1.14	1.02	1.18	36.09	0.38		
SNO.5h.2		Section I	1st	1.17	0.89	1.24	1.02	1.14	36.32	0.57		
SNO.5h.3			2nd	1.19	0.9	2.01	1.02	1.03	37.52	0.67		
		$_{mean}$**SNO**$_{microbial}$		1.17	0.9	1.33	1.02	1.15	36.34	0.58		
SPO.5a.1	ML	Column A	1st	1.14	0.86	1.61	1.03	1.21	38.1	0.6		
SPO.5a.2			2nd	1.17	0.9	1.5	1.02	1.17	36	0.46		
SPO.5a.3			3rd	1.17	0.9	1.39	1.07	1.2	40.63	0.49		
SPO.5b.1		Column B	1st	1.17	0.9	1.31	1.1	1.08	37.75	0.51		
SPO.5b.2			2nd	1.16	0.87	1.33	1	1.17	37.85	0.54		
SPO.5c.2		Column C	1st	1.14	0.87	1.26	1.06	1.21	38.39	0.45	N/A	
SPO.5c.3			2nd	1.18	0.9	1.24	1.02	1.16	35.91	0.58		
SPO.5d.1		Column D	1st	1.14	0.91	2.29	1.08	0.96	36.34	0.51		
SPO.5d.2			2nd	1.17	0.91	1.45	1.05	1.1	37.28	0.57		
SPO.5e.1		Column E	1st	1.12	0.88	1.62	1.04	1.22	37.3	0.69		
SPO.5e.2			2nd	1.17	0.91	1.33	1.07	1.03	36.2	0.58		
SPO.5f.1		Column F	1st	1.1	0.9	1.35	1.08	1.16	38.82	0.47		
SPO.5f.2			2nd	1.16	0.89	1.32	1.03	1.09	36.39	0.63		
SPO.5f.3			3rd	1.17	0.91	1.59	1.1	1.13	37.62	0.72		
SPO.5g.1		Section G	1st	1.15	0.91	1.43	1.11	1.12	36.34	0.62		
SPO.5g.2			2nd	1.15	0.91	1.3	1.08	1.1	38.07	0.56		
SPO.5h		Section H		1.18	0.87	1.32	1.07	1.21	38.29	0.6		
SPO.5i.1		Section I	1st	1.18	0.88	1.42	1.07	1.09	37.71	0.63		
SPO.5i.2			2nd	1.23	0.9	1.97	1.03	1	36.57	0.95		
SPO.5i.3			3rd	1.17	0.91	2	1.04	1.07	35.24	0.85		
SPO.5i.4			4th	1.15	0.93	1.68	1.14	1.1	38.02	0.56		
		$_{mean}$**SPO**$_{microbial}$		1.16	0.9	1.51	1.06	1.12	37.37	0.6		

Table 4: *REE characteristics and SLI ratios of each microdrilled subsample from rocks RT3 to SPO. Sample nature states whether the subsample is from the intercolumn sediment (IS), detrital sediment (DS) or microbial laminae (ML). Horizon indicates at which layer the related subsample came from, numbered bottom to top.*

8.3. Discussion

8.3.1. Subsample REE Patterns

The data share similar broad patterns, with small positive Eu anomalies, superchondritic Y/Ho ratios and moderate HREE enrichment (**Figure 20**) when compared to the bulk rock REY data for the Nama Group reported in Tostevin et al. (2016) (**Figure 21**). However, there are minor differences in the range and average for some of these anomalies. The subsamples have higher average Eu anomalies (1.74 vs. 1.17), lower average Y/Ho ratios (63.9 vs. 75.9), no positive Ce anomalies (0.96 vs. 1.28) and lower ∑REE (0.77 ppm vs. 1.26 ppm). The subsamples also have smoother REE patterns and a smaller range for REE anomalies (**Figure 22**). Overall, the study samples show more consistent data when compared to the bulk rock analysis. Possible reasons may be due to the precision of the micro-drilling technique and / or the preservation capabilities of microbialites. The *in-situ* drilling technique directly targets microbial material, as opposed to bulk rock analysis that included a wider range of carbonate grains, cements and potential contaminants from microbial and non-microbial settings. Furthermore, microbialites are known to excellent preservers of seawater signals (Webb and Kamber, 2000), so by focusing on the laminae, we are increasing the precision of the dataset.

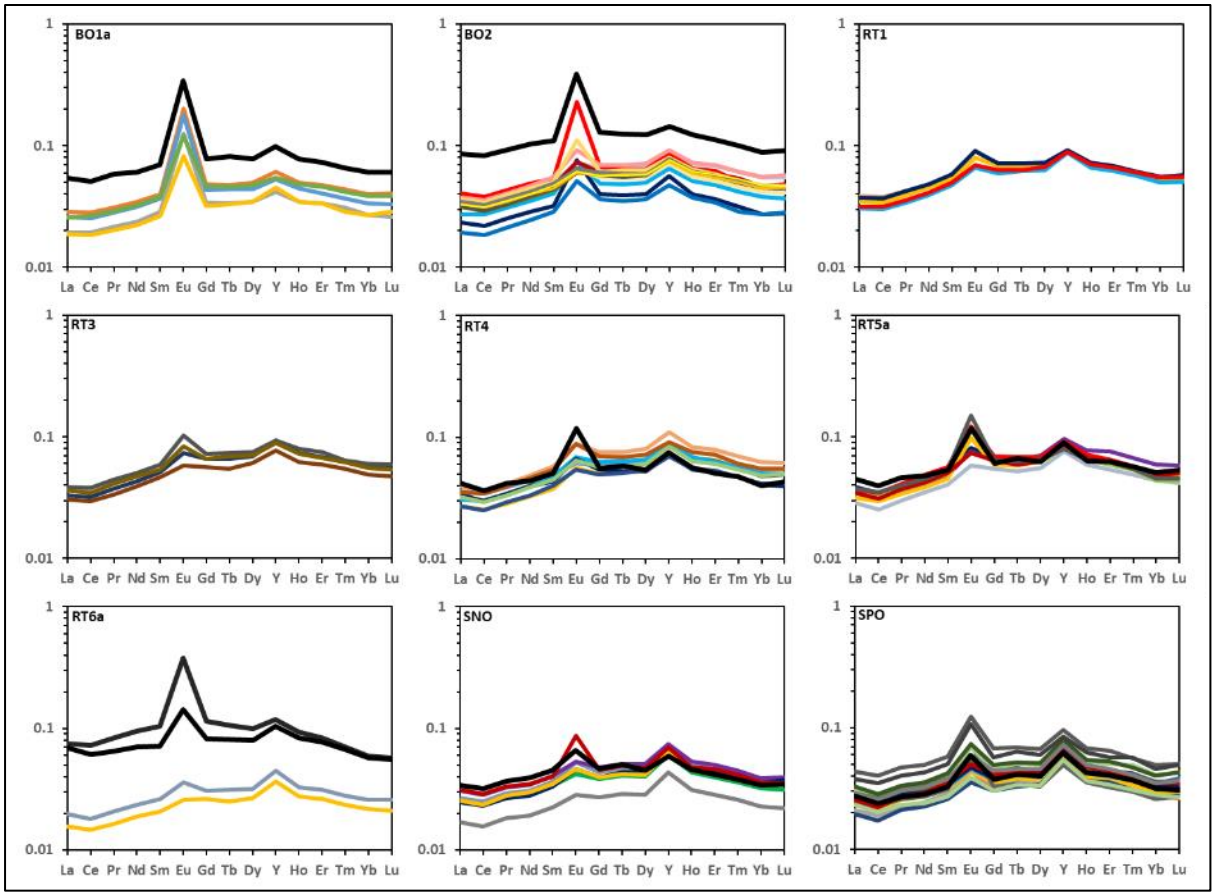

Figure 20*: REE patterns of the nine rigorously sampled specimens. Black lines indicate the detrital or non-microbial samples. Samples are normalised to PAAS (log scale)*

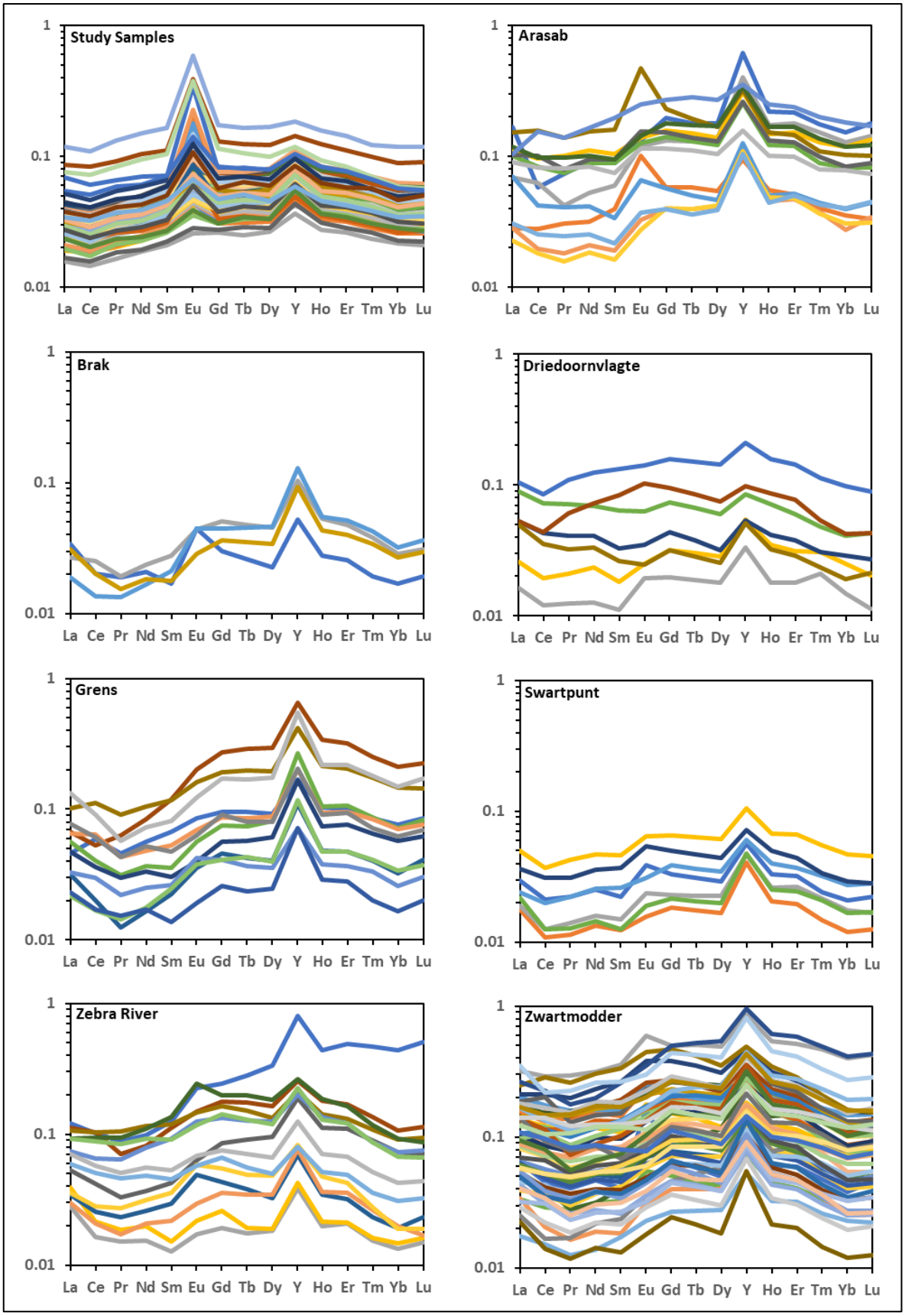

Figure 21: *Comparisons of the REE patterns of this study against the Nama bulk rock collected by Tostevin et al. (2016). The sample sites listed are from contemporaneous carbonates deposited within the Zaris Basin, Namibia (Wood et al., 2015). Samples are normalised to PAAS (log scale)*

The overall REE pattern across the subsamples show preservation of a primary seawater signal (**Figure 21**), evident by depletions in LREE, comparatively enriched HREEs and superchondritic Y anomalies (Frimmel, 2009; Zhang and Nozaki, 1996). Pronounced or consistent Eu anomalies in microbialites have been associated with the mixture of hydrothermal fluid in the water column or the precipitation of Fe-sulphides (Derry and Jacobsen, 1990; Frimmel, 2009; Zhang and Nozaki, 1996). The anomaly can either be positive or negative, depending on the redox state and sulphur activity in the fluid. An alternative theory for a persistent anomaly could be from the biosorption of Eu into microbial mats, whereby Eu passively accumulates within microbial mats through ion-exchange reactions with carboxyl functional groups within the surface of bacterial cells (Kazak et al., 2018; Vijayaraghavan et al., 2010; Vijayaraghavan and Yun, 2008). It is thus possible that the Eu anomalies seen across the microbial sample set may be due to this indirect accumulation of Eu. However, comparing the Eu anomalies of the intercolumn sediments and the columnar microbialites shows there is no preferential elevation in the microbial laminae.

In fact, it is apparent that the subsamples with the highest Eu anomalies are non-microbial (**Figure 23**), with values peaking at 4.62 (**Table 3**). This suggests that the Eu anomalies cannot be an artifact of biosorption, and it is likely an ambient signal, indicating that the seawater had an acidic, reducing hydrothermal component (Frimmel, 2009; German and Elderfield, 1990). Building on this, the non-microbial subsamples have higher Fe, Mn, and Al content than the sampled microbial column material (**Figure 23**). Lastly, subsamples RT6a.4 and BO2.1 come from patches of red-orange sediment and have the highest Fe concentrations (15.98 ppm in **Table 4** and 3.65 ppm in **Table 3** respectively), which suggests that these patches of red-orange sediment found throughout the rock samples contain iron oxides. Altogether, these elevations in typically terrigenous elements could indicate the material from both the intercolumn fill and from detrital clasts embedded within microbial columns are sourced from sediments transported into the microbial reefs. However, contrasting these findings are no significant differences between the Ce anomalies, LREE and HREE enrichments, ∑REE and $\delta^{13}C$ ratios of the microbial and intercolumn material (**Figure 24**). It is likely that further sampling of the intercolumn material would be required to elucidate any real compositional differences.

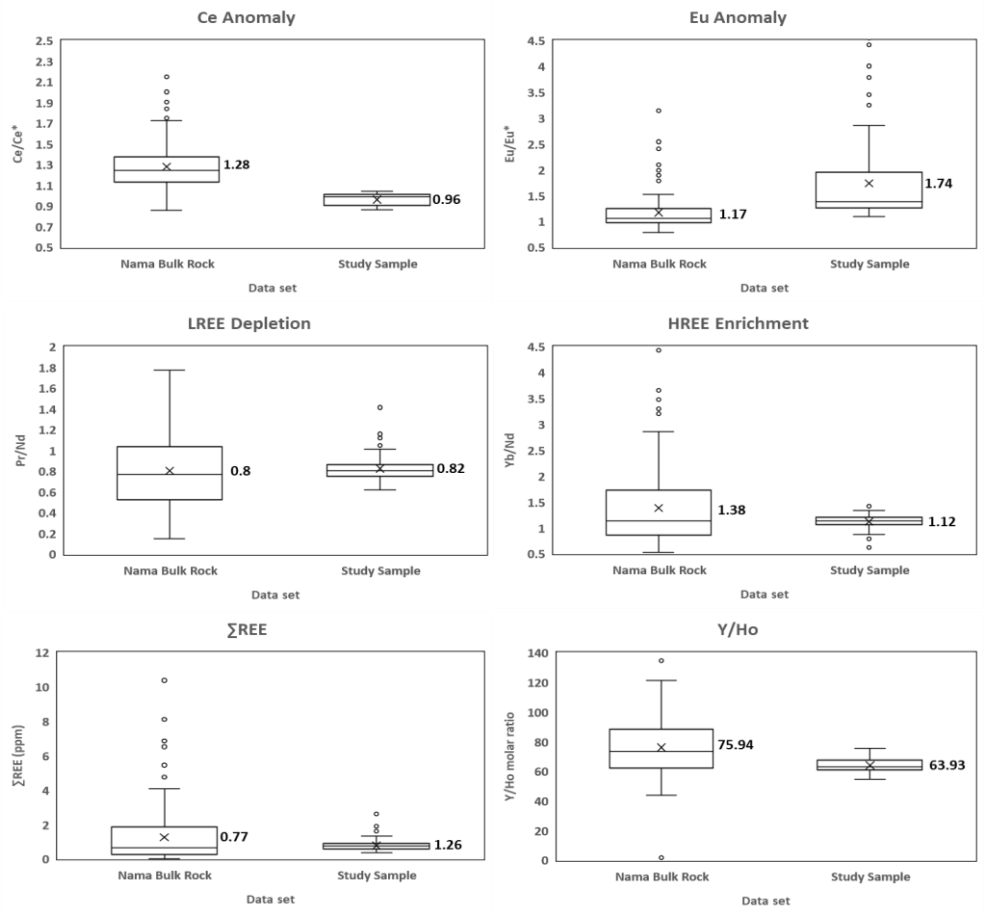

Figure 22: *Comparisons of REE anomaly, ratio and REE content of the bulk Nama Group (Tostevin et al., 2016a) against the targeted analysis of this study.*

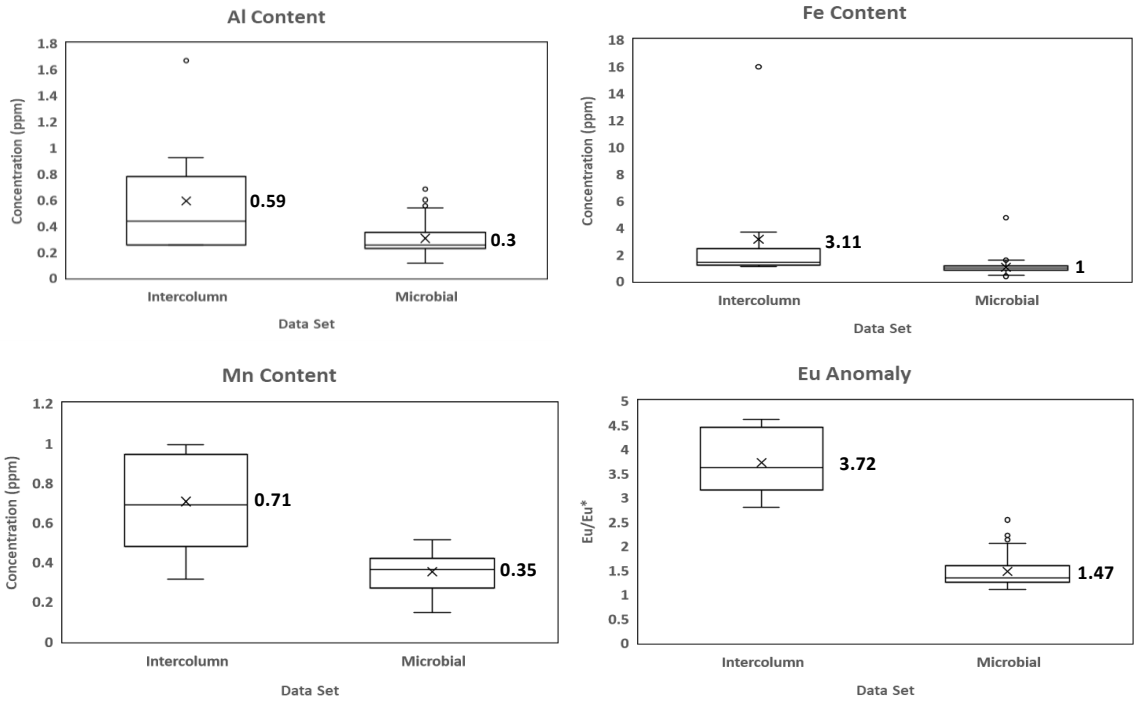

Figure 23: *Comparisons of the chemical parameters of the intercolumn and microbial material with the most significant differences.*

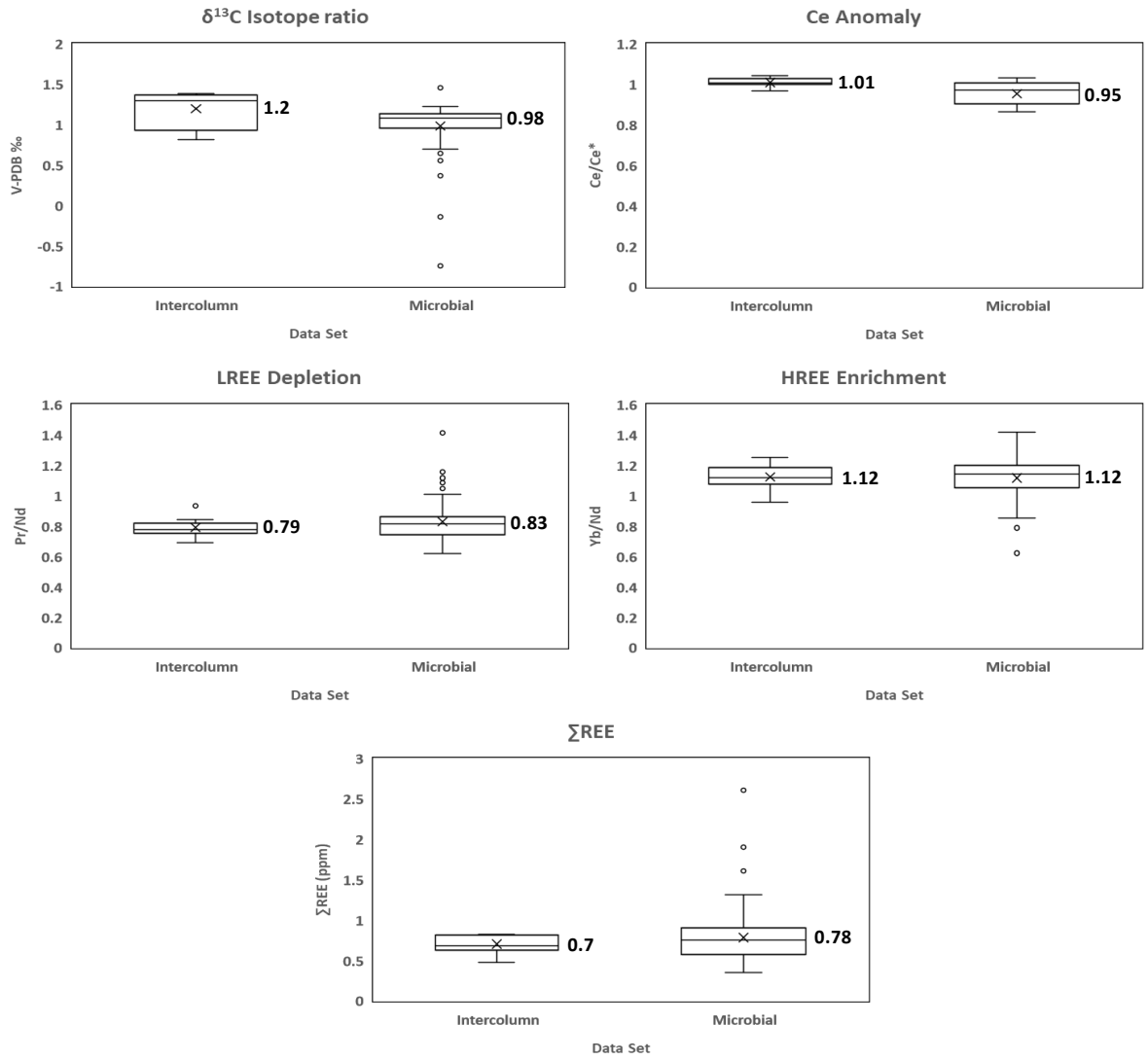

Figure 24*: Comparisons of the chemical parameters of the intercolumn and microbial material with little or no significant differences.*

8.3.2. Ce Anomaly

The subsamples analysed here contain no significant Ce anomalies. The first order implication is that there was not sufficient oxygen in the water from which the carbonate precipitated to oxidise Ce. Rocks with positive Ce anomalies or no significant anomaly were likely deposited in anoxic to suboxic conditions below the oxic chemocline (Elderfield and Sholkovitz, 1987; German and Elderfield, 1990). Therefore, there is an apparent incongruence between the REE chemistry, the palaeoenvironmental features of the stromatolite textures and the palaeoecology of the Late Ediacaran as a whole. The micritic textures, overall shape, growth pattern, and columnar divergence of the dark laminations are consistent with photosynthetic microbial affinity. Furthermore, studies on the sedimentary facies of the Nama Group suggest that the broad limestone successions were deposited in a low energy, shallow water environment (Grotzinger, 2000; Saylor et al., 1995). According to these lines of evidence, the microbialites were generated by photosynthetic bacteria and would have formed within the photic zone in oxic surface waters (<30–200 m depth).

Furthermore, other microbialites in the Nama Group have been found associated with Ediacaran biota fossils (Curtis et al., 2020; Grotzinger et al., 2005; Penny et al., 2017; Wood and Curtis, 2015), as well as potential skeletal fossil fragments between the columns and additional *Cloudina* and *Namacalathus* aggregates discovered in the same locality (Grotzinger, 2000; Grotzinger et al., 2000). If these Ediacaran biota had aerobic metabolisms (See section *2.2 Ediacaran Biota*), they must have inhabited a locally oxic environment. Thus, the absence of an oxic Ce anomaly signal in the micro-drilled microbial horizons is perplexing. How can we reconcile these observations? Several possibilities are explored below.

8.3.2.1. Microenvironmental Complexity

Microbial mats are micro-scale ecosystems, hosting a range of metabolic processes (Louyakis et al., 2017; Mcloughlin et al., 2013; Pace et al., 2018; Ries et al., 2008). Could metabolic variation account for the lack of Ce anomalies? Many bacteria perform anoxygenic photosynthesis, generating elemental sulphur, sulphate, or arsenate ions instead of oxygen (Hamilton et al., 2016; Mcloughlin et al., 2013; Philippot et al., 2007; Qu et al., 2017; Sforna et al., 2014). In theory, these microbes would have the same growth forms as oxygenic photosynthetic bacteria, preferentially growing towards sunlight, forming mats at the water's surface, domes below the surface and columnar networks further below that (**Figure 25**). Structurally, these bacteria can look the same, creating the same peloidal micrite observed within the thin sections (See *section 6.3.3.1. General Microscale Features*). Therefore, the sampled mats may not have been producing oxygen, and the micro-environment and surroundings may have been anoxic, while the local environment itself could have indeed been oxic.

An alternative explanation is that chemical properties of the EPS generated by microbes leads to the passive accumulation of certain REEs, neutralizing any anomalous element signals. Non-nutritive REEs, can passively accumulate within microbial mats through biosorption (Beveridge and Murray, 1976; Buzoleva et al., 2006; Johannesson et al., 2014). This is a process whereby abiotic chemical reactions, such as ion-exchange reactions between carboxyl functional groups and REE ions (Vijayaraghavan et al., 2010; Vijayaraghavan and Yun, 2008), concentrate elements onto the surface or cell walls of microbes, independent of metabolic accumulations (Davis et al., 2003; Gadd, 2009). Due to minor variations in ionic radius, electron configuration, charge, solubility, and reactivity of each REE, there may be a preferential concentration of certain elements over others (Derco and Vrana, 2018; Michalak et al., 2013). This implies elevated REE anomalies, or even reduced anomalies across a sample could reflect this unrelated bioaccumulation (Kazak et al., 2018; Nozaki et al., 1997). However, the extent of this scenario on ancient microbialite REE composition has not been explored beyond explaining the relative elevation of HREE compared to LREE (Johannesson et al., 2014), but it still points to another layer of microenvironmental complexity when performing direct microbial laminae sampling.

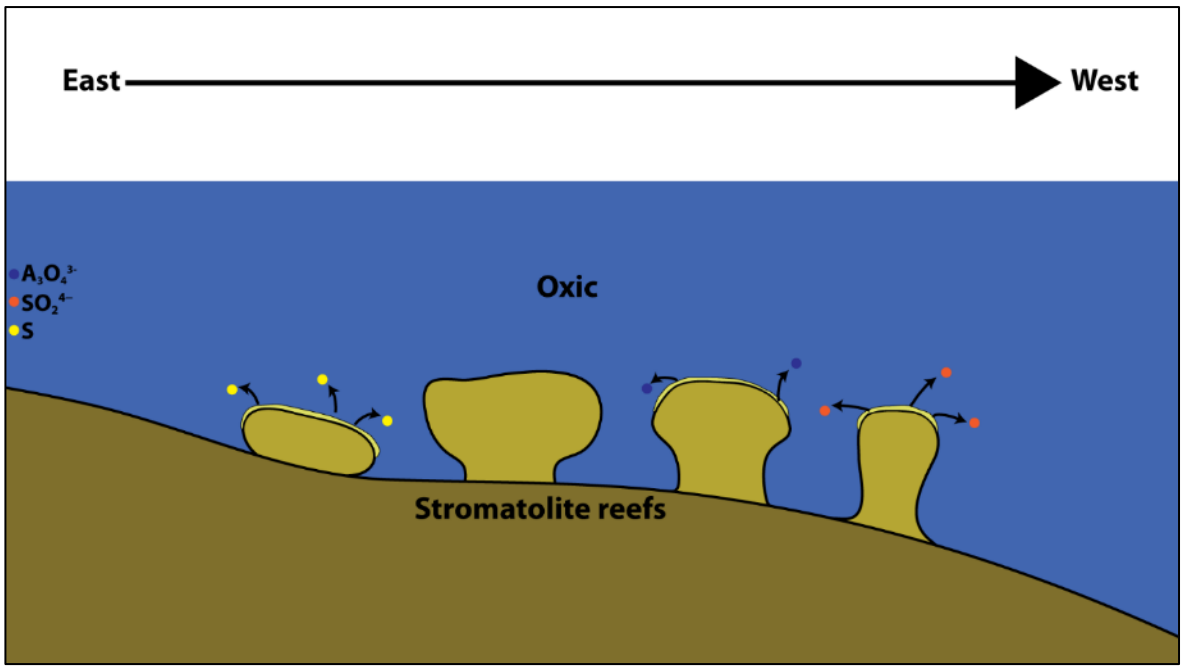

Figure 25: *Visualisation of multiple anoxygenic bacteria building the reefs and releasing products other than oxygen into the surrounding oxic waters. Top yellow layer indicates the active metabolic mat surface.*

8.3.2.2. Are we targeting the right places?

It is possible that the microbial material sampled here does not contain the micro-facies that record negative Ce anomalies. Wilmeth et al. (2022) recently showed that negative Ce anomalies are associated with quartz or calcite filled fenestrae. These fenestrae, essentially oxygen "bubbles," have granular oxides formed along the edges. Wilmeth et al. (2020) also found a clear reduction in negative Ce anomalies as one moves away from these fossilised oxygen "bubbles". None of this study's microdrilling targeted any features that would suggest there was fenestration, although small microsparry domes between laminae were identified after REE analysis was complete (**Figure 15B**). It should be noted that these fenestrae textures are prevalent in the Archean when there was widespread anoxia. They are not documented from the Ediacaran. It is currently unclear whether the lack of prominent fenestrae observed within the microstructural analysis is an accurate indicator of the actual environmental conditions. Alternatively, negative Ce anomalies may be associated with microbial carbonate, but on a scale too fine for us to detect with a micro-drilling technique. Active microbial mats have layers that are several hundred microns thick (Hickman-Lewis et al., 2020), while the drill bit used in sample acquisition was 8 mm thick. Negative Ce anomalies may exist in the local water during active microbial growth, but these may be interspersed with periods of time where the micro-environment was anoxic, even on short timescales such as day-night cycles or periods of reduced productivity. As such, a large drill bit would integrate both these signals (**Figure 26**).

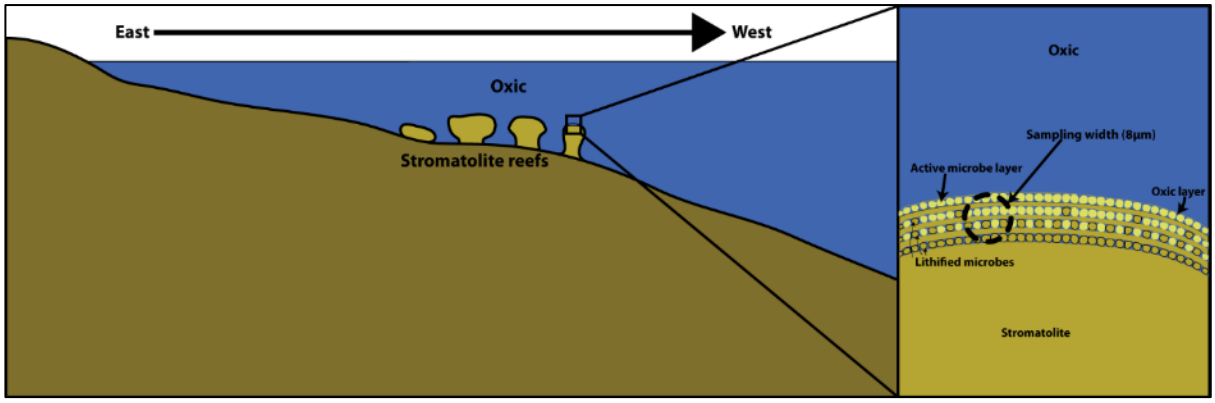

Figure 26: *Microdrilling integrated multiple microbial layers containing both preserved, oxidised Ce and layers without, such as detrital layers or layers of low production or preservation.*

8.3.2.3. Ocean Stratification

Another possibility is that microbialites did produce oxygen, but the carbonate was trapped and bound from the surrounding environment, which was anoxic. The uppermost surface waters in contact with the atmosphere, and the parts of the shelf that hosted metazoans, must have been oxic, but there may have been a shallow chemocline. This anoxia could have been short lived, driven by physical upwelling of anoxic, hydrothermally influenced deeper waters onto the shallow continental shelf periodically, perhaps even triggering microbialite growth through nutrient delivery. These deep waters would have contained no or small positive Ce anomalies and could also be the source of the ambient positive Eu anomalies recorded throughout the drilled subsamples (Derry and Jacobsen, 1990). Such conditions potentially occurred during deposition of Archean microbial carbonates (Danielson et al., 1992; Hickman-Lewis et al., 2020; Hofmann, 2011; Kamber and Webb, 2001; Murphy and Sumner, 2008). Our understanding of how much time a single microbial lamina represents is still uncertain, multiple studies show growth could vary from daily to multiannual scales in the same succession (Gradziński, 2010; Kano et al., 2007; Okumura et al., 2013; Petryshyn et al., 2012; Reitner et al., 2011; Vázquez-Urbez et al., 2010). Therefore, the microbial growth could record unusual and short-lived conditions that were not representative of the steady-state conditions on the shelf. The small amount of oxygen generated by the microbes could have been rapidly consumed by delivery of reduced ions from surrounding anoxic waters, preventing sufficient build-up to trigger Ce oxidation, or the microenvironment may have been oxic, but the carbonate preserved in the mats precipitated in surrounding anoxic waters.

A more likely scenario is that there was some degree of persistent ocean stratification. This is the most likely explanation to account for the consistency of the REE patterns preserved in both the microbialites and intercolumn sediments, which appear to record the same ambient environmental signal. This stratification could have been a regional shallow chemocline (**Figure 27**), but Fe speciation data for the Nama Group indicate that conditions became persistently well-oxygenated by the time of the deposition of the Schwarzrand Subgroup (Bowyer et al., 2020). However, there may have been periodic shallow water ferruginous incursions in the late Ediacaran, coinciding with the relative age of the stromatolite samples. Sampling red sediment intercalations within rock sample RT6a and orange interchannel sediment in BO2 show these sediments have the highest iron contents across all the micro-drilled subsamples (15.98 ppm in **Table 4** and 3.65 ppm in **Table 3** respectively).

This red-orange iron rich sediment is present throughout the whole sample set as either large detrital clasts, near microscopic grains scattered across microbial layers, laminae intercalations, and as large sections of the interchannel fill, indicating Fe-rich conditions. Thus, it is possible the stromatolite samples formed in a ferruginous zone, below depths commonly associated with persistent oxygenation and skeletal metazoan activity. However, it is possible these sediments are the result of widespread secondary oxidation of iron within the sediments, potentially by the percolation of oxygenated groundwater after lithification (Foscolos et al., 1976). Discounting this, the analysis of the microbial structures in section *6. Microbialite Analysis* still points to formation in relatively deep, potentially subtidal waters. Thus, these microbialites may have formed at depths more commonly associated with anoxic waters that prevailed across the deep oceans of the Proterozoic.

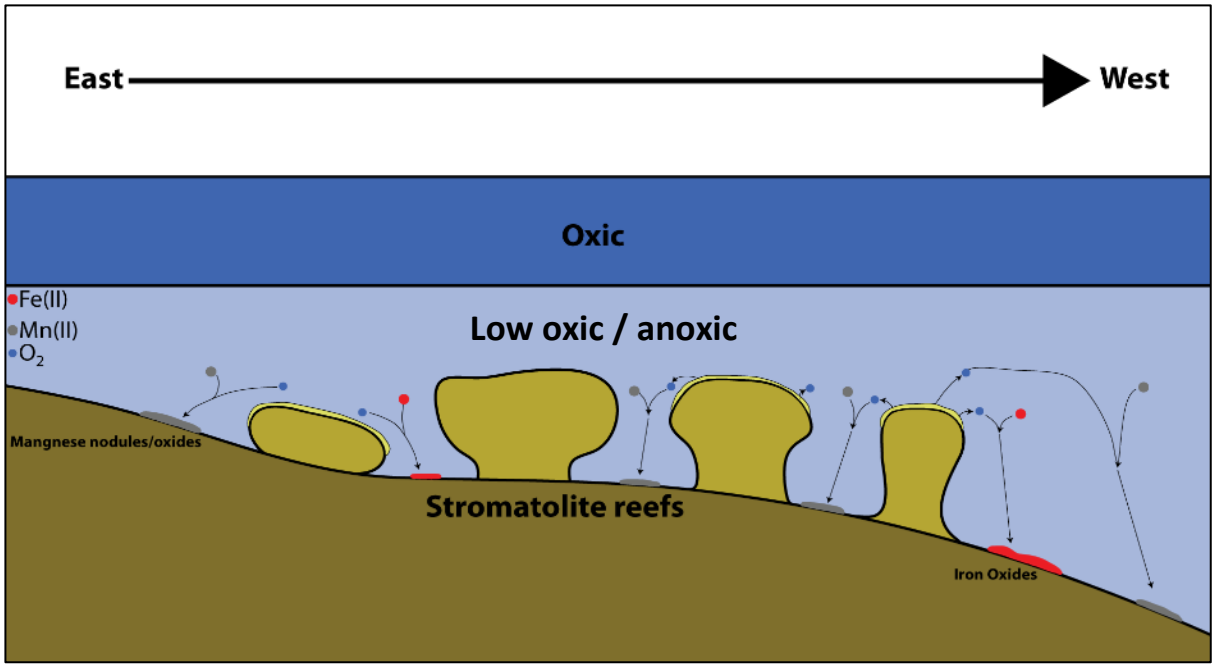

Figure 27: *Visualisation of a persistent low oxic or anoxic ocean stratification, either due to an elevated ferruginous zone or reef formation at the low end of the oxic shallow waters.*

It is also possible that conditions were oxic, but there was either no Mn oxide generation due to low ambient Mn^{2+} in the environment, or the oxygenation was not sufficient to trigger Mn oxidation. An unresolved complication with Ce anomaly analysis is the inability of the anomaly to distinguish between truly anoxic waters and low oxygen waters. The preservation of a negative Ce anomaly implicitly requires the presence of Mn oxides somewhere in the environment. Tostevin et al. (2016b) showed that Mn-oxides are stable in the water column when oxygen levels are above 10 µM. This is to say that persistent negative Ce anomalies could potentially indicate microbial formation within an intermediate, low oxygen water body, and not necessarily true anoxia. This does however still indicate a level of ocean stratification and redox complexity.

Alternatively, the microbialites formed in oxic waters, but localised “pockets” of anoxia could have formed around the microbialites themselves. Microbial reefs would have created relative relief against the flat benthic substrate. Domal and columnar stromatolites could influence the circulation of surrounding water, creating sluggish, stagnant regions where organic matter decomposition occurred. This could have turned the waters around microbialites, and potentially within the microbial columns themselves, into zones of net oxygen consumption. While the samples show no evidence of excessive organic matter accumulation, the darkened fragments and black subrounded clasts in the intercolumn sediments across many samples potentially indicates some degree of organic matter was trapped in the intercolumn spaces (See section *6.4.5. Feature Summary*).

9. Conclusion

9.1. Summary

The detailed petrographic analysis of the microbialite outcrop near the boundary between the Urusis and Nomtsas Formations of the Schwarzrand Subgroup, northern South Africa reveals an extensive domal stromatolite reef, composed of smaller columnar stromatolites spread throughout the cores and outer layers of these domes. The domal stromatolite reef formed within a subtidal region, permanently submerged, unaffected by tidal energies, but influenced by waves. More precisely, the reef grew in the lower shoreface zone, which experienced high energy conditions and turbulence. Prior stratigraphic studies indicate that this reef likely formed on the outer carbonate ramp, bordering the deep, open ocean (See Fig. 2 in Sumner and Grotzinger, 2000; Fig. 2 in Riding et al., 2014; Fig. 31 in Fralick and Riding, 2015). This ramp was situated on the shallow continental shelf of a foreland basin on the Kalahari craton, within the Adamastor or Khomas palaeooceans (Hartnady et al., 1985; Stanistreet et al., 1991). Variations in growth structure on the meter scale suggest different sections formed in different depth regimes, but this could be due to complex topography creating areas of increased turbulence and areas that are shielded from turbulence. It could also point to multiple, rapid sea-level fluctuations, pushing sections of the reef into the offshore transition zone, where energy levels are low and only occasionally disrupted by storm wave events.

The REE data suggest that the columns in between the stromatolite domes and from the centre of these domes formed in anoxic conditions. If these anoxic or low oxygen conditions were localised around the stromatolite columns, the commonly associated Ediacaran Biota could have been attracted to the microbialites as a source of food and shelter, rather than oxygen oases. While the present geochemical data cannot expand upon the nature of this anoxia, whether this was a small scale, reef bound stratification or a regionally shallow chemocline, integration with petrographic observations can help. I interpret the domal stromatolite reef to have formed in the subtidal zone, which was persistently anoxic. A lack of emplaced skeletal metazoans such as those found in shallower microbialite reefs (Grotzinger, 1990; Grotzinger et al., 1995; Walter et al., 1992), as well as potential fragments of skeletal metazoans in my samples, further supports the possibility of the domal reefs forming in turbulent, deeper, potentially hydrothermally influenced anoxic waters. Microbialite reefs across the Neint-Nababeep Plateau were morphologically diverse, evident by the conical reefs observed at Site 2 (**Figure 2C**) as well as the identification of 100 m scale Pinnacle Reefs at the highest elevations of the Plateau (Nelson et al. 2022).

It is thus reasonable to assume that microbialites formed across the entire photic zone depth regime, placing some reefs within the same depth as the skeletal metazoans of the Ediacaran Biota, and others far below these oxic surface waters. 3-D modelling of the Nama Group microbial reefs from Zebra River, Namibia have shown it was likely microbialite reefs grew as compounded domal and stratiform successions throughout the Nama Group deposition (Adams et al., 2005).

9.2. Research Questions

This study set out to answer these questions regarding the microbialites of the Neint-Nababeep Plateau:

1. *Can we extract reliable REE signals from ancient microbialites?*
   Ultimately, yes, the REE signals derived directly from microbial laminae indicate the preservation of a primary seawater signal. The low variation in these signals, regardless of depth or location across the reef indicates the recording of ambient conditions. There was no geochemical difference between the bacterial build-ups, alleged to be photosynthetic cyanobacterial formations, and surrounding carbonate.

2. *Were these microbialites centres of oxygenation in an otherwise low oxygen ocean?*
   Inconclusive. The REE data show no significant Ce anomaly, indicating that there was no fractionation of Ce within the waters that the calcite precipitated from. As such, these reefs do not seem to be "oxygen oases." However, there are several possible explanations for the apparent anoxic signals, some of which are consistent with the reefs being locally oxic. Additional geochemical proxy analysis on these microbial laminae will be required to obtain unequivocal evidence.

3. *Do the REE signals correlate with conditions found within contemporaneous Nama Group deposits based on bulk rock analysis?*
   The stratigraphic correlation of this section to the rest of the Nama Group has only recently been published (Nelson et al. 2022). The redox and environmental conditions recorded from this reef are analogous to the Swartpunt and Pinnacle Reef sections from the Witputs Subbasin (Tostevin et al., 2016a; Tostevin et al., 2016b). The REE Signals are generally consistent, except positive Ce anomalies are common in the bulk rock data but are absent from the microbial samples. Thus, the findings in this study could further constrain the stratigraphic location of the oxic water chemocline across the Nama Group Ediacaran.

4. *Are there notable spatiotemporal variations in the macroscale morphologies, microscale fabrics and REE patterns across these previously unstudied South African Nama Group microbialites?*
   Ultimately this study showed there is extensive centimetre scale variations in microbialite textures through space and time, indicating rapidly changing water depths, energy levels and turbulence.

5. *Can an ecological relationship be established between the formative microbes of the microbialites and their environment?*
   The microbial laminae were created by microbial mat communities that experienced predominantly rapid growth periods with occasional periods of suppression by environmental conditions. However, a lack of clearly preserved bacterial cell structures and no tests for metabolic complexity makes constraining any further palaeoecological relationships difficult.

6. *What was the provenance of the carbonate within the stromatolites? Did the formative microbial mats scavenge carbonate sediments from the water column or was carbonate precipitated in situ? Is there a correlation between the carbonate provenance and different microbial fabrics?*
   The provenance is complicated. The REE chemistry, microscale petrography and XRD analysis indicate a widespread distribution of calcite of the same origin in both the intercolumn sediment and the microbial laminae, likely from calcite supersaturated waters. This suggests the calcite in the microbial laminae was sourced from the same location as the intercolumn sediments, pointing to a sediment accumulation formation. However, the petrographic features point to textural difference in the calcite. The occurrence of subrounded micrite clot fabrics exclusively within the microbial laminae point the in-situ formation of biologically mediated calcite, while unstructured micrite, coarse grained microspar and spar point to the transportation of terrigenous grains in the intercolumn sediments. Sediment intercalations in the columnar material contain the same coarser grained calcite, supporting their origin as patches of detrital particles settling within the microbialite. Thus, there is a correlation between the calcite fabrics and the location within the microbialite reef. A spectrum thus likely exists between biologically precipitated and entrapped carbonate within the rock samples.

9.3. Future Studies

There are many avenues for continued research from this study. The findings in this thesis show potentially unique geochemical and environmental features of the Nama Group, which could help piece together the palaeoenvironmental and palaeoredox puzzle of the southern African Ediacaran Period. Future studies could expand on this work in the following ways:

1. The presence of anoxygenic photosynthetic bacteria could be evaluated using sulphur isotopes to reveal sulphur metabolic affinities (Canfield and Teske, 1996; Grosch et al., 2023; McLoughlin et al., 2023), RAMEN thermometry to test whether the heat thresholds align with oxygenic or anoxygenic microbes (Grosch et al., 2023; Sanders et al., 2023), and biosignatures such as CH_3/CH_2 ratios can determine potential taxonomic affinities (Qu et al., 2015; Qu et al., 2017). Additionally, borehole sampling can help obtain fresher samples from the depth that have experienced comparatively less diagenetic weathering.

2. More extensive fieldwork could identify whether sparry calcite microbial fenestrae and aragonite fans are present in the Nama Group, and test whether these regions contain negative Ce anomalies (Riding et al., 2014; Sumner, 2002; Sumner and Grotzinger, 2000). Wilmeth et al. (2022) had demonstratably shown negative Ce signals from fenestral oxides that form around calcite and quartz filled "oxygen bubble" fenestrae (See Fig. 2 in Wilmeth et al., 2022). Linked to this, extensive fieldwork could determine if the microbial reef at Site 1 is truly bereft of typical Ediacaran skeletal fossils.

3. Detailed sedimentary facies analysis could reveal more information about the specific depositional environments of the domal stromatolite reef (Li et al., 2021; Sanders and Grotzinger, 2021). The potential records of small-scale turbidity should be explored further, by performing detailed measurements of microbialite synoptic relief, which can help determine the topographic height created by the microbial columns with respect to the surrounding sediments. In-depth sedimentary facies analysis could potentially constrain the prevalent palaeocurrent directions across the reef. Nelson et al. (2022) noted increasing rates of sedimentation towards the end of the Schwarzrand Subgroup deposition, coinciding with the location of the studied reef. Vertical comparisons of the laminae composition across multiple microbialite reefs could be made, seeing if increasing occurrence of lighter, detrital influenced laminae coincide with these increasing sedimentation rates.

4. The powdered subsamples could be more extensively run for SLI and XRD analysis, both to better constrain the organic content of the microbialites and to get a more detailed idea of the calcium carbonate minerology. As it stands, the distribution of calcite, aragonite, and dolomite across the microbialite reef is unknown.

5. The degree of redox heterogeneity across the reef could be explored further. Fe speciation on complementary microbial horizons, as well as further sampling of the intercolumn sediment, could be used to constrain the presence of local ferruginous conditions. Similarly, the targeted analysis of any potential Mn nodules associated with the reef could further clarity the redox structure across the reef.

6. Finally, a question which extends to all Precambrian microbialite analysis, what do we know about the volume of oxygen microbial mat bacterium produce? The availability of nitrogen, phosphorus and trace metals was thought to be low throughout the Precambrian (Anbar and Knoll, 2002; Field et al., 1998; Guilbaud et al., 2020), a consequence of insufficient organic matter breakdown and P sequestration (Derry, 2015; Kipp and Stüeken, 2017; Planavsky et al., 2023). A persistent low nutrient abundance would surely limit the volume of oxygen produced by cyanobacteria. The use of biogeochemical and earth system analytic modelling has helped infer relative oxygen concentrations for the Archean oceans (Olson et al., 2013), such techniques could be applied to the Nama Group microbial reefs.

Ultimately, this study exemplifies the complexity of microbialite features and formative conditions and follows decades of research showing the uncertainty of ancient microbialite analysis. Interpretations based on modern microbial build-ups are tentative when the ancient deposits have morphologies or scales unlike forms seen today, and the unlikelihood of a unified model of microbialite formation means each outcrop must be treated as unique (Arenas et al., 2017). Additionally, the apparent lack of any Ce anomaly across these Nama Group formations has been a source of much confoundment. Complementary research from the Namibian Nama Group have found evidence of positive Ce anomalies for the Late Ediacaran (Bowyer et al., 2020; Tostevin et al., 2016b; Wood et al., 2015), with this paper confirming a disparity from Ediacaran sequences from other parts of the world (Li et al., 2021; Ling et al., 2013; Zhang et al., 2021), where clear negative Ce anomalies have been found.

9.4. Closing Remarks

While this study most certainly broadens the areas of research for the Ediacaran Period, showing extensive microbial reefs across a South African Nama Group outcrop, it opens more questions about the search for oxic signals: Could we be overestimating the contribution of microbialites to widespread ocean and atmosphere oxygenation? Microbialite reefs dominate shallow marine waters in the Precambrian. However, shallow marine environments are fractions of the total ocean surface area. Sanchez-Baracaldo (2015) and Sanchez-Baracaldo et al. (2022) suggest that there was a greater contribution to shallow marine oxygenation, and later persistent oxygenation, by newly diversified planktonic cyanobacteria into the open oceans near the end of the Precambrian.

Correlations with similar aged deposits by Sanchez-Baracaldo et al. (2022) shows this adaptive radiation is linked to increases in nutrient availability and pO_2 levels in the Neoproterozoic (Laakso et al., 2020; Reinhard et al., 2017). Simply by occupying far greater expanses of the photic zone, planktonic cyanobacteria could have produced far greater volumes of oxygen than the spatially limited microbial mat cyanobacteria (Sanchez-Baracaldo, 2015; Sanchez-Baracaldo et al., 2022). This late Precambrian colonisation of the ocean oceans could potentially explain why there is a lag-time for widespread oxygenation, the primary oxygen producers were spatially limited. Could these phytoplankton play a larger role in the oxygen oases hypothesis? How would we identify the potential oxic signals of planktonic cyanobacteria? Sanchez-Baracaldo (2015) made use of phylogenetic data to model the evolution of cyanobacteria, not any geochemical proxies directly from preserved phytoplankton. Will their preservation state be dependable enough to record primary seawater signals? Do REE concentrate on their surfaces? Ultimately, where are the negative Ce anomalies from the southern African Nama Group deposits?

10. Supplementary Data

10.1. Appendix 1: B-SEM Images

RT1 Intercolumn Sediment

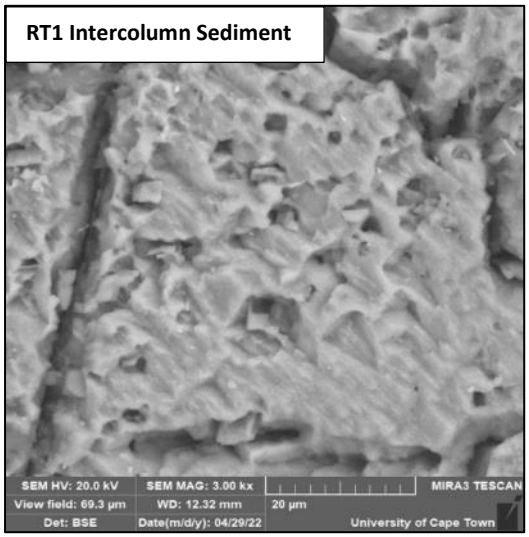

RT1 Intercolumn Sediment

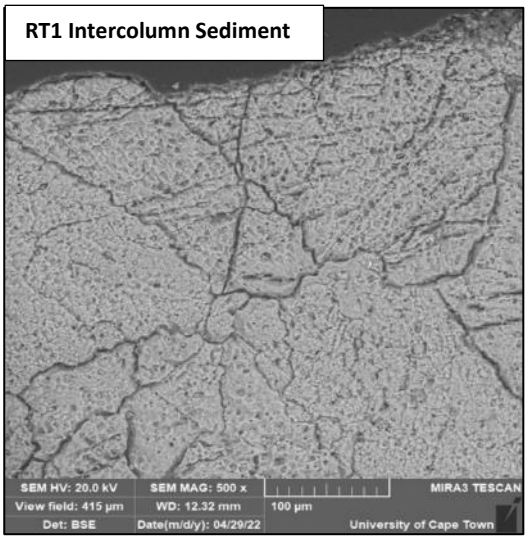

RT1 Microbial Laminae

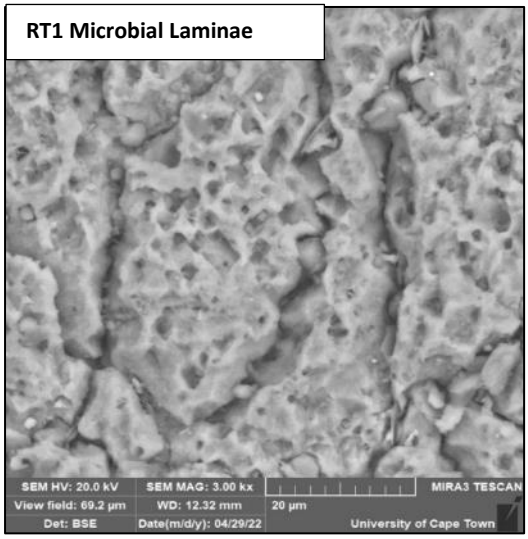

RT1 Microbial Laminae

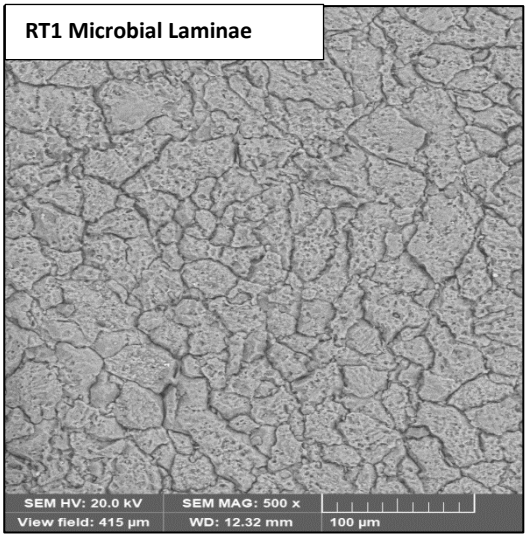

RT1 Red-Orange Sediment

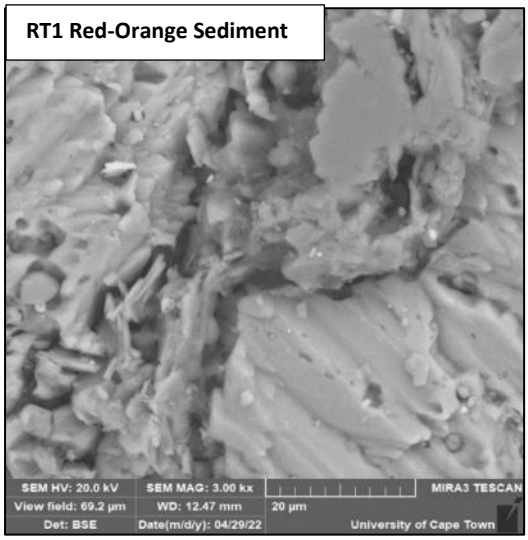

RT1 Red-Orange Sediment

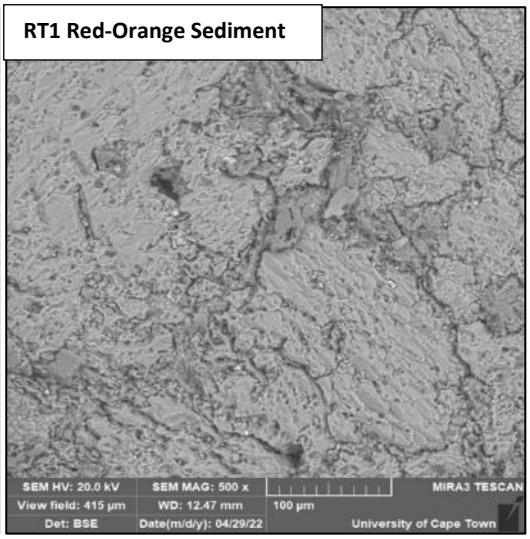

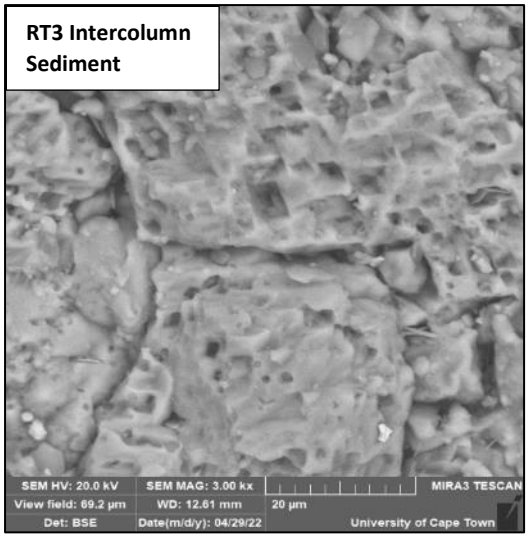
RT3 Intercolumn Sediment
SEM HV: 20.0 kV
SEM MAG: 3.00 kx
MIRA3 TESCAN
View field: 69.2 µm
WD: 12.61 mm
20 µm
Det: BSE
Date(m/d/y): 04/29/22
University of Cape Town

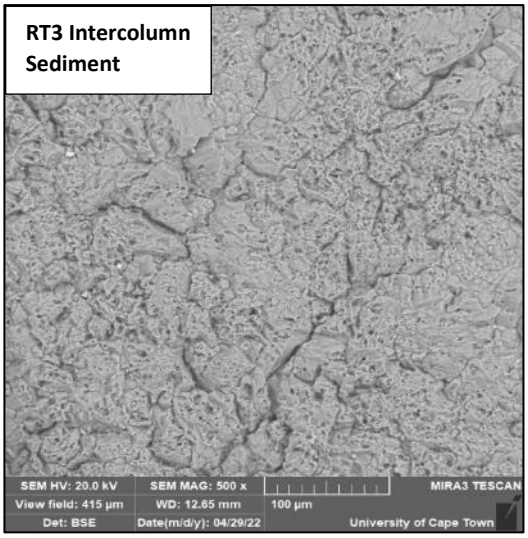
RT3 Intercolumn Sediment
SEM HV: 20.0 kV
SEM MAG: 500 x
MIRA3 TESCAN
View field: 415 µm
WD: 12.65 mm
100 µm
Det: BSE
Date(m/d/y): 04/29/22
University of Cape Town

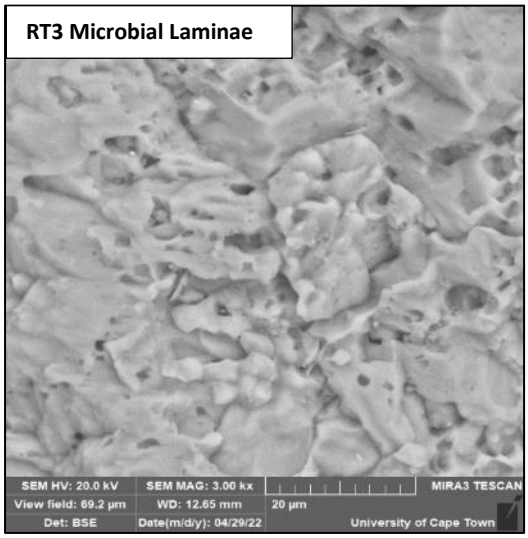
RT3 Microbial Laminae
SEM HV: 20.0 kV
SEM MAG: 3.00 kx
MIRA3 TESCAN
View field: 69.2 µm
WD: 12.65 mm
20 µm
Det: BSE
Date(m/d/y): 04/29/22
University of Cape Town

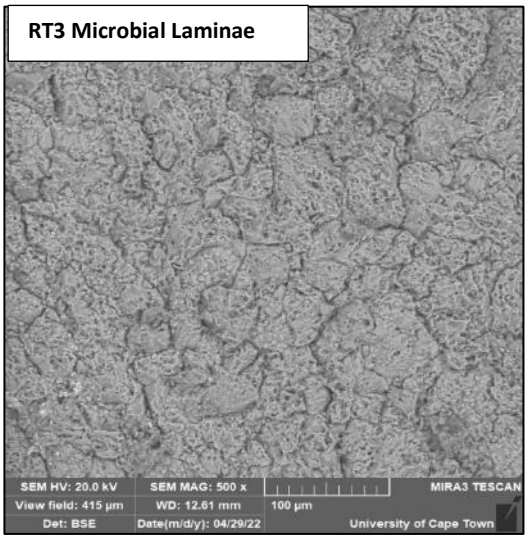
RT3 Microbial Laminae
SEM HV: 20.0 kV
SEM MAG: 500 x
MIRA3 TESCAN
View field: 415 µm
WD: 12.61 mm
100 µm
Det: BSE
Date(m/d/y): 04/29/22
University of Cape Town

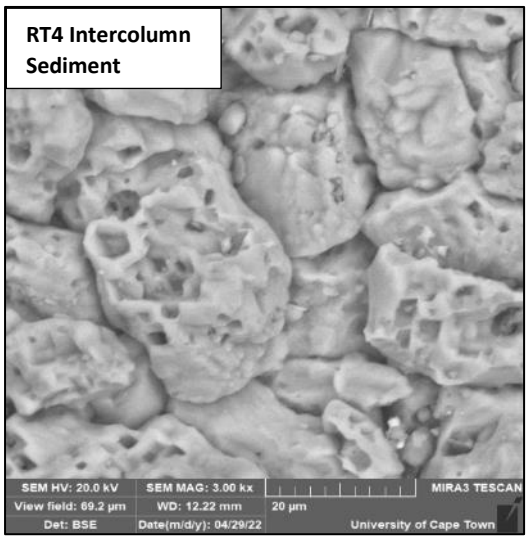
RT4 Intercolumn Sediment
SEM HV: 20.0 kV
SEM MAG: 3.00 kx
MIRA3 TESCAN
View field: 69.2 µm
WD: 12.22 mm
20 µm
Det: BSE
Date(m/d/y): 04/29/22
University of Cape Town

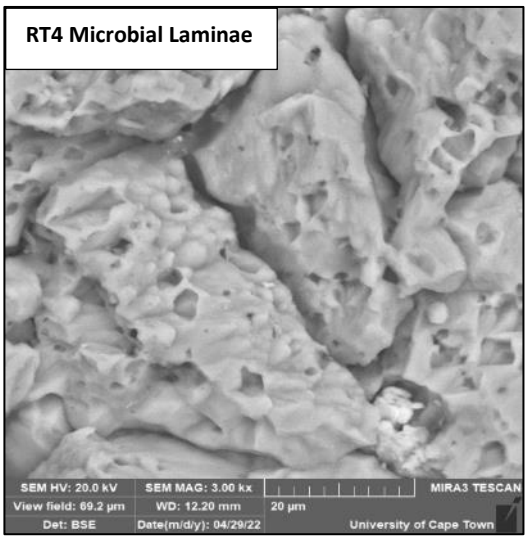
RT4 Microbial Laminae
SEM HV: 20.0 kV
SEM MAG: 3.00 kx
MIRA3 TESCAN
View field: 69.2 µm
WD: 12.20 mm
20 µm
Det: BSE
Date(m/d/y): 04/29/22
University of Cape Town

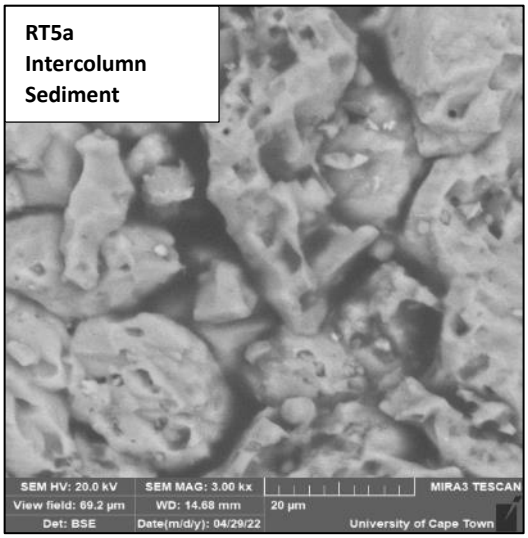
RT5a Intercolumn Sediment
SEM HV: 20.0 kV
SEM MAG: 3.00 kx
MIRA3 TESCAN
View field: 69.2 µm
WD: 14.68 mm
20 µm
Det: BSE
Date(m/d/y): 04/29/22
University of Cape Town

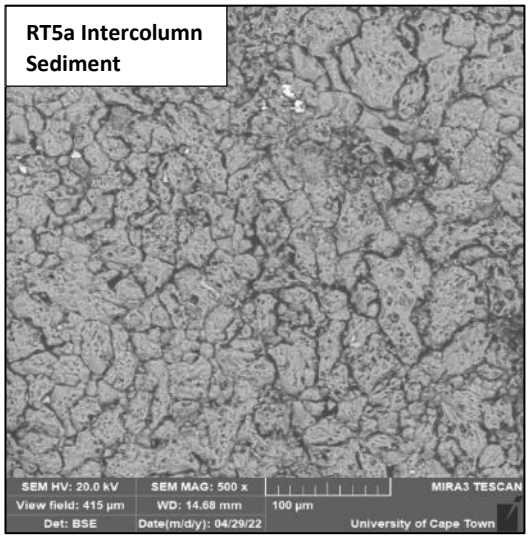
RT5a Intercolumn Sediment
SEM HV: 20.0 kV
SEM MAG: 500 x
MIRA3 TESCAN
View field: 415 µm
WD: 14.68 mm
100 µm
Det: BSE
Date(m/d/y): 04/29/22
University of Cape Town

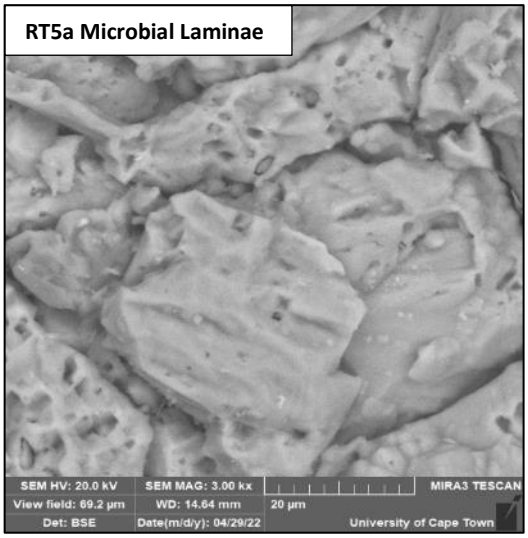
RT5a Microbial Laminae
SEM HV: 20.0 kV
SEM MAG: 3.00 kx
MIRA3 TESCAN
View field: 69.2 µm
WD: 14.64 mm
20 µm
Det: BSE
Date(m/d/y): 04/29/22
University of Cape Town

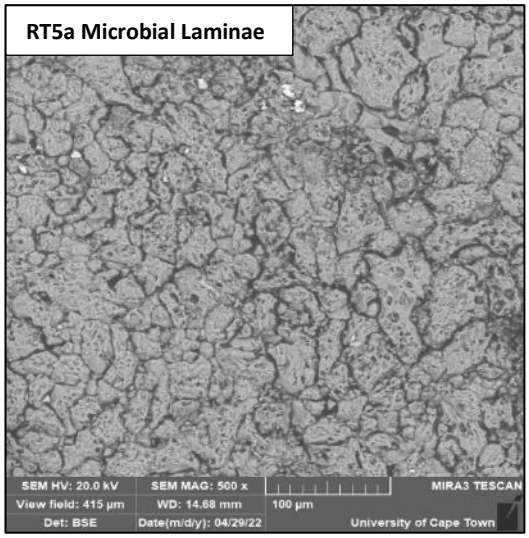
RT5a Microbial Laminae
SEM HV: 20.0 kV
SEM MAG: 500 x
MIRA3 TESCAN
View field: 415 µm
WD: 14.68 mm
100 µm
Det: BSE
Date(m/d/y): 04/29/22
University of Cape Town

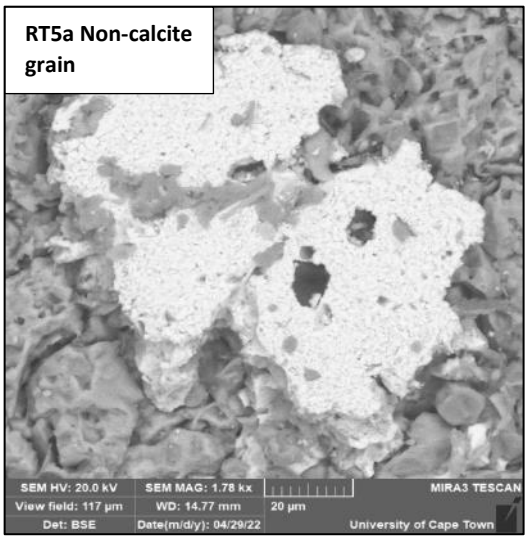
RT5a Non-calcite grain
SEM HV: 20.0 kV
SEM MAG: 1.78 kx
MIRA3 TESCAN
View field: 117 µm
WD: 14.77 mm
20 µm
Det: BSE
Date(m/d/y): 04/29/22
University of Cape Town

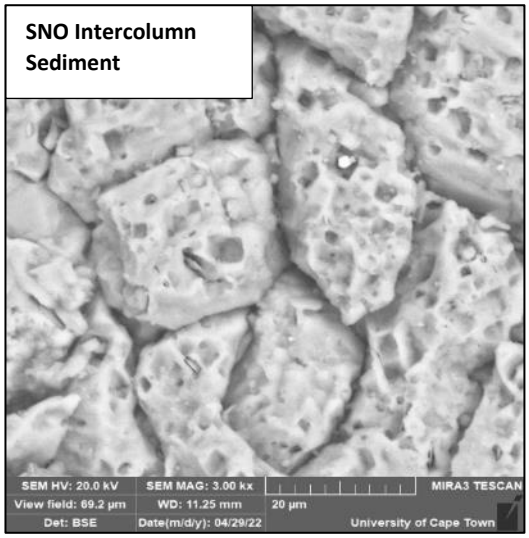
SNO Intercolumn Sediment
SEM HV: 20.0 kV
SEM MAG: 3.00 kx
MIRA3 TESCAN
View field: 69.2 µm
WD: 11.25 mm
20 µm
Det: BSE
Date(m/d/y): 04/29/22
University of Cape Town

SNO Microbial Column Wall

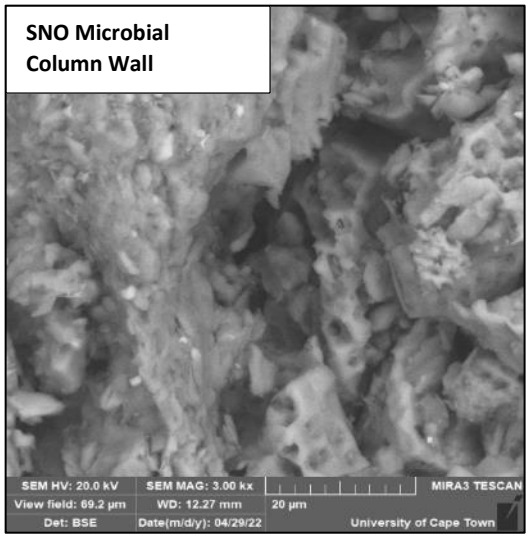

SNO Microbial Laminae

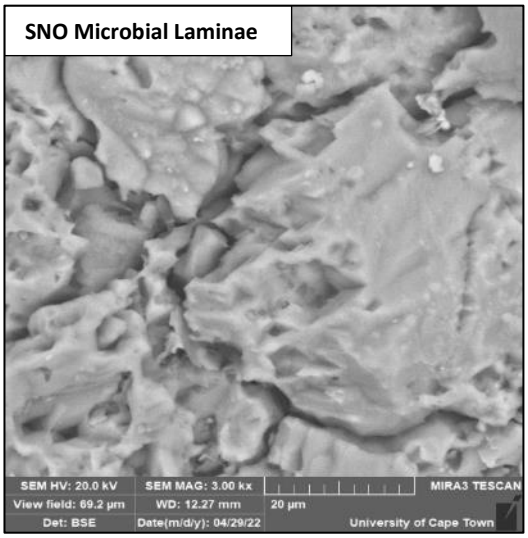

SNO Microbial Laminae

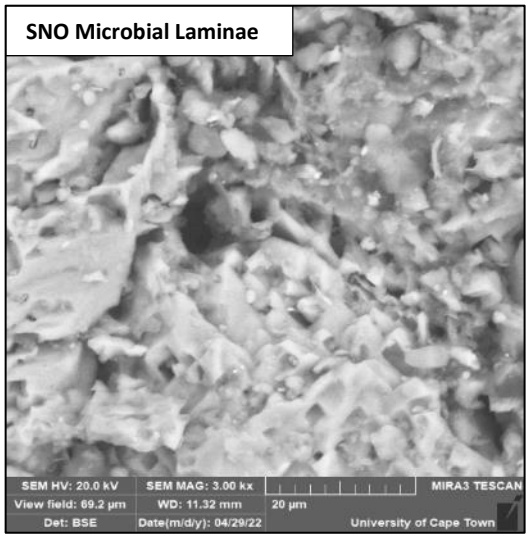

SNO Microbial Laminae

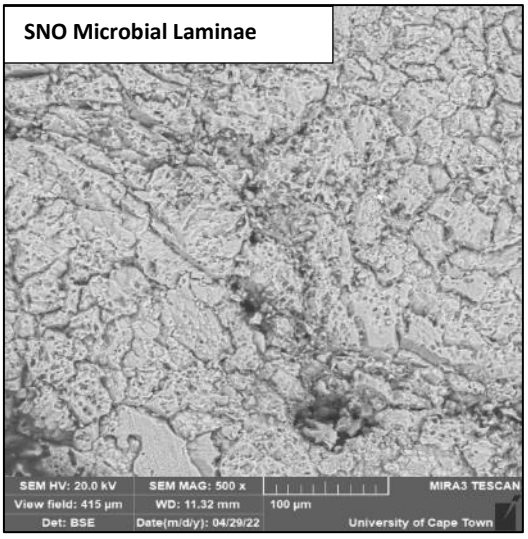

SNO Intercolumn

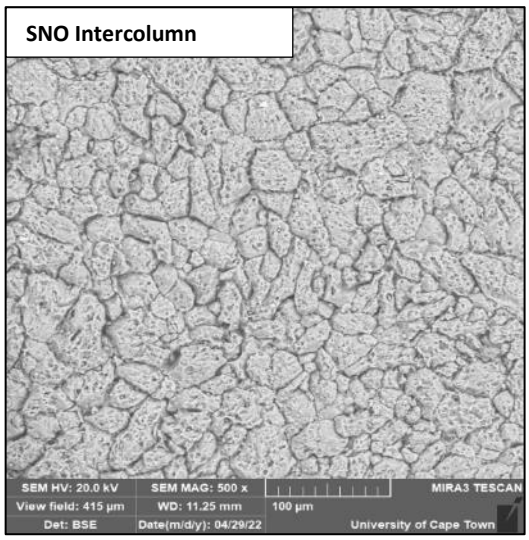

SNO Intercolumn Sediment

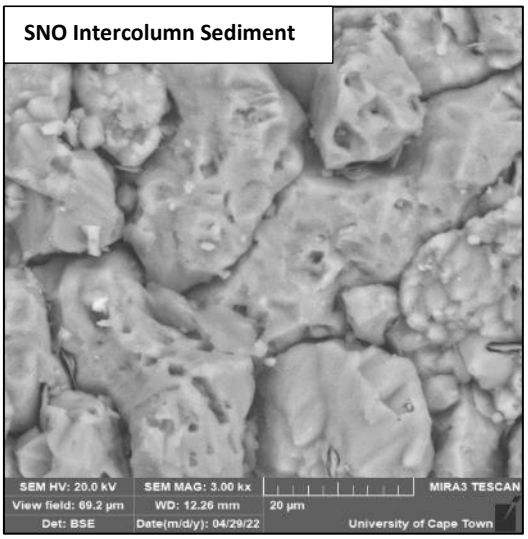

SNO Microbial Laminae

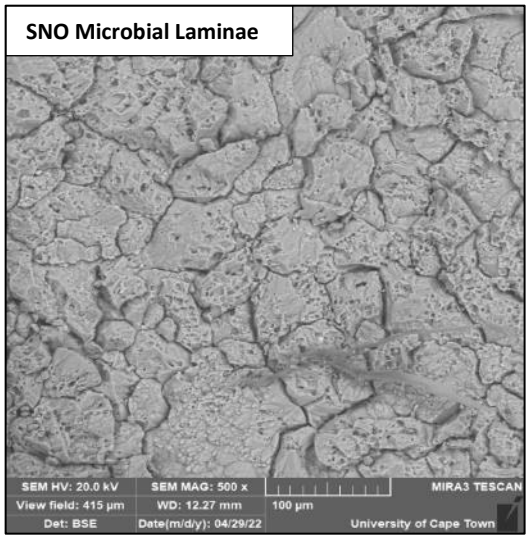

SPO Microbial Column

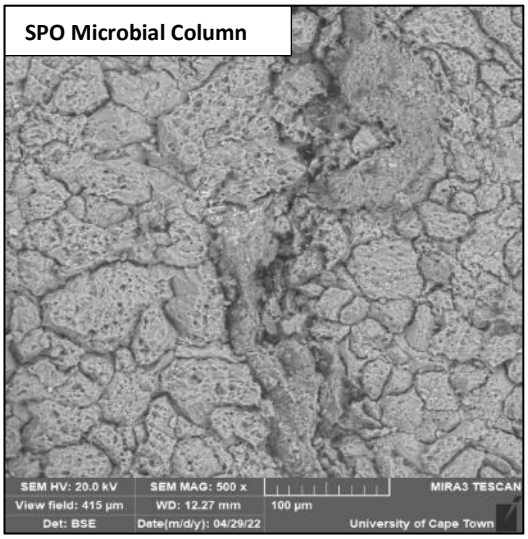

SPO Intercolumn

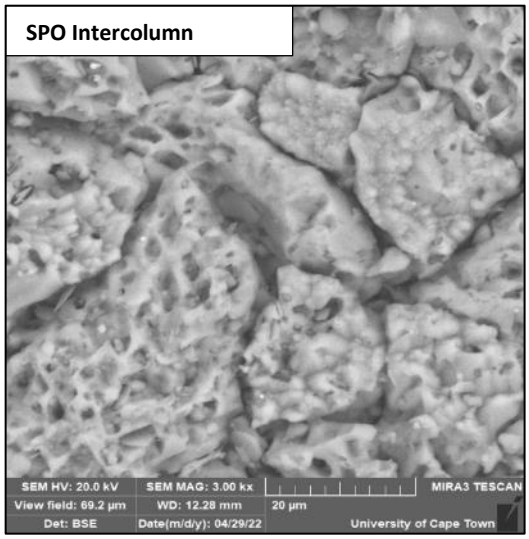

SPO Microbial Sediment

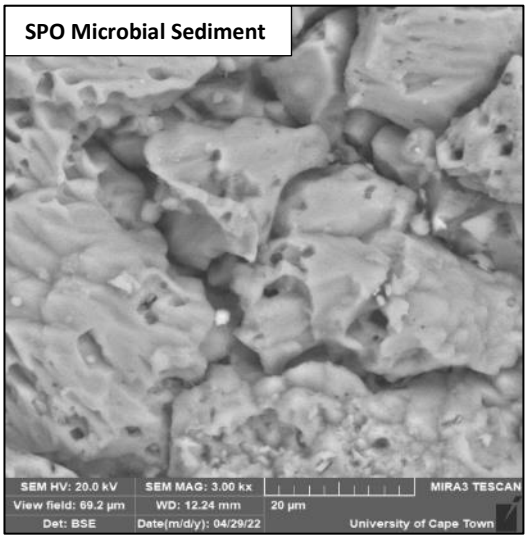

SPO Microbial Sediment

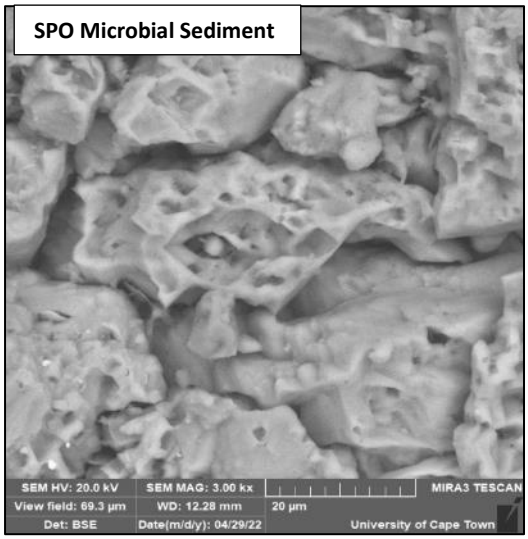

SPO Microbial Sediment

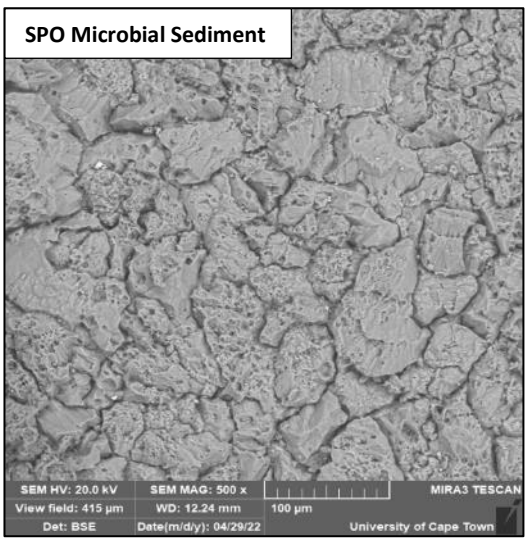

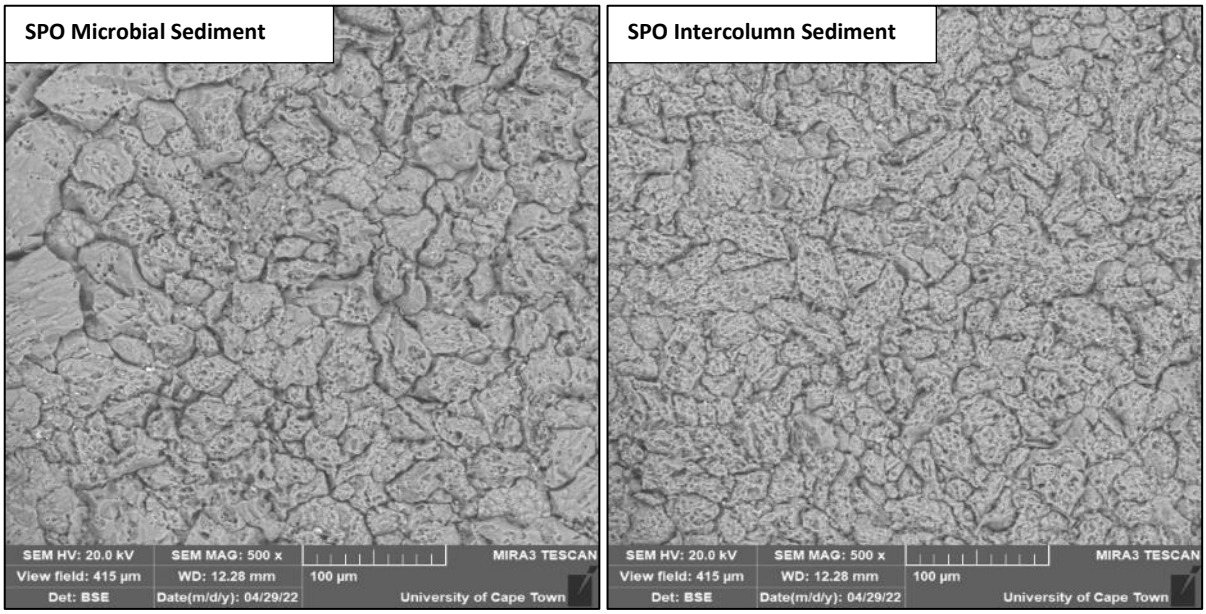

10.2 Appendix 2: Additional Geochemical Comparisons

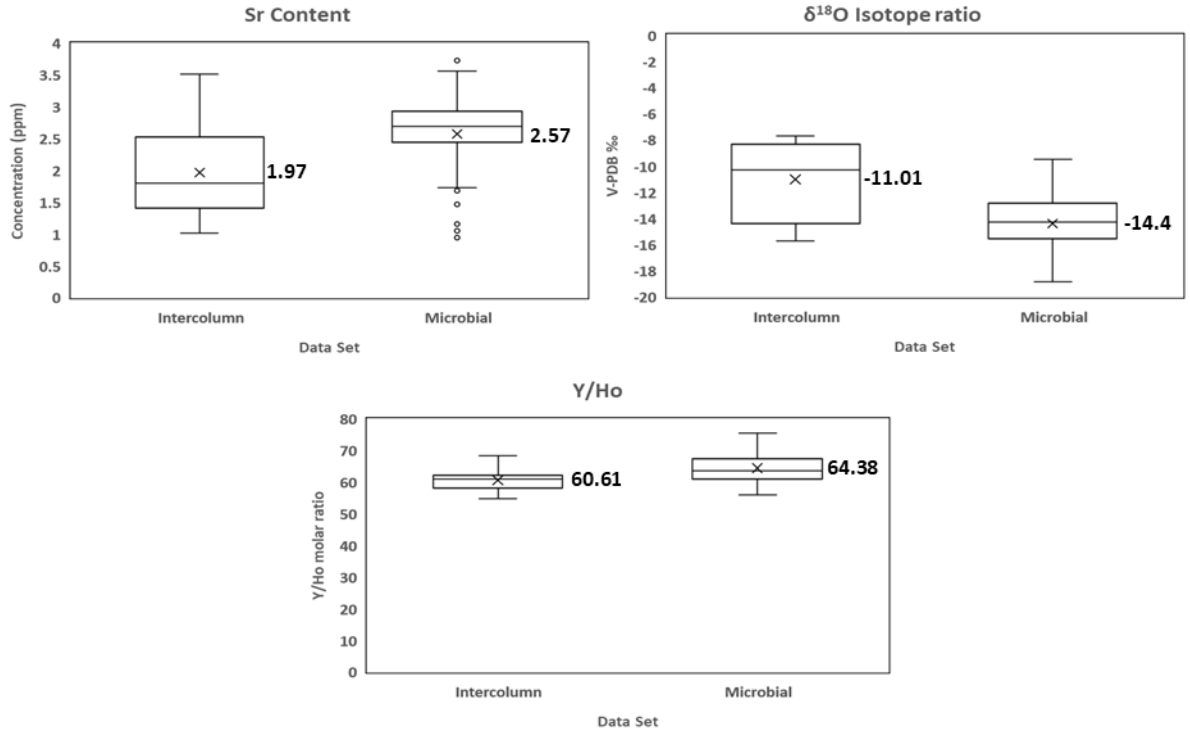

Figure 28: *Comparisons of the Sr content, $\delta^{18}O$ ratios and Y/Ho ratios between microbial and intercolumn material.*

10.3. Appendix 3: Rock Polishing Technique

10.3.1. Equipment

1. Variable speed orbital sander/polisher. I used a 1200W polisher, but any machine that can reach 3000 rpm will work. A random orbit sander will also work, but make sure that it can run at 3000 rpm or lower. Higher speeds will cause the polishing pads to tear, which can be dangerous.

2. 10cm Velcro backing pad for the polishing pads to fit onto the sander/polisher.

3. Seven 10 cm diameter wet diamond polishing pads; 50, 150, 300, 500, 1000, 2000 and 3000 grit sizes.

4. Wool buffing pad. My polisher (Tork Craft POL02) came with a buffing pad, others might not. These must be run at the lowest speed, preferably no higher than 1000 rpm.

5. M3 half face protective respirator mask with a 6035 particulate filter. Any combination of respirator and particulate filter will work, just follow the specific instructions given with the product.

6. Safety goggles, protective gloves, and earmuffs. A lab coat would be recommended, as the polishing creates a lot of mud and dust.

7. A large supply of water.

10.3.2. Method

1. This guide assumes the rocks have been cut, with roughly flat surfaces.

2. I would advise reading the safety and user manual for each instrument before starting. The manual in the polisher box should provide details about the machine and how to place polishing pads on it safely.

3. A well-ventilated room would be ideal, so rock dust does not settle too heavily.

4. The roughness of the target surface will determine which grit pad to start with. Surfaces with rock cutting marks and sharp relief will require starting with the 50 grit pad. Focus on sanding down and levelling the surface. If there are no significant gouges or sharp relief, the 500 grit pad is suitable for calcium carbonate rocks. To summarise; if the surface is not evenly flat, start with the 50 grit pad; if the surface has no deep cuts, start with the 500 grit pad.

5. Begin by wetting the surface to be cut. Place the polisher on the surface then turn it on. Care should be taken not push the machine against the rock, as this will gouge the rock. Polish in one direction with the polisher at the highest speed, making multiple passes in parallel tracts. Never leave the polisher on one spot for more than 5 seconds, as this will gouge the rock. If you are using the 50 or 150 grit, do not let the machine sit in one place for more than 1 or 2 seconds. Ideally, you should begin the polishing tract in the opposite direction of the cut marks on the rock, assuming that there are any. Ensure the surface is constantly wet, reapplying water when required. Once the original cut marks have been sanded off, you should be ready to move onto the next grit size.

6. Once you are satisfied with the first polish, unplug the sander, and remove the pad from the Velcro backing. Place on the finest grid pad after the current one. The pads go from 50 (coarsest), 150, 300, 500, 1000, 2000 to 3000 (finest). Do not skip this fining scale, as it will waste your time to polish it down.

7. Begin the next polishing phase by starting your tract in the opposite direction from the previous tract. The sanding marks of the previous polish will be visible when the rock is dried. Remember to wet the surface first, place the polisher on the rock and then turn it on. As one moves down the fining scale, it will take longer to polish the surface. Maintain a consistent polishing path, never letting the machine sit on one place longer that 3-5 seconds depending on the grit size.

Make multiple and parallel polishing tracts if necessary. Once you are satisfied, begin the next grit size.

8. Continue this polishing process until you get to the 3000 grit pad. At this point, you should notice that the rock is no longer absorbing the water, the water may start running off. You should also see some shine by the transition of the 2000 to 3000 grit. You should also notice that the machine glides very easily over the rock surface.

9. Once the 3000 grit polish is complete, remove both the diamond pad and the backing pad. Fix the wool buffing pad to the polisher. Sprinkle the wool pad with water. Switch the machine to the lowest speed, wet the polished surface, place the polisher with the wet wool buff pad on the surface, and start the machine. Do not apply any pressure on the wool pad, as this will either send the rock flying or the machine spinning out of your hands. Lightly move the machine in small concentric rings over the rock. Do this until both the rock and wool pad are dry. Keep doing this buffing process until you are satisfied with a shiny rock surface.

10. Ideally, the dry polished surface should look as if it was wet.

11. If your rocks specimen is small; small enough to fit comfortably in your hand; it can be difficult to place the polisher against the rock. It may go flying with the slightest pressure. In such cases, you can flip over the polisher, with the polishing pad facing upward. This should be doable if the polishing machine comes with a cross card or D shaped handle. Doing this method actually provides more control but will require you to have one hand constantly on the trigger and the other holding the rock sample. Regardless, follow the same polishing process outlined above with this technique.

10.3. Appendix 3: Raw ICP-MS Data

Sample	^{46}Ca (ppm)	^{27}Al (ppb)	Mn (ppm)	^{58}Fe (ppm)	^{84}Sr (ppm)	^{135}Ba (ppb)	^{139}La (ppb)	^{140}Ce (ppb)	^{141}Pr (ppb)	^{146}Nd (ppb)	^{147}Sm (ppb)	^{151}Eu (ppb)	^{157}Gd (ppb)	^{159}Tb (ppb)	^{163}Dy (ppb)	^{89}Y (ppb)	^{165}Ho (ppb)	^{167}Er (ppb)	^{169}Tm (ppb)	^{174}Yb (ppb)	^{175}Lu (ppb)
BO1a.1c	498.80	1666.33	0.64	1.36	1.47	26.75	3.45	6.40	0.85	3.22	0.69	0.59	0.67	0.10	0.59	3.81	0.12	0.32	0.04	0.26	0.04
BO1a.5a.1	281.72	250.00	<100	0.50	1.16	15.76	1.28	2.48	0.32	1.29	0.28	0.24	0.29	0.04	0.27	1.65	0.05	0.15	0.02	0.12	0.02
BO1a.5a.2	240.27	250.00	<100	0.51	1.05	7.58	0.87	1.72	0.22	0.89	0.20	0.15	0.20	0.03	0.18	1.15	0.04	0.10	0.01	0.08	0.01
BO1a.5a.3	280.53	250.00	<100	0.46	0.96	6.11	0.84	1.62	0.20	0.84	0.18	0.10	0.19	0.03	0.18	1.23	0.04	0.10	0.01	0.08	0.01
BO1a.5g.1	270.63	250.00	<100	0.45	1.47	9.31	1.16	2.24	0.29	1.18	0.25	0.22	0.26	0.04	0.23	1.46	0.05	0.13	0.02	0.10	0.01
BO1a.5g.2	308.00	250.00	<100	0.57	1.73	9.67	1.15	2.33	0.29	1.22	0.26	0.15	0.28	0.04	0.25	1.50	0.05	0.14	0.02	0.12	0.02
BO1b.3	534.84	725.93	0.99	1.98	1.41	11.61	3.29	5.79	0.78	3.10	0.64	0.23	0.59	0.09	0.48	3.16	0.09	0.25	0.03	0.20	0.03
BO2.1	422.40	250.00	<100	3.65	2.52	776.68	3.83	7.32	0.94	3.86	0.76	0.47	0.78	0.11	0.65	3.91	0.13	0.34	0.05	0.27	0.04
BO2.5a.1	299.80	110.11	<100	0.50	1.16	3.58	1.05	1.94	0.26	1.06	0.22	0.09	0.24	0.03	0.21	1.55	0.04	0.11	0.01	0.08	0.01
BO2.5a.2	255.23	181.93	<100	0.35	0.98	3.44	0.86	1.64	0.22	0.92	0.20	0.06	0.22	0.03	0.19	1.29	0.04	0.11	0.01	0.08	0.01
BO2.5a.3	346.60	250.00	<100	0.59	1.68	5.87	1.23	2.41	0.31	1.32	0.28	0.09	0.30	0.04	0.27	1.78	0.05	0.15	0.02	0.11	0.02
BO2.5a.4	392.27	250.00	<100	0.95	2.38	8.80	1.55	3.01	0.38	1.62	0.34	0.09	0.39	0.06	0.36	2.47	0.07	0.21	0.03	0.16	0.02
BO2.5b.1	391.60	250.00	<100	0.92	2.72	10.08	1.45	2.68	0.35	1.53	0.32	0.09	0.36	0.05	0.32	2.24	0.07	0.18	0.02	0.14	0.02
BO2.5b.2	380.13	250.00	<100	0.93	2.67	8.51	1.79	3.35	0.44	1.82	0.37	0.28	0.40	0.06	0.34	2.34	0.07	0.19	0.02	0.14	0.02
BO2.5b.3	464.42	250.00	<100	1.01	2.62	6.86	1.67	3.14	0.41	1.75	0.38	0.11	0.42	0.06	0.38	2.53	0.08	0.21	0.03	0.17	0.03
BO2.5c.1	401.02	201.63	<100	1.33	2.87	9.90	1.42	2.58	0.34	1.43	0.30	0.07	0.35	0.05	0.31	2.18	0.06	0.17	0.02	0.14	0.02
BO2.5c.2	381.41	250.00	<100	1.09	3.22	16.01	1.61	3.01	0.40	1.65	0.35	0.13	0.37	0.06	0.34	2.19	0.07	0.18	0.02	0.14	0.02
BO2.5c.3	393.20	201.12	<100	1.20	2.83	15.17	1.54	2.82	0.36	1.55	0.32	0.08	0.33	0.05	0.29	1.95	0.06	0.16	0.02	0.13	0.02
BO2.5d.1	377.89	180.45	<100	1.25	2.51	7.54	1.42	2.60	0.34	1.47	0.31	0.08	0.34	0.05	0.31	2.12	0.06	0.17	0.02	0.14	0.02
BO2.5d.2	425.06	201.06	<100	1.33	2.71	12.34	1.55	2.85	0.37	1.56	0.34	0.08	0.36	0.05	0.31	2.08	0.06	0.17	0.02	0.14	0.02
BO2.5f	375.26	218.66	<100	1.07	2.72	11.72	1.47	2.73	0.35	1.48	0.31	0.07	0.34	0.05	0.31	2.01	0.06	0.17	0.02	0.13	0.02
BO2.5g	390.45	250.00	<100	1.13	2.79	9.50	1.45	2.74	0.36	1.51	0.32	0.08	0.34	0.05	0.31	2.09	0.06	0.18	0.02	0.14	0.02
PSP.1	305.40	250.00	*off-scale*	1.33	1.01	149.48	5.24	9.68	1.33	5.57	1.14	0.71	1.05	0.15	0.89	5.06	0.17	0.44	0.06	0.35	0.05
RT1.5a	467.33	250.00	<100	1.10	3.52	10.79	1.71	3.34	0.43	1.78	0.37	0.11	0.40	0.06	0.36	2.46	0.07	0.20	0.03	0.17	0.02
RT1.5b.1	454.91	250.00	<100	0.99	3.73	12.85	1.55	3.00	0.40	1.69	0.37	0.10	0.41	0.06	0.36	2.44	0.07	0.21	0.03	0.16	0.02
RT1.5b.2	424.80	250.00	<100	0.98	3.24	16.78	1.68	3.24	0.43	1.80	0.40	0.11	0.43	0.06	0.38	2.50	0.08	0.21	0.03	0.17	0.03
RT1.5c.1	407.69	250.00	<100	0.96	3.18	12.01	1.36	2.66	0.35	1.46	0.33	0.08	0.36	0.06	0.34	2.41	0.07	0.19	0.03	0.15	0.02
RT1.5c.2	404.94	250.00	<100	0.91	3.53	12.77	1.41	2.77	0.36	1.53	0.34	0.08	0.38	0.06	0.36	2.42	0.07	0.20	0.03	0.16	0.02
RT3.5a.2	446.30	250.00	<100	0.85	3.55	18.45	1.47	2.83	0.38	1.62	0.35	0.09	0.40	0.06	0.37	2.56	0.08	0.21	0.03	0.17	0.02
RT3.5d	370.47	280.00	*off-scale*	1.08	3.28	13.38	1.35	2.62	0.34	1.46	0.32	0.07	0.34	0.05	0.33	2.11	0.07	0.18	0.02	0.15	0.02
RT3.5e.1	375.78	280.00	*off-scale*	1.03	2.71	14.43	1.73	3.34	0.45	1.87	0.41	0.12	0.43	0.07	0.40	2.53	0.08	0.23	0.03	0.18	0.03
RT3.5e3	369.23	250.00	<100	0.79	2.69	12.19	1.61	3.06	0.42	1.76	0.37	0.10	0.40	0.06	0.37	2.44	0.08	0.21	0.03	0.17	0.02
RT4.2a	495.77	919.67	0.69	1.45	2.55	16.13	2.65	4.58	0.60	2.32	0.49	0.20	0.48	0.07	0.41	2.91	0.08	0.22	0.03	0.17	0.03
RT4.5a.1	347.20	186.80	*off-scale*	0.91	2.65	9.54	1.43	2.67	0.35	1.49	0.33	0.07	0.36	0.05	0.34	2.39	0.07	0.20	0.03	0.14	0.02
RT4.5a.2	365.82	250.00	<100	0.97	2.66	8.19	1.61	3.01	0.39	1.64	0.35	0.07	0.35	0.06	0.33	2.32	0.07	0.19	0.03	0.15	0.02
RT4.5a.3	361.34	224.35	*off-scale*	0.92	3.22	17.20	1.76	3.20	0.42	1.82	0.40	0.11	0.46	0.07	0.43	3.01	0.09	0.24	0.03	0.19	0.03
RT4.5b.2	401.45	185.04	<100	0.82	2.87	7.34	1.21	2.25	0.29	1.21	0.26	0.07	0.30	0.05	0.28	2.07	0.06	0.16	0.02	0.12	0.02
RT4.5b.3	415.91	250.00	<100	0.95	3.16	9.71	1.38	2.61	0.35	1.47	0.33	0.08	0.38	0.06	0.35	2.40	0.07	0.19	0.03	0.15	0.02
RT4.5c	365.11	215.49	<100	0.81	2.18	21.34	1.51	2.63	0.35	1.47	0.30	0.08	0.33	0.05	0.28	1.97	0.06	0.16	0.02	0.12	0.02
RT4.5d.2	433.13	179.50	<100	0.88	2.53	7.67	1.44	2.58	0.34	1.45	0.31	0.08	0.34	0.05	0.32	2.28	0.07	0.19	0.02	0.15	0.02
RT4.5d.3	361.31	215.46	*off-scale*	1.07	2.84	9.94	1.22	2.21	0.30	1.25	0.28	0.07	0.30	0.05	0.29	1.89	0.06	0.16	0.02	0.12	0.02
RT4.5e	360.98	295.30	*off-scale*	1.11	3.14	131.71	1.59	3.02	0.40	1.72	0.37	0.11	0.42	0.06	0.38	2.49	0.08	0.22	0.03	0.17	0.02
RT5a.3a	529.06	704.39	0.89	1.19	1.62	37.14	2.85	4.92	0.66	2.54	0.52	0.20	0.52	0.08	0.47	3.48	0.10	0.27	0.04	0.22	0.03
RT5a.5a.1	365.37	163.36	*off-scale*	0.88	2.91	10.77	1.27	2.23	0.30	1.32	0.28	0.07	0.33	0.05	0.30	2.09	0.06	0.16	0.02	0.13	0.02
RT5a.5a.3	358.04	251.91	<100	0.82	3.28	13.90	1.71	3.05	0.41	1.74	0.36	0.10	0.41	0.06	0.35	2.46	0.07	0.20	0.02	0.15	0.02
RT5a.5b.2	366.98	214.07	*off-scale*	1.33	2.80	11.48	1.66	2.85	0.37	1.55	0.33	0.09	0.38	0.06	0.38	2.64	0.08	0.23	0.03	0.18	0.03
RT5a.5c.1	374.52	236.02	*off-scale*	1.33	2.93	12.89	1.53	2.85	0.38	1.60	0.34	0.14	0.37	0.05	0.33	2.24	0.07	0.18	0.02	0.13	0.02
RT5a.5c.2	374.95	195.44	*off-scale*	1.23	2.79	9.02	1.40	2.61	0.34	1.43	0.31	0.12	0.36	0.05	0.33	2.31	0.07	0.19	0.02	0.14	0.02
RT5a.5c.3	349.78	250.00	<100	0.73	3.07	13.80	1.63	3.03	0.42	1.81	0.39	0.15	0.42	0.06	0.36	2.51	0.07	0.20	0.03	0.15	0.02
RT5a.5c.4	381.90	215.31	*off-scale*	1.07	3.27	12.28	1.54	2.75	0.38	1.60	0.35	0.09	0.38	0.05	0.34	2.34	0.07	0.19	0.02	0.14	0.02
RT5a.5e.1	371.33	243.55	*off-scale*	1.33	2.60	12.28	1.67	3.11	0.41	1.70	0.37	0.18	0.38	0.06	0.35	2.18	0.07	0.19	0.02	0.14	0.02
RT6a.2	468.96	250.00	<100	1.99	1.98	10.18	3.36	6.41	0.84	3.52	0.71	0.46	0.69	0.09	0.53	3.25	0.10	0.26	0.03	0.18	0.02
RT6a.4	385.75	250.00	<100	15.98	1.40	10.07	3.06	5.39	0.66	2.61	0.49	0.17	0.50	0.07	0.43	2.85	0.09	0.24	0.03	0.17	0.02
RT6a.5a.1	275.32	143.16	<100	0.57	0.95	2.51	0.88	1.60	0.21	0.88	0.18	0.04	0.19	0.03	0.17	1.22	0.03	0.10	0.01	0.08	0.01
RT6a.5e	263.66	134.06	<100	0.68	0.94	2.68	0.70	1.29	0.17	0.70	0.14	0.03	0.16	0.02	0.14	1.00	0.03	0.08	0.01	0.07	0.01
SNO.1d	447.58	618.31	0.31	1.09	2.19	56.89	2.17	4.00	0.53	2.07	0.44	0.11	0.40	0.06	0.34	2.28	0.07	0.18	0.02	0.15	0.02
SNO.5e.1	577.70	489.94	0.26	1.69	2.78	9.82	1.67	3.00	0.40	1.54	0.33	0.07	0.33	0.05	0.30	2.35	0.06	0.17	0.02	0.14	0.02
SNO.5e.2	531.59	627.94	0.25	0.98	2.67	11.12	1.70	3.16	0.42	1.63	0.36	0.09	0.37	0.06	0.35	2.63	0.07	0.20	0.03	0.16	0.02
SNO.5e.3	539.24	536.71	0.19	0.95	2.93	26.89	1.95	3.57	0.47	1.82	0.40	0.09	0.41	0.06	0.38	2.86	0.08	0.22	0.03	0.17	0.02
SNO.5f.1	482.52	550.30	0.20	0.77	2.68	9.65	1.57	2.91	0.39	1.50	0.33	0.08	0.34	0.06	0.33	2.53	0.07	0.19	0.03	0.15	0.02
SNO.5g.1	392.88	347.61	0.14	0.70	2.48	6.71	1.06	1.95	0.26	1.01	0.22	0.05	0.23	0.04	0.21	1.67	0.05	0.12	0.02	0.10	0.01
SNO.5h.2	514.73	576.50	0.22	1.10	2.93	20.04	1.63	2.98	0.41	1.59	0.34	0.08	0.34	0.05	0.32	2.49	0.07	0.18	0.02	0.15	0.02
SNO.5h.3	440.42	620.58	0.19	0.91	2.39	46.92	1.96	3.60	0.48	1.84	0.39	0.15	0.39	0.06	0.35	2.68	0.07	0.20	0.03	0.15	0.02
SPO.5a.1	535.77	426.73	0.51	1.56	2.69	7.91	1.62	2.81	0.39	1.51	0.33	0.10	0.34	0.05	0.32	2.63	0.07	0.20	0.03	0.15	0.02
SPO.5a.2	450.35	375.89	0.36	1.08	2.41	7.24	1.32	2.41	0.33	1.25	0.27	0.08	0.27	0.04	0.26	1.98	0.05	0.14	0.02	0.12	0.02
SPO.5a.3	443.60	300.25	0.36	0.83	2.45	6.28	1.32	2.37	0.33	1.30	0.28	0.08	0.30	0.05	0.27	2.32	0.06	0.16	0.02	0.13	0.02
SPO.5b.1	454.63	394.27	0.34	0.67	2.50	8.18	1.53	2.65	0.37	1.45	0.30	0.08	0.31	0.05	0.28	2.18	0.06	0.16	0.02	0.13	0.02
SPO.5b.2	551.13	359.34	0.43	4.73	2.58	9.42	1.53	2.76	0.38	1.46	0.31	0.08	0.32	0.05	0.30	2.38	0.06	0.17	0.02	0.14	0.02
SPO.5c.2	435.47	270.68	0.30	0.76	2.25	6.59	1.23	2.14	0.30	1.19	0.25	0.06	0.26	0.04	0.25	2.10	0.05	0.15	0.02	0.12	0.02
SPO.5c.3	519.56	524.87	0.40	1.15	2.58	13.48	1.69	3.09	0.42	1.61	0.35	0.08	0.36	0.05	0.32	2.41	0.07	0.18	0.02	0.15	0.02
SPO.5d.1	515.72	339.11	0.43	1.53	1.93	13.11	1.68	2.91	0.38	1.45	0.31	0.13	0.29	0.04	0.25	1.94	0.05	0.14	0.02	0.11	0.02
SPO.5d.2	549.91	445.28	0.43	1.06	2.83	8.57	1.59	2.92	0.39	1.54	0.33	0.09	0.34	0.05	0.31	2.44	0.07	0.18	0.02	0.14	0.02
SPO.5e.1	558.07	244.24	0.36	1.14	2.14	7.06	1.94	3.38	0.46	1.78	0.38	0.12	0.39	0.06	0.37	2.97	0.08	0.22	0.03	0.17	0.03
SPO.5e.2	589.34	504.37	0.41	1.30	2.56	12.18	1.79	3.22	0.43	1.67	0.36	0.09	0.35	0.05	0.32	2.42	0.07	0.18	0.02	0.14	0.02
SPO.5f.1	587.19	309.20	0.33	0.99	2.55	7.77	1.47	2.53	0.33	1.27	0.26	0.07	0.26	0.04	0.25	2.11	0.05	0.15	0.02	0.12	0.02
SPO.5f.2	595.21	454.10	0.41	0.99	2.89	11.19	1.86	3.35	0.46	1.78	0.38	0.09	0.38	0.06	0.34	2.71	0.07	0.20	0.03	0.16	0.02
SPO.5f.3	605.08	301.98	0.47	1.10	2.57	9.47	2.09	3.62	0.49	1.91	0.42	0.13	0.43	0.07	0.39	3.08	0.08	0.23	0.03	0.18	0.03
SPO.5g.1	575.59	329.42	0.40	0.99	2.38	8.75	1.82	3.16	0.43	1.68	0.36	0.10	0.37	0.06	0.33	2.60	0.07	0.19	0.03	0.15	0.02
SPO.5g.2	601.00	334.64	0.40	1.07	2.49	7.81	1.74	3.03	0.40	1.56	0.33	0.08	0.33	0.05	0.31	2.50	0.07	0.18	0.02	0.14	0.02
SPO.5h	589.54	304.54	0.51	0.86	3.00	12.07	1.63	2.82	0.40	1.56	0.35	0.09	0.36	0.06	0.34	2.77	0.07	0.20	0.03	0.15	0.02
SPO.5i.1	582.12	383.77	0.36	0.78	3.03	8.50	1.85	3.21	0.44	1.72	0.38	0.10	0.38	0.06	0.35	2.81	0.07	0.20	0.03	0.15	0.02
SPO.5i.2	571.48	680.37	0.42	1.17	3.00	11.73	2.77	5.08	0.68	2.63	0.57	0.21	0.58	0.09	0.51	3.71	0.10	0.28	0.04	0.21	0.03
SPO.5i.3	570.99	597.71	0.32	0.87	3.16	9.85	2.40	4.37	0.59	2.28	0.49	0.19	0.49	0.08	0.45	3.28	0.09	0.25	0.04	0.20	0.03
SPO.5i.4	582.56	364.03	0.38	0.70	2.71	7.84	1.74	2.98	0.39	1.51	0.32	0.10	0.33	0.05	0.30	2.41	0.06	0.18	0.02	0.13	0.02

10.4. Appendix 4: Analysis Types and Sample Sizes

Internal Specimen Names	Rock Samples	REE Analysis	Laminae	Sediment & Intercalations	Photographs	Thin Sections	SEM Mounts	SLI Analysis	Laminae	Sediment & Intercalations	XRD
A.W S.N Onions	X	X	X	X	X	X	X	X	X	X	X
Onions RT1	RT1	✓	✓	X	✓	✓	✓	✓	✓	X	✓
Onions RT3	RT3	✓	✓	X	✓	✓	✓	✓	✓	X	✓
Onions RT4	RT4	✓	✓	✓ (1 sample)	✓	✓	✓	✓	✓	X	✓
Onions RT5a	RT5a	✓	✓	✓ (1 sample)	✓	✓	✓	✓	✓	X	✓
Onions RT6a	RT6a	✓	✓	✓ (1 sample)	✓	X	X	✓	✓	X	✓
Poofy SP RT AW	PSP	✓	X	✓ (1 sample)	X	X	X	✓	✓	X	✓
S-N Boundary Onion 1a	BO1a	✓	✓	✓ (1 sample)	✓	X	X	✓	✓	X	✓
S-N Boundary Onion 1b	BO1b	✓	X	✓ (1 sample)	X	X	X	X	X	X	✓
S-N Boundary Onion 2	BO2	✓	✓	✓ (1 sample)	✓	X	X	✓	✓	✓	✓
SN Onion	SNO	✓	✓	✓ (2 samples)	✓	✓	✓	X	X	X	✓
SP Onion	SPO	✓	✓	X	✓	✓	✓	X	X	X	✓
Spitzkopf Muffin 1	X	X	X	X	X	X	X	X	X	X	X
SP-NS AW1	X	X	X	X	X	X	X	X	X	X	X
21 collected	**14 polished**	**175 powders collected from 11 rocks**			**14 rocks photographed**	**11 sections made from 6 rocks**	**8 mounts made from 6 rocks**	**51 of the 84 REE powders, from 8 rocks**			**15 powders from 11 rocks, selected randomly from unanalysed drilled powders**
14 named	11 sampled	84 powders plotted for REE			9 rocks described	11 sections described	8 mounts scanned	46 of the 51 aligned with REE plotted powders			15 analysed

11. References

Abell, P. I., Awramik, S. M., Osborne, R. H., and Tomellini, S., 1982, Plio-Pleistocene lacustrine stromatolites from Lake Turkana, Kenya: morphology, stratigraphy, and stable isotopes: Sedimentary Geology, v. 32, p. 1-26.

Adams, E. W., Grotzinger, J. P., Watters, W. A., Schröder, S., McCormick, D. S., and Al-Siyabi, H. A., 2005, Digital characterization of thrombolite-stromatolite reef distribution in a carbonate ramp system (terminal Proterozoic, Nama Group, Namibia): AAPG Bulletin, v. 89, no. 10, p. 1293-1318.

Aitken, J. D., 1967, Classification and environmental significance of cryptalgal limestones and dolomites, with illustrations from the Cambrian and Ordovician of southwestern Alberta: Journal of Sedimentary Research, v. 37, no. 4, p. 1163-1178.

Almond, J., 2009, Contributions to the palaeontology and stratigraphy of the Alexander Bay sheet area (1: 250.000 geological sheet 2816). 117 pp: Unpublished report for the Council for Geoscience. Natura Viva cc, Cape Town.

Amthor, J. E., Grotzinger, J. P., Schröder, S., Bowring, S. A., Ramezani, J., Martin, M. W., and Matter, A., 2003, Extinction of Cloudina and Namacalathus at the Precambrian-Cambrian boundary in Oman: Geology, v. 31, no. 5, p. 431-434.

Anbar, A. D., and Knoll, A. H., 2002, Proterozoic ocean chemistry and evolution: a bioinorganic bridge?: science, v. 297, no. 5584, p. 1137-1142.

Andres, M. S., and Pamela Reid, R., 2006, Growth morphologies of modern marine stromatolites: A case study from Highborne Cay, Bahamas: Sedimentary Geology, v. 185, no. 3-4, p. 319-328.

Arenas, C., Jones, B., and Hollis, C., 2017, Temporal and environmental significance of microbial lamination: Insights from Recent fluvial stromatolites in the River Piedra, Spain: Sedimentology, v. 64, no. 6, p. 1597-1629.

Arp, G., Reimer, A., and Reitner, J., 2001, Photosynthesis-induced biofilm calcification and calcium concentrations in Phanerozoic oceans: Science, v. 292, no. 5522, p. 1701-1704.

Awramik, S. M., 1971, Precambrian Columnar Stromatolite Diversity: Reflection of Metazoan Appearance: Science, v. 174, no. 4011, p. 825-827.

Awramik, S. M., 1992, The history and significance of stromatolites, Early organic evolution, Springer, p. 435-449.

Awramik, S. M., and Grey, K., Stromatolites: biogenicity, biosignatures, and bioconfusion, *in* Proceedings Astrobiology and Planetary Missions2005, Volume 5906, SPIE, p. 227-235.

Awramik, S. M., and Semikhatov, M., 1979, The relationship between morphology, microstructure, and microbiota in three vertically intergrading stromatolites from the Gunflint Iron Formation: Canadian Journal of Earth Sciences, v. 16, no. 3, p. 484-495.

Awramik, S., 1991, Archaean and Proterozoic stromatolites: Calcareous algae and stromatolites, p. 289-304.

Awramik, S., and Margulis, L., 1974, Definition of stromatolite: Stromatolite Newsletter (unpublished), v. 2.
Banner, J. L., Hanson, G., and Meyers, W., 1988, Rare earth element and Nd isotopic variations in regionally extensive dolomites from the Burlington-Keokuk Formation (Mississippian); implications for REE mobility during carbonate diagenesis: Journal of Sedimentary Research, v. 58, no. 3, p. 415-432.
Barbieri, R., and Cavalazzi, B., 2004, Astrobiological implications of microbial morphologies in cold fluid-generated carbonates: Advances in Space Research, v. 33, no. 8, p. 1262-1267.
Bau, M., 1999, Scavenging of dissolved yttrium and rare earths by precipitating iron oxyhydroxide: experimental evidence for Ce oxidation, Y-Ho fractionation, and lanthanide tetrad effect: Geochimica et Cosmochimica Acta, v. 63, no. 1, p. 67-77.
Bau, M., and Dulski, P., 1999, Comparing yttrium and rare earths in hydrothermal fluids from the Mid-Atlantic Ridge: implications for Y and REE behaviour during near-vent mixing and for the Y/Ho ratio of Proterozoic seawater: Chemical Geology, v. 155, no. 1-2, p. 77-90.
Bau, M., Möller, P., and Dulski, P., 1997, Yttrium and lanthanides in eastern Mediterranean seawater and their fractionation during redox-cycling: Marine Chemistry, v. 56, no. 1-2, p. 123-131.
Bekker, A., Holland, H., Wang, P.-L., Rumble Iii, D., Stein, H., Hannah, J., Coetzee, L., and Beukes, N., 2004, Dating the rise of atmospheric oxygen: Nature, v. 427, no. 6970, p. 117-120.
Bekker, A., Planavsky, N., Rasmussen, B., Krapez, B., Hofmann, A., Slack, J., Rouxel, O., and Konhauser, K., 2014, Iron formations: Their origins and implications for ancient seawater chemistry, Treatise on geochemistry, Volume 12, Elsevier, p. 561-628.
Bellefroid, E. J., Planavsky, N. J., Miller, N. R., Brand, U., and Wang, C., 2018, Case studies on the utility of sequential carbonate leaching for radiogenic strontium isotope analysis: Chemical Geology, v. 497, p. 88-99.
Bengtson, S., 2004, Early skeletal fossils: The Paleontological Society Papers, v. 10, p. 67-78.
Beveridge, T., and Murray, R., 1976, Uptake and retention of metals by cell walls of Bacillus subtilis: Journal of Bacteriology, v. 127, no. 3, p. 1502-1518.
Black, M., 1933, The precipitation of calcium carbonate on the Great Bahama Bank: Geological Magazine, v. 70, no. 10, p. 455-466.
Blanco, G., Germs, G. J. B., Rajesh, H. M., Chemale, F., Dussin, I. A., and Justino, D., 2011, Provenance and paleogeography of the Nama Group (Ediacaran to early Palaeozoic, Namibia): Petrography, geochemistry and U–Pb detrital zircon geochronology: Precambrian Research, v. 187, no. 1-2, p. 15-32.
Bolhar, R., and Van Kranendonk, M. J., 2007, A non-marine depositional setting for the northern Fortescue Group, Pilbara Craton, inferred from trace element geochemistry of stromatolitic carbonates: Precambrian Research, v. 155, no. 3-4, p. 229-250.
Bolhar, R., Kamber, B. S., Moorbath, S., Fedo, C. M., and Whitehouse, M. J., 2004, Characterisation of early Archaean chemical sediments by trace element signatures: Earth and Planetary Science Letters, v. 222, no. 1, p. 43-60.
Bosak, T., Mariotti, G., MacDonald, F. A., Perron, J. T., and Pruss, S. B., 2013, Microbial sedimentology of stromatolites in Neoproterozoic cap carbonates: The Paleontological Society Papers, v. 19, p. 51-76.
Bowyer, F. T., Shore, A. J., Wood, R. A., Alcott, L. J., Thomas, A. L., Butler, I. B., Curtis, A., Hainanan, S., Curtis-Walcott, S., Penny, A. M., and Poulton, S. W., 2020, Regional nutrient decrease drove redox stabilisation and metazoan diversification in the late Ediacaran Nama Group, Namibia: Sci Rep, v. 10, no. 1, p. 2240.
Brasier, M., and Lindsay, J., 1998, A billion years of environmental stability and the emergence of eukaryotes: new data from northern Australia: Geology, v. 26, no. 6, p. 555-558.
Buick, R., Des Marais, D. J., and Knoll, A. H., 1995, Stable isotopic compositions of carbonates from the Mesoproterozoic Bangemall Group, northwestern Australia: Chemical Geology, v. 123, no. 1-4, p. 153-171.

Burne, R. V., and Moore, L. S., 1987, Microbialites: organosedimentary deposits of benthic microbial communities: Palaios, p. 241-254.
Buzoleva, L., Bezverbnaya, I., and Kalitina, E., 2006, Microbiological analysis of the contamination of marginal seas in the northwestern part of the Pacific Ocean: Oceanology, v. 46, no. 1, p. 50.
Byrne, R. H., and Kim, K.-H., 1990, Rare earth element scavenging in seawater: Geochimica et Cosmochimica Acta, v. 54, no. 10, p. 2645-2656.
Cabioch, G., Camoin, G., Webb, G. E., Le Cornec, F., Molina, M. G., Pierre, C., and Joachimski, M. M., 2006, Contribution of microbialites to the development of coral reefs during the last deglacial period: case study from Vanuatu (South-West Pacific): Sedimentary Geology, v. 185, no. 3-4, p. 297-318.
Cady, S. L., Farmer, J. D., Grotzinger, J. P., Schopf, J. W., and Steele, A., 2003, Morphological biosignatures and the search for life on Mars: Astrobiology, v. 3, no. 2, p. 351-368.
Canfield, D. E., 2005, The early history of atmospheric oxygen: homage to Robert M. Garrels: Annu. Rev. Earth Planet. Sci., v. 33, p. 1-36.
Canfield, D. E., and Teske, A., 1996, Late Proterozoic rise in atmospheric oxygen concentration inferred from phylogenetic and sulphur-isotope studies: Nature, v. 382, no. 6587, p. 127-132.
Canfield, D. E., Ngombi-Pemba, L., Hammarlund, E. U., Bengtson, S., Chaussidon, M., Gauthier-Lafaye, F., Meunier, A., Riboulleau, A., Rollion-Bard, C., Rouxel, O., Asael, D., Pierson-Wickmann, A. C., and El Albani, A., 2013, Oxygen dynamics in the aftermath of the Great Oxidation of Earth's atmosphere: Proc Natl Acad Sci U S A, v. 110, no. 42, p. 16736-16741.
Canfield, D. E., Poulton, S. W., and Narbonne, G. M., 2007, Late-Neoproterozoic deep-ocean oxygenation and the rise of animal life: Science, v. 315, no. 5808, p. 92-95.
Canfield, D. E., Poulton, S. W., Knoll, A. H., Narbonne, G. M., Ross, G., Goldberg, T., and Strauss, H., 2008, Ferruginous conditions dominated later Neoproterozoic deep-water chemistry: Science, v. 321, no. 5891, p. 949-952.
Cao, R., 2003, History and current status of study on stromatolitic nomenclature and classification in the Precambrian: Geological Survey and Research, v. 26, no. 2, p. 80-83.
Chandler, F. W., 1980, Proterozoic redbed sequences of Canada.
Cloud, P. E., and Semikhatov, M., 1969, Proterozoic stromatolite zonation: American Journal of Science, v. 267, no. 9, p. 1017-1061.
Cloud, P., and Drake, E., 1968, Pre-metazoan evolution and the origins of the Metazoa: Evolution and environment, v. 72.
Corkeron, M., Webb, G. E., Moulds, J., and Grey, K., 2012, Discriminating stromatolite formation modes using rare earth element geochemistry: Trapping and binding versus in situ precipitation of stromatolites from the Neoproterozoic Bitter Springs Formation, Northern Territory, Australia: Precambrian Research, v. 212-213, p. 194-206.
Cortijo, I., Cai, Y., Hua, H., Schiffbauer, J. D., and Xiao, S., 2015, Life history and autecology of an Ediacaran index fossil: Development and dispersal of Cloudina: Gondwana Research, v. 28, no. 1, p. 419-424.
Criado-Reyes, J., Otalora, F., Canals, A., Verdugo-Escamilla, C., and Garcia-Ruiz, J. M., 2023, Mechanisms shaping the gypsum stromatolite-like structures in the Salar de Llamara (Atacama Desert, Chile): Sci Rep, v. 13, no. 1, p. 678.
Crowe, S. A., Døssing, L. N., Beukes, N. J., Bau, M., Kruger, S. J., Frei, R., and Canfield, D. E., 2013, Atmospheric oxygenation three billion years ago: Nature, v. 501, no. 7468, p. 535-538.
Curtis, A., Wood, R., Bowyer, F., Shore, A., Curtis-Walcott, A., Robertsson, J., and Brasier, A., 2020, Modelling Ediacaran metazoan–microbial reef growth: Sedimentology, v. 68, no. 5, p. 1877-1892.

Dahl, T. W., Hammarlund, E. U., Anbar, A. D., Bond, D. P., Gill, B. C., Gordon, G. W., Knoll, A. H., Nielsen, A. T., Schovsbo, N. H., and Canfield, D. E., 2010, Devonian rise in atmospheric oxygen correlated to the radiations of terrestrial plants and large predatory fish: Proceedings of the National Academy of Sciences, v. 107, no. 42, p. 17911-17915.

Danielson, A., Möller, P., and Dulski, P., 1992, The europium anomalies in banded iron formations and the thermal history of the oceanic crust: Chemical geology, v. 97, no. 1-2, p. 89-100.

Darroch, S. A., Boag, T. H., Racicot, R. A., Tweedt, S., Mason, S. J., Erwin, D. H., and Laflamme, M., 2016, A mixed Ediacaran-metazoan assemblage from the Zaris Sub-basin, Namibia: Palaeogeography, Palaeoclimatology, Palaeoecology, v. 459, p. 198-208.

Darroch, S. A., Sperling, E. A., Boag, T. H., Racicot, R. A., Mason, S. J., Morgan, A. S., Tweedt, S., Myrow, P., Johnston, D. T., Erwin, D. H., and Laflamme, M., 2015, Biotic replacement and mass extinction of the Ediacara biota: Proc Biol Sci, v. 282, no. 1814.

Davis, T. A., Volesky, B., and Mucci, A., 2003, A review of the biochemistry of heavy metal biosorption by brown algae: Water research, v. 37, no. 18, p. 4311-4330.

De Carlo, E. H., and Green, W. J., 2002, Rare earth elements in the water column of Lake Vanda, McMurdo Dry Valleys, Antarctica: Geochimica et Cosmochimica Acta, v. 66, no. 8, p. 1323-1333.

Derco, J., and Vrana, B., 2018, Introductory Chapter: Biosorption, Biosorption.

Derry, L. A., 2015, Causes and consequences of mid-Proterozoic anoxia: Geophysical Research Letters, v. 42, no. 20, p. 8538-8546.

Derry, L. A., and Jacobsen, S. B., 1990, The chemical evolution of Precambrian seawater: evidence from REEs in banded iron formations: Geochimica et Cosmochimica Acta, v. 54, no. 11, p. 2965-2977.

Diakonov, I., Ragnarsdottir, K., and Tagirov, B., 1998, Standard thermodynamic properties and heat capacity equations of rare earth hydroxides:: II. Ce (III)-, Pr-, Sm-, Eu (III)-, Gd-, Tb-, Dy-, Ho-, Er-, Tm-, Yb-, and Y-hydroxides. Comparison of thermochemical and solubility data: Chemical geology, v. 151, no. 1-4, p. 327-347.

Diamond, C. W., and Lyons, T. W., 2018, Mid-Proterozoic redox evolution and the possibility of transient oxygenation events: Emerging Topics in Life Sciences, v. 2, no. 2, p. 235-245.

Dill, R. F., Shinn, E. A., Jones, A. T., Kelly, K., and Steinen, R. P., 1986, Giant subtidal stromatolites forming in normal salinity waters: Nature, v. 324, no. 6092, p. 55-58.

Droser, M. L., and Gehling, J. G., 2015, The advent of animals: the view from the Ediacaran: Proceedings of the National Academy of Sciences, v. 112, no. 16, p. 4865-4870.

Droser, M. L., Tarhan, L. G., and Gehling, J. G., 2017, The Rise of Animals in a Changing Environment: Global Ecological Innovation in the Late Ediacaran: Annual Review of Earth and Planetary Sciences, v. 45, no. 1, p. 593-617.

Dumoulin, J. A., Slack, J. F., Whalen, M. T., and Harris, A. G., 2011, Depositional setting and geochemistry of phosphorites and metalliferous black shales in the carboniferous-permian lisburne group, northern Alaska: US Geological Survey, 2330-7102.

Dupraz, C., Pattisina, R., and Verrecchia, E. P., 2006, Translation of energy into morphology: Simulation of stromatolite morphospace using a stochastic model: Sedimentary Geology, v. 185, no. 3-4, p. 185-203.

Dupraz, C., Reid, R. P., Braissant, O., Decho, A. W., Norman, R. S., and Visscher, P. T., 2009, Processes of carbonate precipitation in modern microbial mats: Earth-Science Reviews, v. 96, no. 3, p. 141-162.

Dupraz, C., Visscher, P. T., Baumgartner, L., and Reid, R., 2004, Microbe–mineral interactions: early carbonate precipitation in a hypersaline lake (Eleuthera Island, Bahamas): Sedimentology, v. 51, no. 4, p. 745-765.

Eguchi, J., Seales, J., and Dasgupta, R., 2020, Great Oxidation and Lomagundi events linked by deep cycling and enhanced degassing of carbon: Nature geoscience, v. 13, no. 1, p. 71-76.

El Tabakh, M., Grey, K., Pirajno, F., and Charlotte Schreiber, B., 1999, Pseudomorphs after evaporitic minerals interbedded with 2.2 Ga stromatolites of the Yerrida basin, Western Australia: origin and significance: Geology, v. 27, no. 10, p. 871-874.
Elderfield, H., 1988, The oceanic chemistry of the rare-earth elements: Philosophical Transactions of the Royal Society of London. Series A, Mathematical and Physical Sciences, v. 325, no. 1583, p. 105-126.
Elderfield, H., and Greaves, M., 1981, Negative cerium anomalies in the rare earth element patterns of oceanic ferromanganese nodules: Earth and Planetary Science Letters, v. 55, no. 1, p. 163-170.
Elderfield, H., and Pagett, R., 1986, Rare earth elements in ichthyoliths: variations with redox conditions and depositional environment: Science of the Total Environment, v. 49, p. 175-197.
Elderfield, H., and Sholkovitz, E. t., 1987, Rare earth elements in the pore waters of reducing nearshore sediments: Earth and Planetary Science Letters, v. 82, no. 3-4, p. 280-288.
Fairchild, I. J., 1991, Origins of carbonate in Neoproterozoic stromatolites and the identification of modern analogues: Precambrian Research, v. 53, no. 3-4, p. 281-299.
Fani, R., 2012, The origin and evolution of metabolic pathways: why and how did primordial cells construct metabolic routes?: Evolution: Education and Outreach, v. 5, no. 3, p. 367-381.
Fedonkin, M. A., Gehling, J. G., Grey, K., Narbonne, G. M., and Vickers-Rich, P., 2007a, The rise of animals: evolution and diversification of the kingdom Animalia, JHU Press.
Fedonkin, M. A., Simonetta, A., and Ivantsov, A. Y., 2007b, New data on Kimberella, the Vendian mollusc-like organism (White Sea region, Russia): palaeoecological and evolutionary implications: Geological Society, London, Special Publications, v. 286, no. 1, p. 157-179.
Field, C. B., Behrenfeld, M. J., Randerson, J. T., and Falkowski, P., 1998, Primary production of the biosphere: integrating terrestrial and oceanic components: science, v. 281, no. 5374, p. 237-240.
Fike, D., Grotzinger, J., Pratt, L., and Summons, R., 2006, Oxidation of the Ediacaran ocean: nature, v. 444, no. 7120, p. 744-747.
Fischer, A. G., 1965, Fossils, early life, and atmospheric history, National Acad Sciences.
Foscolos, A.E., Powell, T. G., and Gunther, P. R., 1976, The use of clay minerals and inorganic and organic geochemical indicators for evaluating the degree of diagenesis and oil generating potential of shales: Geochimica et Cosmochimica Acta., v. 8, no. 40, p. 953–966.
Fournier, G., Moore, K., Rangel, L., Payette, J., Momper, L., and Bosak, T., 2021, The Archean origin of oxygenic photosynthesis and extant cyanobacterial lineages: Proceedings of the Royal Society B, v. 288, no. 1959, p. 20210675.
Fralick, P., and Riding, R., 2015, Steep Rock Lake: Sedimentology and geochemistry of an Archean carbonate platform: Earth-Science Reviews, v. 151, p. 132-175.
Frei, R., Crowe, S. A., Bau, M., Polat, A., Fowle, D. A., and Døssing, L. N., 2016, Oxidative elemental cycling under the low O2 Eoarchean atmosphere: Scientific reports, v. 6, no. 1, p. 21058.
Frimmel, H. E., 2009, Trace element distribution in Neoproterozoic carbonates as palaeoenvironmental indicator: Chemical Geology, v. 258, no. 3-4, p. 338-353.
Furuyama, S., Kano, A., Kunimitsu, Y., Osanai, Y., Adachi, T., Liu, X., and Wang, W., 2013, Ediacaran mineralized microfossils from the basinal facies of the Doushantuo Formation in northwestern Hunan Province, South China: Paleontological Research, v. 17, no. 3, p. 241-250.
Gabelein, C. D., 1974, Biologic control of stromatolite microstructure: implications for Precambrian time stratigraphy: American Journal of Science, v. 274, no. 6, p. 575-598.
Gadd, G. M., 2009, Biosorption: critical review of scientific rationale, environmental importance and significance for pollution treatment: Journal of Chemical Technology & Biotechnology: International Research in Process, Environmental & Clean Technology, v. 84, no. 1, p. 13-28.

Gandin, A., and Debrenne, F., 2010, Distribution of the archaeocyath-calcimicrobial bioconstructions on the Early Cambrian shelves: Palaeoworld, v. 19, no. 3-4, p. 222-241.
German, C. R., and Elderfield, H., 1990, Application of the Ce anomaly as a paleoredox indicator: the ground rules: Paleoceanography, v. 5, no. 5, p. 823-833.
Germs, 1995, The Neoproterozoic of southwestern Africa, with emphasis on platform stratigraphy and paleontology: Precambrian Research, v. 73, no. 1-4, p. 137-151.
Germs, G. J. B., Knoll, A. H., and Vidal, G., 1986, Latest Proterozoic microfossils from the Nama Group, Namibia (South West Africa): Precambrian Research, v. 32, p. 45-62.
Germs, G. J., 1972, New shelly fossils from Nama Group, South West Africa: American Journal of Science, v. 272, p. 752-761.
Germs, G. J., 1974, The Nama Group in South West Africa and its relationship to the Pan-African geosyncline: The Journal of Geology, v. 82, no. 3, p. 301-317.
Germs, G. J., 1995, The Neoproterozoic of southwestern Africa, with emphasis on platform stratigraphy and paleontology: Precambrian Research, v. 73, no. 1-4, p. 137-151.
Germs, G., and Gresse, P., 1991, The foreland basin of the Damara and Gariep orogens in Namaqualand and southern Namibia: stratigraphic correlations and basin dynamics: South African Journal of Geology, v. 94, no. 2, p. 159-169.
Geyer, G., 2005, The Fish River Subgroup in Namibia: stratigraphy, depositional environments and the Proterozoic–Cambrian boundary problem revisited: Geological Magazine, v. 142, no. 5, p. 465-498.
Gibson Jr, E. K., McKay, D. S., Thomas-Keprta, K. L., Wentworth, S., Westall, F., Steele, A., Romanek, C. S., Bell, M., and Toporski, J., 2001, Life on Mars: evaluation of the evidence within Martian meteorites ALH84001, Nakhla, and Shergotty: Precambrian research, v. 106, no. 1-2, p. 15-34.
Glaessner, M., 1976, Early Phanerozoic annelid worms and their geological and biological significance: Journal of the Geological Society, v. 132, no. 3, p. 259-275.
Golubić, S., 1973, Green algae and carbonate deposits: The biology of blue-green algae, v. 9, p. 434.
Gradziński, M., 2010, Factors controlling growth of modern tufa: results of a field experiment: Geological Society, London, Special Publications, v. 336, no. 1, p. 143-191.
Grandjean, P., and Albarède, F., 1989, Ion probe measurement of rare earth elements in biogenic phosphates: Geochimica et Cosmochimica Acta, v. 53, no. 12, p. 3179-3183.
Grandjean, P., Cappetta, H., Michard, A., and Albarede, F., 1987, The assessment of REE patterns and $^{143}Nd/^{144}Nd$ ratios in fish remains: Earth and Planetary Science Letters, v. 84, no. 2-3, p. 181-196.
Grant, S., 1990, Shell structure and distribution of Cloudina, a potential index fossil for the terminal Proterozoic: American Journal of Science, v. 290, p. 261-294.
Grey, K., and Awramik, S., 2020, Handbook for the study and description of microbialites: GSWA Bull, v. 147, p. 279p.
Grosch, E. G., McLoughlin, N., and Whitehouse, M., 2023, Multiple sulphur isotope record of Paleoarchean sedimentary rocks across the Onverwacht Group, Barberton Greenstone Belt, South Africa: Geobiology, v. 21, no. 2, p. 153-167.
Grotzinger, J. P., 2000, Facies and paleoenvironmental setting of thrombolite-stromatolite reefs, terminal Proterozoic Nama Group (ca. 550–543 Ma), central and southern Namibia: Communications of the Geological Survey of Namibia, v. 12, p. 221-233.
Grotzinger, J. P., and James, N. P., 2000a, Carbonate Sedimentation and Diagenesis in the Evolving Precambrian World, SEPM Society for Sedimentary Geology.
Grotzinger, J. P., and James, N. P., 2000b, Precambrian carbonates: evolution of understanding: Society of Economic Paleontologists and Mineralogists, no. Special Publication 67, p. p. 3–22.
Grotzinger, J. P., and Knoll, A. H., 1999, Stromatolites in Precambrian carbonates: evolutionary mileposts or environmental dipsticks?: Annual review of earth and planetary sciences, v. 27, no. 1, p. 313-358.

Grotzinger, J. P., Arvidson, R., Bell Iii, J., Calvin, W., Clark, B., Fike, D., Golombek, M., Greeley, R., Haldemann, A., and Herkenhoff, K. E., 2005, Stratigraphy and sedimentology of a dry to wet eolian depositional system, Burns formation, Meridiani Planum, Mars: Earth and Planetary Science Letters, v. 240, no. 1, p. 11-72.
Grotzinger, J. P., Bowring, S. A., Saylor, B. Z., and Kaufman, A. J., 1995, Biostratigraphic and geochronologic constraints on early animal evolution: Science, v. 270, no. 5236, p. 598-604.
Grotzinger, J. P., Watters, W. A., and Knoll, A. H., 2000, Calcified metazoans in thrombolite-stromatolite reefs of the terminal Proterozoic Nama Group, Namibia: Paleobiology, v. 26, no. 3, p. 334-359.
Grotzinger, J., 1990, Geochemical model for Proterozoic stromatolite decline: American Journal of Science, v. 290, no. A, p. 80-103.
Grotzinger, J., 1994, Trends in Precambrian carbonate sediments and their implication for understanding evolution: Early life on Earth, p. 245-258.
Grotzinger, J., Adams, E. W., and SchrÖDer, S., 2005, Microbial–metazoan reefs of the terminal Proterozoic Nama Group (c. 550–543 Ma), Namibia: Geological Magazine, v. 142, no. 5, p. 499-517.
Guilbaud, R., Poulton, S. W., Butterfield, N. J., Zhu, M., and Shields-Zhou, G. A., 2015, A global transition to ferruginous conditions in the early Neoproterozoic oceans: Nature Geoscience, v. 8, no. 6, p. 466-470.
Guilbaud, R., Poulton, S. W., Thompson, J., Husband, K. F., Zhu, M., Zhou, Y., Shields, G. A., and Lenton, T. M., 2020, Phosphorus-limited conditions in the early Neoproterozoic ocean maintained low levels of atmospheric oxygen: Nature Geoscience, v. 13, no. 4, p. 296-301.
Haley, B. A., Klinkhammer, G. P., and Mix, A. C., 2005, Revisiting the rare earth elements in foraminiferal tests: Earth and Planetary Science Letters, v. 239, no. 1-2, p. 79-97.
Hamilton, T. L., Bryant, D. A., and Macalady, J. L., 2016, The role of biology in planetary evolution: cyanobacterial primary production in low-oxygen Proterozoic oceans: Environ Microbiol, v. 18, no. 2, p. 325-340.
Han, T. M., and Runnegar, B., 1992, Megascopic eukaryotic algae from the 2.1-billion-year-old Negaunee iron-formation, Michigan: Science, v. 257, no. 5067, p. 232–235.
Hand, B. M., and Bartberger, C. E., 1988, Leeside sediment fallout patterns and the stability of angular bedforms: Journal of Sedimentary Research, v. 58, no. 1, p. 33-43.
Hanson, J., 1948, Formation and breakdown of serpulid tubes: Nature, v. 161, no. 4094, p. 610-611.
Hardisty, D. S., Lu, Z., Bekker, A., Diamond, C. W., Gill, B. C., Jiang, G., Kah, L. C., Knoll, A. H., Loyd, S. J., and Osburn, M. R., 2017, Perspectives on Proterozoic surface ocean redox from iodine contents in ancient and recent carbonate: Earth and Planetary Science Letters, v. 463, p. 159-170.
Haris, V., 1990, Sessile animals of the sea shore, Springer Science and Business Media.
Hartnady, C., Joubert, P., and Stowe, C., 1985, Proterozoic crustal evolution in southwestern Africa: Episodes, v. 8, no. 4, p. 236-244.
Hedley, R., 1958, Tube formation by Pomatoceros triqueter (Polychaeta): Journal of the Marine Biological Association of the United Kingdom, v. 37, no. 2, p. 315-322.
Herman, E., and Kump, L., 2005, Biogeochemistry of microbial mats under Precambrian environmental conditions: a modelling study: Geobiology, v. 3, no. 2, p. 77-92.
Hickman-Lewis, K., Gourcerol, B., Westall, F., Manzini, D., and Cavalazzi, B., 2020, Reconstructing Palaeoarchaean microbial biomes flourishing in the presence of emergent landmasses using trace and rare earth element systematics: Precambrian Research, v. 342.
Hoffman, P., 1973, Recent and ancient algal stromatolites: seventy years of pedagogic cross-pollination: Evolving concepts in sedimentology, p. 178-191.
Hofmann, A., 2011, Archaean hydrothermal systems in the Barberton greenstone belt and their significance as a habitat for early life: Earliest life on earth: habitats, environments and methods of detection, p. 51-78.

Hofmann, H. J., 2000, Archean Stromatolites as Microbial Archives, *in* Riding, R. E., and Awramik, S. M., eds., Microbial Sediments: Berlin, Heidelberg, Springer Berlin Heidelberg, p. 315-327.
Hofmann, H., 1973, Stromatolites: characteristics and utility: Earth-Science Reviews, v. 9, no. 4, p. 339-373.
Hofmann, H., Grey, K., Hickman, A., and Thorpe, R., 1999, Origin of 3.45 Ga coniform stromatolites in Warrawoona group, Western Australia: Geological Society of America Bulletin, v. 111, no. 8, p. 1256-1262.
Holland, H. D., 2006, The oxygenation of the atmosphere and oceans: Philosophical Transactions of the Royal Society B: Biological Sciences, v. 361, no. 1470, p. 903-915.
Holland, H. D., 2020, The chemical evolution of the atmosphere and oceans, Princeton University Press.
Hua, H., Chen, Z., Yuan, X., Zhang, L., and Xiao, S., 2005, Skeletogenesis and asexual reproduction in the earliest biomineralizing animal Cloudina: Geology, v. 33, no. 4.
Hummer, D. R., Golden, J. J., Hystad, G., Downs, R. T., Eleish, A., Liu, C., Ralph, J., Morrison, S. M., Meyer, M. B., and Hazen, R. M., 2022, Evidence for the oxidation of Earth's crust from the evolution of manganese minerals: Nature communications, v. 13, no. 1, p. 1-7.
Jahnert, R. J., and Collins, L. B., 2011, Significance of subtidal microbial deposits in Shark Bay, Australia: Marine Geology, v. 286, no. 1-4, p. 106-111.
Jahnert, R. J., Collins, L. B., and Ariztegui, D., 2013, Controls on microbial activity and tidal flat evolution in Shark Bay, Western Australia: Sedimentology, v. 60, no. 4, p. 1071-1099.
James, N. P., and Gravestock, D. I., 1990, Lower Cambrian shelf and shelf margin buildups, Flinders Ranges, South Australia 1: Sedimentology, v. 37, no. 3, p. 455-480.
James, R., Elderfield, H., and Palmer, M., 1995, The chemistry of hydrothermal fluids from the Broken Spur site, 29 N Mid-Atlantic Ridge: Geochimica et Cosmochimica Acta, v. 59, no. 4, p. 651-659.
Johannesson, K. H., Telfeyan, K., Chevis, D. A., Rosenheim, B. E., and Leybourne, M. I., 2014, Rare earth elements in stromatolites—1. Evidence that modern terrestrial stromatolites fractionate rare earth elements during incorporation from ambient waters, Evolution of Archean crust and early life, Springer, p. 385-411.
Johnston, D. T., Poulton, S., Tosca, N., O'brien, T., Halverson, G., Schrag, D. P., and Macdonald, F. A., 2013, Searching for an oxygenation event in the fossiliferous Ediacaran of northwestern Canada: Chemical Geology, v. 362, p. 273-286.
Kamber, B. S., and Webb, G. E., 2001, The geochemistry of late Archaean microbial carbonate: implications for ocean chemistry and continental erosion history: Geochimica et Cosmochimica Acta, v. 65, no. 15, p. 2509-2525.
Kamber, B. S., Bolhar, R., and Webb, G. E., 2004, Geochemistry of late Archaean stromatolites from Zimbabwe: evidence for microbial life in restricted epicontinental seas: Precambrian Research, v. 132, no. 4, p. 379-399.
Kamennaya, N. A., Ajo-Franklin, C. M., Northen, T., and Jansson, C., 2012, Cyanobacteria as biocatalysts for carbonate mineralization: Minerals, v. 2, no. 4, p. 338-364.
Kano, A., Hagiwara, R., Kawai, T., Hori, M., and Matsuoka, J., 2007, Climatic Conditions and Hydrological Change Recorded in a High-Resolution Stable-Isotope Profile of a Recent Laminated Tufa on a Subtropical Island, Southern Japan: Journal of Sedimentary Research, v. 77, no. 1, p. 59-67.
Kawaguchi, T., and Decho, A. W., 2002, Isolation and biochemical characterization of extracellular polymeric secretions (EPS) from modern soft marine stromatolites (Bahamas) and its inhibitory effect on CaCO3 precipitation: Preparative Biochemistry and Biotechnology, v. 32, no. 1, p. 51-63.
Kazak, E., Kalitina, E., Kharitonova, N., Chelnokov, G., Elovskii, E., and Bragin, I., 2018, Biosorption of rare-earth elements and yttrium by heterotrophic bacteria in an aqueous environment: Moscow University Geology Bulletin, v. 73, p. 287-294.

Kennard, J. M., and James, N. P., 1986, Thrombolites and stromatolites; two distinct types of microbial structures: Palaios, v. 1, no. 5, p. 492-503.
Kipp, M. A., and Stüeken, E. E., 2017, Biomass recycling and Earth's early phosphorus cycle: Science Advances, v. 3, no. 11, p. eaao 4795.
Knoll, A. H., 2003, Biomineralization and Evolutionary History: Reviews in Mineralogy and Geochemistry, v. 54, no. 1, p. 329-356.
Knoll, A. H., and Nowak, M. A., 2017, The timetable of evolution: Science advances, v. 3, no. 5, p. e1603076.
Knoll, A., and Swett, K., 1990, Carbonate deposition during the late Proterozoic Era: an example from Spitsbergen: American Journal of Science, v. 290, p. 104-132.
Komiya, T., Hirata, T., Kitajima, K., Yamamoto, S., Shibuya, T., Sawaki, Y., Ishikawa, T., Shu, D., Li, Y., and Han, J., 2008, Evolution of the composition of seawater through geologic time, and its influence on the evolution of life: Gondwana Research, v. 14, no. 1-2, p. 159-174.
Kopp, R. E., Kirschvink, J. L., Hilburn, I. A., and Nash, C. Z., 2005, The Paleoproterozoic snowball Earth: a climate disaster triggered by the evolution of oxygenic photosynthesis: Proceedings of the National Academy of Sciences, v. 102, no. 32, p. 11131-11136.
Kump, L. R., and Barley, M. E., 2007, Increased subaerial volcanism and the rise of atmospheric oxygen 2.5 billion years ago: Nature, v. 448, no. 7157, p. 1033-1036.
Kunzmann, M., Gibson, T. M., Halverson, G. P., Hodgskiss, M. S., Bui, T. H., Carozza, D. A., Sperling, E. A., Poirier, A., Cox, G. M., and Wing, B. A., 2017, Iron isotope biogeochemistry of Neoproterozoic marine shales: Geochimica et Cosmochimica Acta, v. 209, p. 85-105.
Laakso, T. A., Sperling, E. A., Johnston, D. T., and Knoll, A. H., 2020, Ediacaran reorganization of the marine phosphorus cycle: Proceedings of the National Academy of Sciences, v. 117, no. 22, p. 11961-11967.
Laflamme, M., Darroch, S. A. F., Tweedt, S. M., Peterson, K. J., and Erwin, D. H., 2013, The end of the Ediacara biota: Extinction, biotic replacement, or Cheshire Cat?: Gondwana Research, v. 23, no. 2, p. 558-573.
Lalonde, S. V., and Konhauser, K. O., 2015, Benthic perspective on Earth's oldest evidence for oxygenic photosynthesis: Proceedings of the National Academy of Sciences, v. 112, no. 4, p. 995-1000.
Lan, Z.-W., and Chen, Z.-Q., 2012, Exceptionally preserved microbially induced sedimentary structures from the Ediacaran post-glacial successions in the Kimberley region, northwestern Australia: Precambrian Research, v. 200-203, p. 1-25.
Lau, K. V., Macdonald, F. A., Maher, K., and Payne, J. L., 2017, Uranium isotope evidence for temporary ocean oxygenation in the aftermath of the Sturtian Snowball Earth: Earth and Planetary Science Letters, v. 458, p. 282-292.
Lenton, T. M., Dahl, T. W., Daines, S. J., Mills, B. J., Ozaki, K., Saltzman, M. R., and Porada, P., 2016, Earliest land plants created modern levels of atmospheric oxygen: Proceedings of the National Academy of Sciences, v. 113, no. 35, p. 9704-9709.
Li, C. W., Chen, J. Y., Lipps, J. H., Gao, F., Chi, H. M., and Wu, H. J., 2022, Ciliated protozoans from the Precambrian Doushantuo Formation, Wengan, South China: Geological Society, London, Special Publications, v. 286, no. 1, p. 151-156.
Li, C., Love, G. D., Lyons, T. W., Fike, D. A., Sessions, A. L., and Chu, X., 2010, A stratified redox model for the Ediacaran ocean: Science, v. 328, no. 5974, p. 80-83.
Li, C.-W., Chen, J.-Y., Lipps, J. H., Gao, F., Chi, H.-M., and Wu, H.-J., 2007, Ciliated protozoans from the Precambrian Doushantuo Formation, Wengan, South China: Geological Society, London, Special Publications, v. 286, no. 1, p. 151-156.
Li, F., Deng, J., Kershaw, S., Burne, R., Gong, Q., Tang, H., Lu, C., Qu, H., Zheng, B., Luo, S., Jin, Z., and Tan, X., 2021, Microbialite development through the Ediacaran–Cambrian transition in China: Distribution, characteristics, and paleoceanographic implications: Global and Planetary Change, v. 205.

Ling, H.-F., Chen, X., Li, D., Wang, D., Shields-Zhou, G. A., and Zhu, M., 2013, Cerium anomaly variations in Ediacaran–earliest Cambrian carbonates from the Yangtze Gorges area, South China: Implications for oxygenation of coeval shallow seawater: Precambrian Research, v. 225, p. 110-127.

Linnemann, U., Ovtcharova, M., Schaltegger, U., Gärtner, A., Hautmann, M., Geyer, G., Vickers-Rich, P., Rich, T., Plessen, B., Hofmann, M., Zieger, J., Krause, R., Kriesfeld, L., and Smith, J., 2019, New high-resolution age data from the Ediacaran-Cambrian boundary indicate rapid, ecologically driven onset of the Cambrian explosion: Terra Nova, v. 31, no. 1, p. 49-58.

Liu, A. G., Kenchington, C. G., and Mitchell, E. G., 2015, Remarkable insights into the paleoecology of the Avalonian Ediacaran macrobiota: Gondwana Research, v. 27, no. 4, p. 1355-1380.

Liu, X. M., Kah, L. C., Knoll, A. H., Cui, H., Wang, C., Bekker, A., and Hazen, R. M., 2021, A persistently low level of atmospheric oxygen in Earth's middle age: Nat Commun, v. 12, no. 1, p. 351.

Liu, Y., and Schmitt, R., 1984, Chemical profiles in sediment and basalt samples from deep-sea drilling project LEG-74, HOLE 525A, Walvis Ridge: Initial Reports of the Deep Sea Drilling Project, v. 74, no. MAR, p. 713-730.

Liu, Y.-G., Miah, M., and Schmitt, R., 1988, Cerium: a chemical tracer for paleo-oceanic redox conditions: Geochimica et Cosmochimica Acta, v. 52, no. 6, p. 1361-1371.

Logan, B. W., 1961, Cryptozoon and associate stromatolites from the recent, Shark Bay, Western Australia: The Journal of Geology, v. 69, no. 5, p. 517-533.

Logan, B. W., Rezak, R., and Ginsburg, R. N., 1964, Classification and environmental significance of algal stromatolites: The Journal of Geology, v. 72, no. 1, p. 68-83.

Louyakis, A. S., Mobberley, J. M., Vitek, B. E., Visscher, P. T., Hagan, P. D., Reid, R. P., Kozdon, R., Orland, I. J., Valley, J. W., Planavsky, N. J., Casaburi, G., and Foster, J. S., 2017, A Study of the Microbial Spatial Heterogeneity of Bahamian Thrombolites Using Molecular, Biochemical, and Stable Isotope Analyses: Astrobiology, v. 17, no. 5, p. 413-430.

Lowe, D. R., 1980, Stromatolites 3,400-myr old from the Archean of Western Australia: Nature, v. 284, no. 5755, p. 441-443.

Lowenstam, H. A., and Weiner, S., 1989, On biomineralization, Oxford University Press on Demand.

Lu, W., Ridgwell, A., Thomas, E., Hardisty, D. S., Luo, G., Algeo, T. J., Saltzman, M. R., Gill, B. C., Shen, Y., and Ling, H.-F., 2018, Late inception of a resiliently oxygenated upper ocean: Science, v. 361, no. 6398, p. 174-177.

Luyt, J., Hare, V. J., and Sealy, J., 2019, The relationship of ungulate δ13C and environment in the temperate biome of southern Africa, and its palaeoclimatic application: Palaeogeography, Palaeoclimatology, Palaeoecology, v. 514, p. 282-291.

Marais, D. J. D., Strauss, H., Summons, R. E., and Hayes, J., 1992, Carbon isotope evidence for the stepwise oxidation of the Proterozoic environment: Nature, v. 359, no. 6396, p. 605-609.

Martin-Bello, L., Arenas, C., Jones, B., and Brasier, A., 2019, Lacustrine stromatolites: Useful structures for environmental interpretation – an example from the Miocene Ebro Basin: Sedimentology, v. 66, no. 6, p. 2098-2133.

Martin, E. E., Blair, S. W., Kamenov, G. D., Scher, H. D., Bourbon, E., Basak, C., and Newkirk, D. N., 2010, Extraction of Nd isotopes from bulk deep sea sediments for paleoceanographic studies on Cenozoic time scales: Chemical Geology, v. 269, no. 3-4, p. 414-431.

Mastandrea, A., Barca, D., Guido, A., Tosti, F., and Russo, F., 2010, Rare earth element signatures in the Messinian pre-evaporitic Calcare di Base formation (Northern Calabria, Italy): evidence of normal seawater deposition: Carbonates and Evaporites, v. 25, no. 2, p. 133-143.

McArthur, J., and Walsh, J., 1984, Rare-earth geochemistry of phosphorites: Chemical Geology, v. 47, no. 3-4, p. 191-220.

McFadden, K. A., Huang, J., Chu, X., Jiang, G., Kaufman, A. J., Zhou, C., Yuan, X., and Xiao, S., 2008, Pulsed oxidation and biological evolution in the Ediacaran Doushantuo Formation: Proceedings of the National Academy of Sciences, v. 105, no. 9, p. 3197-3202.

McLoughlin, N., Li, M., Wacey, D., Martin, L. A., Shen, Y., and Beukes, N. J., 2023, Microbial sulphur-cycling and atmospheric signatures in the 2.52 Ga Gamohaan Formation, South Africa: Earth and Planetary Science Letters, v. 602, p. 117941.

Mcloughlin, N., Melezhik, V. A., Brasier, A. T., and Medvedev, P. V., 2013, Palaeoproterozoic stromatolites from the Lomagundi-Jatuli interval of the Fennoscandian Shield, Reading the Archive of Earth's Oxygenation: Global Events and the Fennoscandian Arctic Russia-Drilling Early Earth Project, Springer-Verlag Berlin Heidelberg, p. 1298-1352.

Mehra, A., Watters, W. A., Grotzinger, J. P., and Maloof, A. C., 2020, Three-dimensional reconstructions of the putative metazoan Namapoikia show that it was a microbial construction: Proc Natl Acad Sci U S A, v. 117, no. 33, p. 19760-19766.

Mercedes-Martín, R., Salas, R., and Arenas, C., 2014, Microbial-dominated carbonate platforms during the Ladinian rifting: sequence stratigraphy and evolution of accommodation in a fault-controlled setting (Catalan Coastal Ranges, NE Spain): Basin Research, v. 26, no. 2, p. 269-296.

Michalak, I., Chojnacka, K., and Witek-Krowiak, A., 2013, State of the art for the biosorption process--a review: Appl Biochem Biotechnol, v. 170, no. 6, p. 1389-1416.

Monty, C. L. V., 1976, Chapter 5.1 The Origin and Development of Cryptalgal Fabrics, Stromatolites, p. 193-249.

Monty, C., 1977, Evolving concepts on the nature and the ecological significance of stromatolites, Fossil algae, Springer, p. 15-35.

Murphy, M. A., and Sumner, D. Y., 2008, Variations in Neoarchean microbialite morphologies: clues to controls on microbialite morphologies through time: Sedimentology, v. 55, no. 5, p. 1189-1202.

Narbonne, G. M., 2005, The Ediacara biota: Neoproterozoic origin of animals and their ecosystems: Annu. Rev. Earth Planet. Sci., v. 33, p. 421-442.

Narbonne, G. M., Saylor, B. Z., and Grotzinger, J. P., 1997, The youngest Ediacaran fossils from southern Africa: Journal of paleontology, v. 71, no. 6, p. 953-967.

Narbonne, G. M., Xiao, S., Shields, G. A., and Gehling, J. G., 2012, The Ediacaran Period: The geologic time scale, v. 1, p. 413-435.

Nelson, L. L., Ramezani, J., Almond, J. E., Darroch, S. A. F., Taylor, W. L., Brenner, D. C., Furey, R. P., Turner, M., and Smith, E. F., 2022, Pushing the boundary: A calibrated Ediacaran-Cambrian stratigraphic record from the Nama Group in northwestern Republic of South Africa: Earth and Planetary Science Letters, v. 580.

Neuweiler, F., d'Orazio, V., Immenhauser, A., Geipel, G., Heise, K.-H., Cocozza, C., and Miano, T. M., 2003, Fulvic acid–like organic compounds control nucleation of marine calcite under suboxic conditions: Geology, v. 31, no. 8, p. 681-684.

Nothdurft, L. D., Webb, G. E., and Kamber, B. S., 2004, Rare earth element geochemistry of Late Devonian reefal carbonates, Canning Basin, Western Australia: confirmation of a seawater REE proxy in ancient limestones: Geochimica et Cosmochimica Acta, v. 68, no. 2, p. 263-283.

Nott, J., and Parkes, K., 1975, Calcium accumulation and secretion in the serpulid polychaete Spirorbis spirorbis L. at settlement: Journal of the Marine Biological Association of the United Kingdom, v. 55, no. 4, p. 911-923.

Nozaki, Y., and Zhang, J., 1995, The rare earth elements and yttrium in the coastal/offshore mixing zone of Tokyo Bay waters and the Kuroshio In Sakai H., & Nozaki Y.(Eds.), Biogeochemical processes and ocean flux in the Western Pacific (pp. 171–184), Tokyo: Terra Scientific Publishing Company.[Google Scholar].

Nozaki, Y., Zhang, J., and Amakawa, H., 1997, The fractionation between Y and Ho in the marine environment: Earth and Planetary Science Letters, v. 148, no. 1-2, p. 329-340.

Och, L. M., and Shields-Zhou, G. A., 2012, The Neoproterozoic oxygenation event: Environmental perturbations and biogeochemical cycling: Earth-Science Reviews, v. 110, no. 1-4, p. 26-57.

O'Connell, B., Wallace, M. W., vS Hood, A., Lechte, M. A., and Planavsky, N. J., 2020, Iron-rich carbonate tidal deposits, Angepena Formation, South Australia: a redox-stratified Cryogenian basin: Precambrian Research, v. 342, p. 105668

Okumura, T., Takashima, C., Shiraishi, F., Nishida, S., and Kano, A., 2013, Processes forming daily lamination in a microbe-rich travertine under low flow condition at the Nagano-yu hot spring, southwestern Japan: Geomicrobiology Journal, v. 30, no. 10, p. 910-927.

Olivier, N., and Boyet, M., 2006, Rare earth and trace elements of microbialites in Upper Jurassic coral-and sponge-microbialite reefs: Chemical Geology, v. 230, no. 1-2, p. 105-123.

Olson, S. L., Kump, L. R., and Kasting, J. F., 2013, Quantifying the areal extent and dissolved oxygen concentrations of Archean oxygen oases: Chemical Geology, v. 362, p. 35-43.

Omelon, C. R., Brady, A. L., Slater, G. F., Laval, B., Lim, D. S. S., and Southam, G., 2013, Microstructure variability in freshwater microbialites, Pavilion Lake, Canada: Palaeogeography, Palaeoclimatology, Palaeoecology, v. 392, p. 62-70.

Pace, A., Bourillot, R., Bouton, A., Vennin, E., Braissant, O., Dupraz, C., Duteil, T., Bundeleva, I., Patrier, P., Galaup, S., Yokoyama, Y., Franceschi, M., Virgone, A., and Visscher, P. T., 2018, Formation of stromatolite lamina at the interface of oxygenic-anoxygenic photosynthesis: Geobiology, v. 16, no. 4, p. 378-398.

Penny, A. M., Wood, R. A., Zhuravlev, A. Y., Curtis, A., Bowyer, F., and Tostevin, R., 2017, Intraspecific variation in an Ediacaran skeletal metazoan: Namacalathus from the Nama Group, Namibia: Geobiology, v. 15, no. 1, p. 81-93.

Penny, A. M., Wood, R., Curtis, A., Bowyer, F., Tostevin, R., and Hoffman, K.-H., 2014, Ediacaran metazoan reefs from the Nama Group, Namibia: Science, v. 344, no. 6191, p. 1504-1506.

Petryshyn, V. A., Corsetti, F. A., Berelson, W. M., Beaumont, W., and Lund, S. P., 2012, Stromatolite lamination frequency, Walker Lake, Nevada: Implications for stromatolites as biosignatures: Geology, v. 40, no. 6, p. 499-502.

Petryshyn, V., and Corsetti, F., 2011, Analysis of growth directions of columnar stromatolites from Walker Lake, western Nevada: Geobiology, v. 9, no. 5, p. 425-435.

Philippot, P., Van Zuilen, M., Lepot, K., Thomazo, C., Farquhar, J., and Van Kranendonk, M. J., 2007, Early Archaean microorganisms preferred elemental sulfur, not sulfate: science, v. 317, no. 5844, p. 1534-1537.

Pierson, B. K., Bauld, J., Castenholz, R. W., D'Amelio, E., Marais, D. J. D., Farmer, J. D., Grotzinger, J. P., Jørgensen, B. B., Nelson, D. C., Palmisano, A. C., Schopf, J. W., Summons, R. E., Walter, M. R., and Ward, D. M., 1992, Modern Mat-Building Microbial Communities: a Key to the Interpretation of Proterozoic Stromatolitic Communities, The Proterozoic Biosphere, p. 245-342.

Pierson, B. K., Bauld, J., Castenholz, R. W., D'Amelio, E., Marais, D. J. D., Farmer, J. D., Grotzinger, J. P., Jørgensen, B. B., Nelson, D. C., Palmisano, A. C., Schopf, J. W., Summons, R. E., Walter, M. R., and Ward, D. M., 1992, Modern Mat-Building Microbial Communities: a Key to the Interpretation of Proterozoic Stromatolitic Communities, The Proterozoic Biosphere, p. 245-342.

Planavsky, N. J., Asael, D., Rooney, A. D., Robbins, L. J., Gill, B. C., Dehler, C. M., Cole, D. B., Porter, S. M., Love, G. D., and Konhauser, K. O., 2023, A sedimentary record of the evolution of the global marine phosphorus cycle: Geobiology, v. 21, no. 2, p. 168-174.

Planavsky, N. J., Slack, J. F., Cannon, W. F., O'Connell, B., Isson, T. T., Asael, D., Jackson, J. C., Hardisty, D. S., Lyons, T. W., and Bekker, A., 2018, Evidence for episodic oxygenation in a weakly redox-buffered deep mid-Proterozoic ocean: Chemical Geology, v. 483, p. 581-594.

Planavsky, N., Bekker, A., Rouxel, O. J., Kamber, B., Hofmann, A., Knudsen, A., and Lyons, T. W., 2010, Rare Earth Element and yttrium compositions of Archean and Paleoproterozoic Fe formations revisited: New perspectives on the significance and mechanisms of deposition: Geochimica et Cosmochimica Acta, v. 74, no. 22, p. 6387-6405.

Porter, S. M., 2010, Calcite and aragonite seas and the de novo acquisition of carbonate skeletons: Geobiology, v. 8, no. 4, p. 256-277.
Poulton, S. W., and Canfield, D. E., 2011, Ferruginous Conditions: A Dominant Feature of the Ocean through Earth's History: Elements, v. 7, no. 2, p. 107-112.
Poulton, S. W., Bekker, A., Cumming, V. M., Zerkle, A. L., Canfield, D. E., and Johnston, D. T., 2021, A 200-million-year delay in permanent atmospheric oxygenation: Nature, v. 592, no. 7853, p. 232-236.
Qu, Y., Engdahl, A., Zhu, S., Vajda, V., and McLoughlin, N., 2015, Ultrastructural heterogeneity of carbonaceous material in ancient cherts: Investigating biosignature origin and preservation: Astrobiology, v. 15, no. 10, p. 825-842.
Qu, Y., Wang, J., Xiao, S., Whitehouse, M., Engdahl, A., Wang, G., and McLoughlin, N., 2017, Carbonaceous biosignatures of diverse chemotrophic microbial communities from chert nodules of the Ediacaran Doushantuo Formation: Precambrian Research, v. 290, p. 184-196.
Raaben, M. a. E. e., Sinha, A. K., and Sharma, M., 2001, Precambrian stromatolites of India and Russia, Birbal Sahni Institute of Palaeobotany.
Raaben, M., 1969, Columnar stromatolites and late Precambrian stratigraphy: American Journal of Science, v. 267, no. 1, p. 1-18.
Reid, R. P., and Browne, K. M., 1991, Intertidal stromatolites in a fringing Holocene reef complex, Bahamas: Geology, v. 19, no. 1, p. 15-18.
Reinhard, C. T., Planavsky, N. J., Gill, B. C., Ozaki, K., Robbins, L. J., Lyons, T. W., Fischer, W. W., Wang, C., Cole, D. B., and Konhauser, K. O., 2017, Evolution of the global phosphorus cycle: Nature, v. 541, no. 7637, p. 386-389.
Reitner, J., Quéric, N.-V., Arp, G., and Van Kranendonk, M. J., 2011, Morphology as an indictor of biogenicity for 3.5–3.2 Ga fossil stromatolites from the Pilbara Craton, Western Australia: Advances in stromatolite geobiology, p. 537-554.
Riding, R., 1991, Classification of microbial carbonates, Calcareous algae and stromatolites, Springer, p. 21-51.
Riding, R., 2000, Microbial carbonates: the geological record of calcified bacterial–algal mats and biofilms: Sedimentology, v. 47, p. 179-214.
Riding, R., 2006, Microbial carbonate abundance compared with fluctuations in metazoan diversity over geological time: Sedimentary Geology, v. 185, no. 3-4, p. 229-238.
Riding, R., 2008, Abiogenic, microbial and hybrid authigenic carbonate crusts: components of Precambrian stromatolites: Geologia Croatica, v. 61, no. 2-3, p. 73-103.
Riding, R., 2008, Abiogenic, microbial and hybrid authigenic carbonate crusts: components of Precambrian stromatolites: Geologia Croatica, v. 61, no. 2-3, p. 73-103.
Riding, R., 2011a, Microbialites, stromatolites, and thrombolites, Encyclopedia of geobiology.
Riding, R., 2011b, The nature of stromatolites: 3,500 million years of history and a century of research, Advances in stromatolite geobiology, Springer, p. 29-74.
Riding, R., Fralick, P., and Liang, L., 2014, Identification of an Archean marine oxygen oasis: Precambrian Research, v. 251, p. 232-237.
Riding, R., Interaction between accretionary process, relative relief, and external shape in stromatolites and related microbial deposits, *in* Proceedings International Alpine Algae Symposium and Field-Meeting 1993.
Ries, J. B., Anderson, M. A., and Hill, R. T., 2008, Seawater Mg/Ca controls polymorph mineralogy of microbial CaCO3: a potential proxy for calcite-aragonite seas in Precambrian time: Geobiology, v. 6, no. 2, p. 106-119.
Rowland, S. M., and Shapiro, R. S., 2002, Reef patterns and environmental influences in the Cambrian and earliest Ordovician.
Rye, R., and Holland, H. D., 1998, Paleosols and the evolution of atmospheric oxygen; a critical review: American Journal of Science, v. 298, no. 8, p. 621-672.

Sahoo, S. K., Planavsky, N. J., Jiang, G., Kendall, B., Owens, J. D., Wang, X., Shi, X., Anbar, A. D., and Lyons, T. W., 2016, Oceanic oxygenation events in the anoxic Ediacaran ocean: Geobiology, v. 14, no. 5, p. 457-468.
Sahoo, S. K., Planavsky, N. J., Kendall, B., Wang, X., Shi, X., Scott, C., Anbar, A. D., Lyons, T. W., and Jiang, G., 2012, Ocean oxygenation in the wake of the Marinoan glaciation: Nature, v. 489, no. 7417, p. 546-549.
Sanchez-Baracaldo, P., 2015, Origin of marine planktonic cyanobacteria: Sci Rep, v. 5, p. 17418.
Sanchez-Baracaldo, P., Bianchini, G., Wilson, J. D., and Knoll, A. H., 2022, Cyanobacteria and biogeochemical cycles through Earth history: Trends Microbiol, v. 30, no. 2, p. 143-157.
Sanders, C. B., Eiler, J. C., and Grotzinger, J. P., 2023, Paragenesis of an Ediacaran carbonate-platform phosphorite: Constraints from optical petrography and texture-specific clumped isotope paleothermometry: Sedimentary Geology, v. 444.
Sanders, C., and Grotzinger, J., 2021, Sedimentological and stratigraphic constraints on depositional environment for Ediacaran carbonate rocks of the São Francisco Craton: Implications for phosphogenesis and paleoecology: Precambrian Research, v. 363.
Saylor, B. Z., Grotzinger, J. P., and Germs, G. J., 1995, Sequence stratigraphy and sedimentology of the Neoproterozoic Kuibis and Schwarzrand subgroups (Nama Group), southwestern Namibia: Precambrian Research, v. 73, no. 1-4, p. 153-171.
Saylor, B. Z., Kaufman, A. J., Grotzinger, J. P., and Urban, F., 1998, A composite reference section for terminal Proterozoic strata of southern Namibia: Journal of Sedimentary Research, v. 68, no. 6, p. 1223-1235.
Scherer, M., and Seitz, H., 1980, Rare-earth element distribution in Holocene and Pleistocene corals and their redistribution during diagenesis: Chemical Geology, v. 28, p. 279-289.
Schopf, J., and Walter, M., 1982, The biology of cyanobacteria: Origin and Early Evolution of Cyanobacteria: The Geological Evidence, edited by NG Carr and BA Whitton, Blackwell, Oxford, and University of California Press, Berkeley, p. 543-564.
Scott, C., Lyons, T., Bekker, A., Shen, Y.-a., Poulton, S., Chu, X.-l., and Anbar, A., 2008, Tracing the stepwise oxygenation of the Proterozoic ocean: Nature, v. 452, no. 7186, p. 456-459.
Seilacher, A., 1984, Late Precambrian and Early Cambrian Metazoa: preservational or real extinctions?, Patterns of change in earth evolution, Springer, p. 159-168.
Seilacher, A., 1985, Discussion of Precambrian metazoans: Philosophical Transactions of the Royal Society of London. B, Biological Sciences, v. 311, no. 1148, p. 47-48.
Seilacher, A., 1989, Vendozoa: organismic construction in the Proterozoic biosphere: Lethaia, v. 22, no. 3, p. 229-239.
Seilacher, A., 1992, Vendobionta and Psammocorallia: lost constructions of Precambrian evolution: Journal of the Geological Society, v. 149, no. 4, p. 607-613.
Seilacher, A., 1999, Biomat-related lifestyles in the Precambrian: Palaios, v. 14, no. 1, p. 86-93.
Seilacher, A., Grazhdankin, D., and Legouta, A., 2003, Ediacaran biota: The dawn of animal life in the shadow of giant protists: Paleontological research, v. 7, no. 1, p. 43-54.
Semikhatov, M. A., and Raaben, M. E., 2000, Proterozoic stromatolite taxonomy and biostratigraphy, Microbial sediments, Springer, p. 295-306.
Semikhatov, M., 1976, Experience in stromatolite studies in the USSR, Developments in sedimentology, Volume 20, Elsevier, p. 337-357.
Semikhatov, M., Gebelein, C., Cloud, P., Awramik, S., and Benmore, W., 1979, Stromatolite morphogenesis—progress and problems: Canadian Journal of Earth Sciences, v. 16, no. 5, p. 992-1015.
Serebryakov, S. N., Komar, V. A., and Semikahatov, M. A., 1972, Dependance of the morphology of Riphean stromatolites on conditions of the depositional environment: News of the Academy of Sciences of the USSR, v. 7, p. 140-148.
Serebryakov, S., 1976, Biotic and abiotic factors controlling the morphology of Riphean stromatolites, Developments in sedimentology, Volume 20, Elsevier, p. 321-336.

Sforna, M. C., Philippot, P., Somogyi, A., Van Zuilen, M. A., Medjoubi, K., Schoepp-Cothenet, B., Nitschke, W., and Visscher, P. T., 2014, Evidence for arsenic metabolism and cycling by microorganisms 2.7 billion years ago: Nature Geoscience, v. 7, no. 11, p. 811-815.
Shaojun, Z., and Mucci, A., 1993, Calcite precipitation in seawater using a constant addition technique: A new overall reaction kinetic expression: Geochimica et Cosmochimica Acta, v. 57, no. 7, p. 1409-1417.
Shapiro, H. M., 2000, Microbial analysis at the single-cell level: tasks and techniques: Journal of microbiological methods, v. 42, no. 1, p. 3-16.
Shapiro, R., and Wilmeth, D., 2020, Treatise Online no. 134: Part B, Volume 2, Chapter 8: Microbialites: Treatise Online.
Shaw, H., and Wasserburg, G., 1985, Sm-Nd in marine carbonates and phosphates: Implications for Nd isotopes in seawater and crustal ages: Geochimica et Cosmochimica Acta, v. 49, no. 2, p. 503-518.
Shields, G. A., 2017, Earth system transition during the Tonian–Cambrian interval of biological innovation: nutrients, climate, oxygen and the marine organic carbon capacitor: Geological Society, London, Special Publications, v. 448, no. 1, p. 161-177.
Shields, G. A., and Webb, G. E., 2004, Has the REE composition of seawater changed over geological time?
Shields-Zhou, G., and Och, L., 2011, The case for a Neoproterozoic oxygenation event: geochemical evidence and biological consequences: GSa Today, v. 21, no. 3, p. 4-11.
Shore, A., Wood, R., Curtis, A., and Bowyer, F., 2020, Multiple branching and attachment structures in cloudinomorphs, Nama Group, Namibia: Geology, v. 48, no. 9, p. 877-881.
Simonson, B. M., and Carney, K. E., 1999, Roll-up structures; evidence of in situ microbial mats in late Archean deep shelf environments: Palaios, v. 14, no. 1, p. 13-24.
Slack, J. F., Grenne, T., and Bekker, A., 2009, Seafloor-hydrothermal Si-Fe-Mn exhalites in the Pecos greenstone belt, New Mexico, and the redox state of ca. 1720 Ma deep seawater: Geosphere, v. 5, no. 3, p. 302-314.
Slack, J., Grenne, T., Bekker, A., Rouxel, O., and Lindberg, P., 2007, Suboxic deep seawater in the late Paleoproterozoic: evidence from hematitic chert and iron formation related to seafloor-hydrothermal sulfide deposits, central Arizona, USA: Earth and Planetary Science Letters, v. 255, no. 1-2, p. 243-256.
Smith, R. M., and Mason, T. R., 1998, Sedimentary environments and trace fossils of Tertiary oasis deposits in the central Namib Desert, Namibia: Palaios, v. 13, no. 6, p. 547-559.
Solari, M., Hervé, F., Le Roux, J., Airo, A., and Sial, A., 2010, Paleoclimatic significance of lacustrine microbialites: A stable isotope case study of two lakes at Torres del Paine, southern Chile: Palaeogeography, Palaeoclimatology, Palaeoecology, v. 297, no. 1, p. 70-82.
Soyol-Erdene, T.-O., and Huh, Y., 2013, Rare earth element cycling in the pore waters of the Bering Sea Slope (IODP Exp. 323): Chemical Geology, v. 358, p. 75-89.
Sperling, E. A., Rooney, A. D., Hays, L., Sergeev, V., Vorob'Eva, N., Sergeeva, N., Selby, D., Johnston, D. T., and Knoll, A. H., 2014, Redox heterogeneity of subsurface waters in the M esoproterozoic ocean: Geobiology, v. 12, no. 5, p. 373-386.
Sperling, E. A., Wolock, C. J., Morgan, A. S., Gill, B. C., Kunzmann, M., Halverson, G. P., Macdonald, F. A., Knoll, A. H., and Johnston, D. T., 2015, Statistical analysis of iron geochemical data suggests limited late Proterozoic oxygenation: Nature, v. 523, no. 7561, p. 451-454.
Stanistreet, I. G., Kukla, P. A., and Henry, G., 1991, Sedimentary basinal responses to a late Precambrian Wilson cycle: The Damara orogen and Nama foreland, Namibia: Journal of African Earth Sciences (and the Middle East), v. 13, no. 1, p. 141-156.
Stolper, D. A., and Keller, C. B., 2018, A record of deep-ocean dissolved O2 from the oxidation state of iron in submarine basalts: Nature, v. 553, no. 7688, p. 323-327.
Stüeken, E. E., Buick, R., and Anbar, A. D., 2015, Selenium isotopes support free O2 in the latest Archean: Geology, v. 43, no. 3, p. 259-262.

Sumner, D. Y., 2000, Microbial vs environmental influences on the morphology of Late Archean fenestrate microbialites, Microbial sediments, Springer, p. 307-314.
Sumner, D. Y., 2004, Implications for Neoarchaean ocean chemistry from primary carbonate mineralogy of the Campbellrand-Malmani Platform, South Africa: Sedimentology, v. 51, no. 6, p. 1273-1299.
Sumner, D. Y., and Grotzinger, J. P., 1996, Were kinetics of Archean calcium carbonate precipitation related to oxygen concentration?: Geology, v. 24, no. 2, p. 119-122.
Sumner, D. Y., and Grotzinger, J. P., 2000, Late Archean aragonite precipitation: petrography, facies associations, and environmental significance: Carbonate Sedimentation and Diagenesis in the Evolving Precambrian World, v. 67.
Sumner, D. Y., Hawes, I., Mackey, T. J., Jungblut, A. D., and Doran, P. T., 2015, Antarctic microbial mats: A modern analog for Archean lacustrine oxygen oases: Geology, v. 43, no. 10, p. 887-890.
Sumner, D., 2002, Decimetre-Thick Encrustations of Calcite and Aragonite on the Sea-Floor and Implications for Neoarchaean and Neoproterozoic Ocean Chemistry: Precambrian sedimentary environments: A modern approach to ancient depositional systems, p. 107-120.
Taber, C. W., and Thomas, C. L., 1940, Taber's Cyclopedic medical dictionary, Philadelphia, F.A. Davis Company.
Tachikawa, K., Jeandel, C., and Roy-Barman, M., 1999, A new approach to the Nd residence time in the ocean: the role of atmospheric inputs: Earth and Planetary Science Letters, v. 170, no. 4, p. 433-446.
Taylor, S. R., and McLennan, S. M., 1985, The continental crust: its composition and evolution.
Tostevin, R., and Mills, B. J. W., 2020, Reconciling proxy records and models of Earth's oxygenation during the Neoproterozoic and Palaeozoic: Interface Focus, v. 10, no. 4, p. 20190137.
Tostevin, R., Bradbury, H. J., Shields, G. A., Wood, R. A., Bowyer, F., Penny, A. M., and Turchyn, A. V., 2019, Calcium isotopes as a record of the marine calcium cycle versus carbonate diagenesis during the late Ediacaran: Chemical Geology, v. 529.
Tostevin, R., Shields, G. A., Tarbuck, G. M., He, T., Clarkson, M. O., and Wood, R. A., 2016a, Effective use of cerium anomalies as a redox proxy in carbonate-dominated marine settings: Chemical Geology, v. 438, p. 146-162.
Tostevin, R., Wood, R. A., Shields, G. A., Poulton, S. W., Guilbaud, R., Bowyer, F., Penny, A. M., He, T., Curtis, A., Hoffmann, K. H., and Clarkson, M. O., 2016b, Low-oxygen waters limited habitable space for early animals: Nat Commun, v. 7, p. 12818.
Tosti, F., and Riding, R., 2017a, Current molded, storm damaged, sinuous columnar stromatolites: Mesoproterozoic of northern China: Palaeogeography, Palaeoclimatology, Palaeoecology, v. 465, p. 93-102.
Tosti, F., and Riding, R., 2017b, Fine-grained agglutinated elongate columnar stromatolites: Tieling Formation, ca 1420 Ma, North China: Sedimentology, v. 64, no. 4, p. 871-902.
Van Kranendonk, M. J., Webb, G. E., and Kamber, B. S., 2003, Geological and trace element evidence for a marine sedimentary environment of deposition and biogenicity of 3.45 Ga stromatolitic carbonates in the Pilbara Craton, and support for a reducing Archaean ocean: Geobiology, v. 1, no. 2, p. 91-108.
Vandenbroucke, M., and Largeau, C., 2007, Kerogen origin, evolution and structure: Organic Geochemistry, v. 38, no. 5, p. 719-833.
Vázquez-Urbez, M., Arenas, C., Sancho, C., Osácar, C., Auqué, L., and Pardo, G., 2010, Factors controlling present-day tufa dynamics in the Monasterio de Piedra Natural Park (Iberian Range, Spain): depositional environmental settings, sedimentation rates and hydrochemistry: International Journal of Earth Sciences, v. 99, p. 1027-1049.
Vijayaraghavan, K., and Yun, Y.-S., 2008, Bacterial biosorbents and biosorption: Biotechnology advances, v. 26, no. 3, p. 266-291.

Vijayaraghavan, K., Sathishkumar, M., and Balasubramanian, R., 2010, Biosorption of lanthanum, cerium, europium, and ytterbium by a brown marine alga, Turbinaria conoides: Industrial & engineering chemistry research, v. 49, no. 9, p. 4405-4411.
Visscher, P. T., Reid, R. P., and Bebout, B. M., 2000, Microscale observations of sulfate reduction: correlation of microbial activity with lithified micritic laminae in modern marine stromatolites: Geology, v. 28, no. 10, p. 919-922.
Vouelle, J., Grasset, M., and Truchet, M., 1991, Sites of biomineralization in the polychaete *Pomatoceros-Triqueter* (Serpulidae) with comments on some other species: Ophelia, p. 661-667.
Wallace, M. W., Hood, A. v., Shuster, A., Greig, A., Planavsky, N. J., and Reed, C. P., 2017, Oxygenation history of the Neoproterozoic to early Phanerozoic and the rise of land plants: Earth and Planetary Science Letters, v. 466, p. 12-19.
Walter, M. R., 1972, Stromatolites and the biostratigraphy of the Australian Precambrian and Cambrian, Palaeontological Association, v. 11.
Walter, M. R., Grotzinger, J., and Schopf, J. W., 1992, Proterozoic Stromatolites, *in* Schopf, J. W., and Klein, C., eds., The Proterozoic Biosphere: Cambridge, Cambridge University Press, p. 253-285.
Walter, M. R., Oehler, J. H., and Oehler, D. Z., 1976, Megascopic algae 1,300 million years old from the Belt supergroup, Montana: a reinterpretation of Walcott's Helminthoidichnites: Journal of Paleontology, v. 5, no. 50, p. 872–881.
Walter, M., and Heys, G., 1985, Links between the rise of the metazoa and the decline of stromatolites: Precambrian Research, v. 29, no. 1-3, p. 149-174.
Walter, M., Buick, R., and Dunlop, J., 1980, Stromatolites 3,400–3,500 Myr old from the North pole area, Western Australia: Nature, v. 284, no. 5755, p. 443-445.
Wang, X., Planavsky, N. J., Hofmann, A., Saupe, E. E., De Corte, B. P., Philippot, P., LaLonde, S. V., Jemison, N. E., Zou, H., and Ossa, F. O., 2018, A Mesoarchean shift in uranium isotope systematics: Geochimica et Cosmochimica Acta, v. 238, p. 438-452.
Wang, Y., Liu, Y.-G., and Schmitt, R., 1986, Rare earth element geochemistry of South Atlantic deep sea sediments: Ce anomaly change at~ 54 My: Geochimica et Cosmochimica Acta, v. 50, no. 7, p. 1337-1355.
Warén, A., Bengtson, S., Goffredi, S. K., and Van Dover, C. L., 2003, A hot-vent gastropod with iron sulfide dermal sclerites: Science, v. 302, no. 5647, p. 1007-1007.
Warren, L. V., Quaglio, F., Riccomini, C., Simões, M. G., Poiré, D. G., Strikis, N. M., Anelli, L. E., and Strikis, P. C., 2014, The puzzle assembled: Ediacaran guide fossil Cloudina reveals an old proto-Gondwana seaway: Geology, v. 42, no. 5, p. 391-394.
Webb, G. E., and Kamber, B. S., 2000, Rare earth elements in Holocene reefal microbialites: a new shallow seawater proxy: Geochimica et Cosmochimica Acta, v. 64, no. 9, p. 1557-1565.
Webb, G. E., and Kamber, B. S., 2011, Trace Element Geochemistry as a Tool for Interpreting Microbialites, Earliest Life on Earth: Habitats, Environments and Methods of Detection, p. 127-170.
Webb, G. E., Baker, J. C., and Jell, J. S., 1998, Inferred syngenetic textural evolution in Holocene cryptic reefal microbialites, Heron Reef, Great Barrier Reef, Australia: Geology, v. 26, no. 4, p. 355-358.
Weiner, S., and Dove, P. M., 2003, An overview of biomineralization processes and the problem of the vital effect: Reviews in mineralogy and geochemistry, v. 54, no. 1, p. 1-29.
Whalen, M. T., Eberli, G. P., and Homewood, P. W., 2002, Microbial carbonates as indicators of environmental change and biotic crises in carbonate systems: Examples from the Late Devonian, Alberta Basin, Canada: Palaeogeography, Palaeoclimatology, Palaeoecology, v. 181, p. 127-151.
Wilmeth, D. T., Corsetti, F. A., Beukes, N. J., Awramik, S. M., Petryshyn, V., Spear, J. R., and Celestian, A. J., 2019, Neoarchean (2.7 Ga) lacustrine stromatolite deposits in the Hartbeesfontein

Basin, Ventersdorp Supergroup, South Africa: Implications for oxygen oases: Precambrian Research, v. 320, p. 291-302.
Wilmeth, D. T., Lalonde, S. V., Berelson, W. M., Petryshyn, V., Celestian, A. J., Beukes, N. J., Awramik, S. M., Spear, J. R., Mahseredjian, T., and Corsetti, F. A., 2022, Evidence for benthic oxygen production in Neoarchean lacustrine stromatolites: Geology.
Wood, R. A., 2011, Paleoecology of the earliest skeletal metazoan communities: Implications for early biomineralization: Earth-Science Reviews, v. 106, no. 1-2, p. 184-190.
Wood, R. A., Grotzinger, J. P., and Dickson, J., 2002, Proterozoic modular biomineralized metazoan from the Nama Group, Namibia: Science, v. 296, no. 5577, p. 2383-2386.
Wood, R. A., Poulton, S. W., Prave, A. R., Hoffmann, K. H., Clarkson, M. O., Guilbaud, R., Lyne, J. W., Tostevin, R., Bowyer, F., Penny, A. M., Curtis, A., and Kasemann, S. A., 2015, Dynamic redox conditions control late Ediacaran metazoan ecosystems in the Nama Group, Namibia: Precambrian Research, v. 261, p. 252-271.
Wood, R., 1999, Reef evolution, Oxford University Press on Demand.
Wood, R., 2017, Palaeoecology of Ediacaran metazoan reefs: Geological Society, London, Special Publications, v. 448, no. 1, p. 195-210.
Wood, R., 2018, Exploring the drivers of early biomineralization: Emerging topics in life sciences, v. 2, no. 2, p. 201-212.
Wood, R., and Curtis, A., 2015, Extensive metazoan reefs from the Ediacaran Nama Group, Namibia: the rise of benthic suspension feeding: Geobiology, v. 13, no. 2, p. 112-122.
Wood, R., and Erwin, D. H., 2018, Innovation not recovery: dynamic redox promotes metazoan radiations: Biological Reviews, v. 93, no. 2, p. 863-873.
Wood, R., and Penny, A., 2018, Substrate growth dynamics and biomineralization of an Ediacaran encrusting poriferan: Proc Biol Sci, v. 285, no. 1870.
Wright, J., Schrader, H., and Holser, W. T., 1987, Paleoredox variations in ancient oceans recorded by rare earth elements in fossil apatite: Geochimica et Cosmochimica Acta, v. 51, no. 3, p. 631-644.
Xiao, S., and Laflamme, M., 2009, On the eve of animal radiation: phylogeny, ecology and evolution of the Ediacara biota: Trends in Ecology and Evolution, v. 24, no. 1, p. 31-40.
Yamamoto, A., and Isozaki, Y., 2013, Historical Review and Current Perspective of Stromatolite Studies: Journal Of Geography-Chigaku Zasshi, v. 122, no. 5, p. 791-806.
Yamamoto, K., Itoh, N., Matsumoto, T., Tanaka, T., and Adachi, M., 2004, Geochemistry of Precambrian carbonate intercalated in pillows and its host basalt: implications for the REE composition of circa 3.4 Ga seawater: Precambrian Research, v. 135, no. 4, p. 331-344.
Yun, Z., and Hofmann, H. J., 1982, Precambrian Stromatolites: Image Analysis of Lamina Shape: The Journal of Geology, v. 90, no. 3, p. 253-268.
Zhang, F., Xiao, S., Romaniello, S. J., Hardisty, D., Li, C., Melezhik, V., Pokrovsky, B., Cheng, M., Shi, W., and Lenton, T. M., 2019a, Global marine redox changes drove the rise and fall of the Ediacara biota: Geobiology, v. 17, no. 6, p. 594-610.
Zhang, J., and Nozaki, Y., 1996, Rare earth elements and yttrium in seawater: ICP-MS determinations in the East Caroline, Coral Sea, and South Fiji basins of the western South Pacific Ocean: Geochimica et Cosmochimica Acta, v. 60, no. 23, p. 4631-4644.
Zhang, K., and Shields, G. A., 2022, Sedimentary Ce anomalies: Secular change and implications for paleoenvironmental evolution: Earth-Science Reviews, v. 229.
Zhang, K., Zhu, X., Wood, R. A., Shi, Y., Gao, Z., and Poulton, S. W., 2018, Oxygenation of the Mesoproterozoic ocean and the evolution of complex eukaryotes: Nature Geoscience, v. 11, no. 5, p. 345-350.
Zhang, S., Wang, X., Wang, H., Bjerrum, C. J., Hammarlund, E. U., Costa, M. M., Connelly, J. N., Zhang, B., Su, J., and Canfield, D. E., 2016, Sufficient oxygen for animal respiration 1,400 million years ago: Proceedings of the National Academy of Sciences, v. 113, no. 7, p. 1731-1736.

Zhang, X., Dai, M., Wang, M., and Qi, Y., 2019b, Calcified coccoid from Cambrian Miaolingian: Revealing the potential cellular structure of Epiphyton: PLoS One, v. 14, no. 3, p. e0213695.
Zhang, Y., Li, J., Chen, L., Wei, Y., Shi, Q., Wang, D.-G., Wu, Q.-M., Song, L.-Y., Tian, M., Kuang, H.-W., Liu, Y.-Q., Mänd, K., Bai, H.-Q., Liu, Z.-L., Wang, Y.-C., Qiao, D.-W., and Zhu, W.-J., 2021, Manganese carbonate stromatolites of the Ediacaran Doushantuo Formation in Chengkou, northern Yangtze Craton, China: Journal of Palaeogeography, v. 10, no. 1.
Zhuravlev, A. Y., Wood, R. A., and Penny, A. M., 2015, Ediacaran skeletal metazoan interpreted as a lophophorate: Proc Biol Sci, v. 282, no. 1818, p. 20151860.

12. Acknowledgements

I would acknowledge the GENUS DST-NRF Centre of Excellence as well as KW Johnston Bequest Bursary. Without these bursaries, I would not have had the opportunity to pursue my Master's degree. I would like to thank my family, friends and my partner, Sarah Lampert, for their consistent support and encouragement as well as the numerous YouTube study playlists that have helped during writing sessions over the last 2 years. I would like to thank Rosalie Tostevin's ALE research group for helping during lab work, everyday encouragement, and transportation assistance. For their assistance in sample preparation and analysis, I would like to thank John McArthur from UCL for REE analysis and Christel Tinguely from UCT's Geology department for REE sample preparation, René van der Merwe from UCT's Geology department for thin section and mount creation, John Harrison from UWC for rock cutting, Rachel Cupido and Miranda Waldron from UCT's Chemical Engineering for XRD and SEM analysis respectively and Julie Luyt from UCT's Archaeology department for lab access and SLI analysis. Finally, I would like to thank Rosalie Tostevin for being an all-round amazing supervisor, her constant guidance, research expertise, readily available supervision, and research fundings as well as Wendy Taylor, whose passion and encouragement for palaeontology helped elevate my interest in this field of research.